CONTROLLER DESIGN FOR PSS AND FACTS DEVICES TO ENHANCE DAMPING OF LOW-FREQUENCY POWER OSCILLATIONS IN POWER SYSTEMS

by

Ruhua You

A dissertation submitted in partial fulfillment
of the requirement for the degree

of

Doctor of Philosophy

in

Engineering

MONTANA STATE UNIVERSITY
Bozeman, Montana

March 2006

APPROVAL

of a dissertation submitted by

Ruhua You

This dissertation has been read by each member of the dissertation committee and has been found to be satisfactory regarding content, English usage, format, citations, bibliographic style, and consistency, and is ready for submission to the Division of Graduate Education.

Dr. M. Hashem Nehrir

Approved for the Department of Electrical and Computer Engineering

Dr. James N. Peterson

Approved for the Division of Graduate Education

Dr. Joseph J. Fedock

STATEMENT OF PERMISSION TO USE

In presenting this dissertation in partial fulfillment of the requirements for a doctoral degree at Montana State University, I agree that the Library shall make it available to borrowers under rules of the Library. I further agree that copying of this dissertation is allowable only for scholarly purposes, consistent with "fair use" as prescribed in the U.S. Copyright Law. Requests for extensive copying or reproduction of this dissertation should be referred to ProQuest Information and Learning, 300 North Zeeb Road, Ann Arbor, Michigan 48106, to whom I have granted "the exclusive right to reproduce and distribute my dissertation in and from microform along with the non-exclusive right to reproduce and distribute my abstract in any format in whole or in part."

Ruhua You

March 24, 2006

TABLE OF CONTENTS

TABLE OF CONTENTS - CONTINUED

LIST OF FIGURES

Figures Page

LIST OF FIGURES - CONTINUED

Figures Page

LIST OF FIGURES - CONTINUED

Figures Page

LIST OF FIGURES - CONTINUED

Figures Page

LIST OF FIGURES - CONTINUED

Figures Page

LIST OF TABLES

ABSTRACT

Low frequency electromechanical oscillations are inevitable characteristics of power systems and they greatly affect the transmission line transfer capability and power system stability. PSS and FACTS devices can help the damping of power system oscillations. The objective of this dissertation is to design an advanced PSS and propose a systematic approach for damping controller design for FACTS devices. Intelligent control strategy which combines the knowledge of system identification, fuzzy logic control, and the neural networks are applied to the PSS design. A fuzzy logic based PSS is developed and tuned by neural network strategy. The proposed PSS improved the damping of power system oscillations over a conventional PSS.

But the same control strategy is not satisfactory for the FACTS damping controller design, mainly because of the different location and role of FACTS devices in power system oscillations compared to PSS. A systematic approach is proposed to design damping controllers for FACTS devices. The problem is considered from a control point of view and treated as a feedback control problem. A low order plant transfer function is obtained by PRONY method; proper control input is selected and a damping controller is designed combining the eigenvalue sensitivity analysis and the root locus method. A gain varying strategy is proposed to change the controller gain according to the transmission line loading condition for better damping effect. This approach is successfully applied in damping controller design for SVC, TCSC, and UPFC. Simulation results demonstrate good damping effects of these controllers

Another work accomplished in this dissertation is the modeling of UPFC, a voltage-sourced converter-based FACTS device who simultaneously control bus voltage and power flows on transmission lines. The UPFC brings quite a few challenges to power system simulation and study including power flow calculations, modeling of converter control and UPFC dynamics, interfacing UPFC with the power system for transient simulation program development and physical and operating constraint modeling. The proposed model accurately represented the behavior of UPFC in quasi-steady state and well demonstrated the unique capability of the UPFC to control both the load flow and the bus voltage rapidly and independently.

CHAPTER 1

INTRODUCTION

The Nature of Power System Oscillations

In an interconnected power system, the synchronous generators should rotate at the same speed and power flows over tie-lines should remain constant under normal operating conditions. However, low frequency electromechanical oscillations may occur when a disturbance is applied to the power system. These oscillations can be observed in most power system variables like bus voltage, line current, generator speed and power.

Power system oscillations were first observed as soon as synchronous generators were interconnected to provide more generation capacity and more reliability to power system. Originally, the fairly closely connected generators were observed to swing against each other at frequencies of around 1-2 Hz. Damper windings on the generator's rotor were used to prevent the amplitude of oscillations from increasing. After fast excitation systems were introduced to prevent the generators from loosing synchronism following a system fault, it was noticed that this kind of excitation system always tends to reduce the damping of the system oscillations. Power System Stabilizers (PSSs), which are the excitation system based damping controllers, were then widely used to add damping torque and increase the damping of these oscillations.

In the 1950s and 1960s, power utilities started connecting to other utilities through a very long transmission line to achieve more reliability and better economy. However,

very low frequency oscillations (0.1-1Hz) were observed as a result of this interconnection, where the generators in one area swing very slowly against those in the neighboring areas. In some cases, these low frequency growing oscillations prevented the interconnection from being retained and caused loss of power supply to custom loads [1].

Power system oscillations are a characteristic of the system and they are inevitable. However, from an operating point of view, oscillations are acceptable as long as they decay. Power system oscillations are initiated by normal small changes in system loads, and they become much worse following a large disturbance. Fig. 1-1 shows the power flow in the major transmission line for the August 1996 collapse of the western US/Canada interconnected system [1]. The initial fault (occurred at about 400*s* in Fig. 1-1) causes a system oscillation at about 0.26 Hz; the cascading disturbances (faults and protective relaying operation) made the oscillation grow in magnitude, and this growing oscillation caused the final collapse of the whole system. As a result, the system split into disconnected regions and a considerable number of customers lost their power supplies. A similar blackout occurred on August 14, 2003.

Power system oscillations are generally associated with the dynamics of generators, turbine governors and excitation systems and can be represented by the linearized swing equation of a synchronous generator around an operating condition as follows:

$$\frac{d}{dt}\Delta\omega_r = \frac{1}{2H}(\Delta T_m - \Delta T_e - D\Delta\omega_r) \tag{1-1}$$

$$\frac{d}{dt}\Delta\delta = \omega_0\Delta\omega_r \tag{1-2}$$

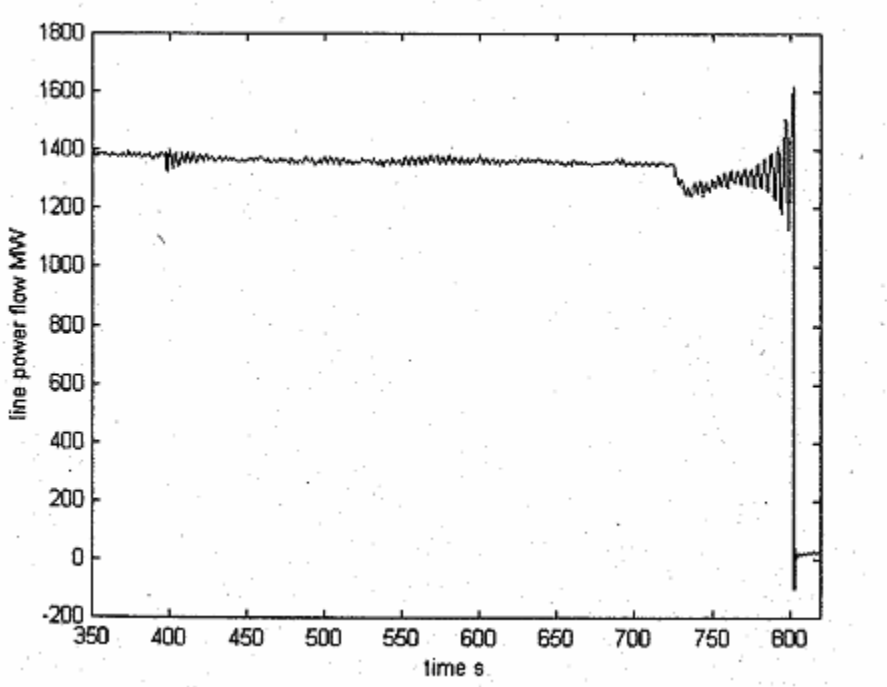

Fig. 1-1 Line Flow Transient – August 10, 1996 western USA/Canada System

where

$\Delta\omega_r$ is the per unit speed deviation of the generator (radians/sec)

$\Delta\delta$ is the rotor angle deviation (radians)

ω_0 is the base rotor electrical speed (radians/second)

T_m, T_e are the mechanical torque and electrical torque, respectively

H is the inertia of the generator

D is the inherent damping coefficient

The electrical torque can be further represented as [59]

$$\Delta T_e = K_S(s)\Delta\delta + K_D(s)\Delta\omega_r \tag{1-3}$$

where K_S and K_D are synchronizing torque and damping torque, respectively. They are sensitive to generator operating conditions, power system network parameters, and

excitation system parameters.

By substituting (1-2) and (1-3) into (1-1), with $\Delta T_m = 0$, we obtain

$$\frac{2H}{\omega_0}\Delta\ddot{\delta} + (D + K_D)\cdot\Delta\dot{\delta} + K_S \cdot \Delta\delta = 0. \tag{1-4}$$

The characteristic equation for (1-4) is given by

$$s^2 + \frac{K_D + D}{2H}s + \frac{K_S\omega_0}{2H} = 0. \tag{1-5}$$

For the system to be stable, both K_D+D and K_S have to be positive. If K_S is negative, the system will have at least one positive real root and the generator will slip out of synchronism without any oscillation. If K_D+D is negative, the system will have at least one root with positive real part. Normally, the effect of AVR in an excitation system with moderate or high response is to introduce a positive synchronizing torque component and a negative damping torque component. Therefore, K_S is positive and K_D+D could be negative. In the case of K_D+D being negative, the system will have complex roots with positive real parts and exhibits oscillations with increasing magnitude. This dissertation explores the controller designs for enhancing the damping of low frequency power oscillations.

For multi-machine systems, the problem is much more complicated. The order of the equations is higher, and interactions between machines have to be considered. However, the physical nature of the oscillations remain the same. Analysis of practical large power systems involves the simultaneous solution of differential equations representing the dynamics of machine rotor circuits, excitation system, prime mover and other devices and the algebraic equations representing power system transmission

network equations (power flow equations) including static loads. The linearized model of these dynamic devices can be represented by

$$\dot{x} = A_D x + B_D \Delta v \tag{1-6}$$

$$\Delta i = C_D x - Y_D \Delta v \tag{1-7}$$

where x is the state vector whose elements are the perturbed values of the device state variables, v is the vector of the network bus voltages and i is the node current injection. The transmission network can be represented by the node equation

$$\Delta i = Y_N \Delta v \tag{1-8}$$

Combining (1.6), (1.7) and (1.8) yields the overall system state equation

$$\dot{x} = Ax = (A_D + B_D (Y_N + Y_D)^{-1} C_D) x \tag{1-9}$$

The stability information of the system can be obtained from the system matrix A.

Power engineers have been working on the stability issue since the 1960's and have conducted numerous theoretical studies and field tests. They developed two different categories of approaches to solve the problem. One category is to follow the understanding of the physical aspects of the power system (nature of power system oscillations) and develop a controller to increase the damping torque. Conventional PSS design is a very good example of this approach [3]. The other is to consider this problem from a control point of view; a power system can be represented as

$$\begin{aligned} \dot{X}_1 &= f(X_1, X_2, u) \\ 0 &= g(X_1, X_2, u) \end{aligned} \tag{1-10}$$

where X_1 denotes system state variables, X_2 denotes network node voltages, and u is an output signal for any specific controller of interest. The controller input can be

represented as

$$Y = h(X_1, X_2, u) \tag{1-11}$$

Different control methods can be applied to the system represented by equations (1.10) & (1.11). And different devices, like PSS and Flexible AC Transmission Systems (FACTS) devices can be used in the power system to enhance the damping of power oscillations. PSSs are widely used to suppress generator electromechanical oscillations and enhance the overall stability of power systems. They are installed in the generator excitation systems and are effective in damping of power system oscillations in a direct way. They normally take generator speed or electrical power as input. Unlike PSS, most FACTS devices are installed on a transmission line far away from any generator. These devices are installed mainly for reasons other than increasing the damping of low frequency oscillations, such as power flow control or voltage enhancement. However, FACTS devices are very expensive and a supplementary controller may be designed for each FACTS device to increase the damping of certain electromechanical oscillatory modes (inter-area modes), while meeting the primary goal of the device. Since electronic devices are not directly involved with electromechanical oscillations, the damping controller design is not as straightforward as those of the PSS.

Literature Review on Control for Power System Damping

Numerous works have been done and published on the damping of power system low frequency oscillations. This section will review some of the published work in this area.

DeMello and Concordia [2] used a single-machine infinite bus system to analyze the nature of the low frequency electro-mechanical oscillations in power systems. They

were the first to explain the phenomena of oscillation by the concepts of synchronous and damping torques, and stated that lack of adequate damping torque is the cause of oscillation or instability. They developed a linearized model of a synchronous generator and its excitation system connected to an infinite bus in the form of a block diagram. Based on this block diagram, the authors came up with expressions of torques and thus revealed the effect of excitation system on stability: normally, the AVR actions increases the synchronizing torque and decreases the damping torque inadvertently. Based on this understanding, the authors used frequency domain methods to develop a speed-based PSS to compensate this negative impact on damping torque caused by the excitation system and demonstrated the effectiveness through analog simulation.

Kundur et al. [3], provided the analytical work and systematic method to determine PSS parameters for large power generation in a practical power system. The basic PSS design idea in this paper is based on the stabilizer proposed in [2]. However, the phase characteristics were obtained using a multi-machine eigenvalue program instead of a single machine model. This work emphasized enhancement of overall system stability, and the authors considered simultaneous damping of inter-area and local modes and discussed the performance of the PSS under different system conditions. In addition to small signal stability performance, the authors also tested the transient stability performance of the PSS and the performance during system islanding. The authors also demonstrated the importance of appropriate choice of washout time constant, stabilizer output limits and other excitation system control parameters. The authors claimed that the frequency response method used to compensate the lag between the excitation input and the electrical torque was fairly robust.

Chow and Sanchez-Gasca [4], proposed four pole-placement techniques for the design of power system stabilizers, with the emphasis on frequency response characteristics of the controller. For controllers to exhibit desirable frequency response characteristics, a simple procedure was proposed to obtain controllers suitable for multiple operating conditions. The issue of robustness of state space designed controllers was investigated.

Hsu and Cheng [5] proposed a power system stabilizer (PSS) based on fuzzy set theory. Speed deviation $\Delta\omega$ and acceleration ($\Delta\dot{\omega}$) were chosen as the input signals to the fuzzy stabilizer. A classical Mamdani type fuzzy system [70] was used to build a mapping relationship from inputs to control output. A seven-by-seven rule table was employed, and all the membership functions were determined based on the authors' experience and no optimization on these membership functions was considered in their paper. The proposed PSS was tested on a two-machine nine-bus system including an infinite bus. The results reported showed better damping as compared with a conventional lead-lag PSS.

Hiyama published a series of papers on applying rule-based fuzzy logic controllers to stabilize power systems [6,7,8,9]. He used speed deviation and acceleration as two inputs and constructed a phase plane. The phase plane was divided into several sectors which represent different control regions and require different control actions. Most parameters used in this controller are represented in a linguistic form. For example, the gain levels high and low were used to implement "strong" and "slight" controls respectively. The gain of the controller is also dependent on how far the state is from the origin of the phase plane, which is the equilibrium point of the generator: it is

proportional to the distance from the origin within a given threshold, and is a constant beyond that. To achieve optimal performance, an optimization routine is used to determine the optimal parameter setting. A time-domain summation of squared errors is used as the performance index, and the parameters are optimized sequentially. Simulations were performed on a single machine infinite bus system and a 3-machine 9-bus system. The results showed damping improvement over conventional stabilizers. In [8] Hiyama presented a modified version of the rule-based stabilizers. Instead of using two gain levels and sign of the control signal to realize the control strategy as reported above, he introduced a fuzzy logic scheme to describe the transition of different controls. The same sequential optimization technique was again used to get a minimal oscillation. However, inferior performances or even instability associated with a condition was reported in [10] when the acceleration and speed deviation were close to zero while the phase was not at its steady-state value. A PID Type fuzzy logic stabilizer was introduced to solve this problem: the information of the integration of the speed deviation was also used as one input and the origin of the phase plane was moved leftward or rightward depending on the sign of the integral. Both simulations and experiments were performed to demonstrate the effectiveness of the modification. Hiyama's heuristic based approach showed some success in his series of research works. However, in his work, the fuzzy PSS parameters were not optimized in a global sense because he claimed the parameters are reasonably insensitive to external conditions. In reality, this approach is only considered robust in the cases considered in his design.

Malik is another person who has done a lot of work in designing fuzzy logic based and neural network based PSS. In [11], Hariri and Malik proposed a fuzzy logic based

PSS; the parameters of their PSS were trained off-line so that it works like the self-optimizing pole shifting APSS proposed in [12]. The training was performed over a wide range of conditions for the generating unit and a wide spectrum of possible disturbances was used for the training. Malik and He presented a recurrent neural network based adaptive PSS in [13]. The basic architecture has two recurrent neural networks. One works as a tracker to learn the dynamic characteristics of the power plant and the other as a controller to damp the oscillations. The weights of the neural network are updated on-line using real time recurrent learning. Both of the proposed PSSs were tested only on a one machine infinite bus system and they both showed better damping results than a conventional PSS for that small system. In [14], Shamsollahi and Malik also proposed a neural adaptive PSS with a similar architecture as the PSS proposed in [13]. However, the training process and training method are different than their former work. In this work, the adaptive neural identifier was first trained offline before being used in the final configuration. Further training of the adaptive neural controller and adaptive neural controller is carried out in every sampling period employing the on-line version of the back propagation method. They applied this neural adaptive PSS both in a SMIB system and a 5 machine system [15]. Also, they investigated the coordination of CPSS and proposed PSS and the self-coordination ability of the proposed PSSs by simulation. It was shown that the proposed PSS not only provides better damping than CPSS, but also coordinates itself with existing PSSs already installed in the system due to its on-line learning ability. The implementation and experimental test of this PSS was performed in the Power System Research Lab at the University of Calgary and the work was reported in [16]. The digital control system

composed of a micro-alternator, a Programmable Logic Controller acting as AVR, a data acquisition system and a PC-based Man-Machine-Interface routine and a DSP board as the controller. The proposed PSS was tested for a variety of operating conditions and disturbances. The experimental results verified the simulation results and conclusion in [15].

Another research effort on this topic is the application of Genetic Algorithm, Fuzzy Logic, Neural network or other intelligent methods to adjust or select an optimal set of parameters for PSS. In [17], a neural network was used to tune the parameters of a conventional PI type PSS. Wen, Cheng and Malik [18] designed an optimal fuzzy logic excitation controller by applying GA in the design process to select all the parameters of the fuzzy controller. Abido [19] designed a hybrid rule based PSS by incorporating GA to search for optimal settings of his proposed PSS parameters. In [20], the simultaneous stabilization of a power system over a wide range of operating conditions via a single-setting conventional power system stabilizer using GA is investigated. The authors wanted to select a single set of power system stabilizer parameters which can make the PSS simultaneously stabilize the power system over a wide range of operating conditions. They treated the power system operating at various loadings as a finite set of plants. The problem was converted to a simple optimization problem which is solved by a genetic algorithm and an eigenvalue based objective function. Two objective functions were presented, allowing the selection of the stabilizer parameters to shift all or some of the system eigenvalues to the left-hand side of a vertical line and a wedge-shape sector in the complex s-plane. The authors proposed in [21] a similar idea to design a PSS. However, another optimization method, tabu search was used to select PSS

parameters. Lu, Nehrir and Pierre [22] proposed a power system stabilizer with a fuzzy logic based parameter tuner. Reduced order linear models for the synchronous generator at a large number of operating points were obtained and the optimal PSS at each operating point were designed by the traditional frequency domain method. In addition, a fuzzy signal synthesizer is introduced to achieve adaptiveness based on the operating condition. They also applied a similar idea for Static Var Compensator (SVC) controller design [23].

Various approaches were also proposed to design damping controllers for different FACTS devices. Larsen, Sanchez-Gasca and Chow [24] tried to represent each electromechanical swing mode in terms of a synchronizing and a damping torque with control loops built around it. They proposed the idea of modal decomposition. In this paper, the impact of the synchronizing and damping components of torque on each electromechanical mode of oscillation in a multi-machine system is determined by decomposing the system variables into their modal components. For each power swing mode, the block diagram representation of modal synchronizing and damping torques similar to [2] is derived and a similar controller design method is used. This method was applied in a Thyristor-controlled Series Capacitor (TCSC) damping controller design in [25]. However, the authors used the multi-modal decomposition on an identified low-order system model rather than on the exact system model.

Noroozian, et al, proposed a very interesting control strategy for SVC and TCSC in [26]. The author incorporated the model of SVC and TCSC in an energy function and then derived the control law by taking the derivative of the energy function and making this derivative be negative. The author also claimed that by using this method, each

device can contribute to the damping of power swings without coordination with other power oscillation damping devices. In [27], Ghandhari, Andersson and Hiskens applied Lyapunov function theory to design a controller for controllable series devices. They derived the control strategy by making the derivative of the energy function be negative. However, the model used in the development of the control laws has a specific form. It is made convenient for obtaining a Lyapunov function, but it doesn't precisely describe actual power system behavior. Ramirez Arredondo represented the power system in the form of a Hamiltonian system and designed a passivity-based nonlinear controller for a TCSC to enhance power system stability in [28]. This control strategy was only tested on a one machine infinite bus system. Rosso, Canizares and Dona proposed a hierarchical control strategy for both dynamic and steady state stability enhancement [29]. Control Strategies to mitigate adverse interactions among the TCSC hierarchical controls are also presented. In this paper, the authors analyzed and compared various locally measurable input signals qualitatively using the equal area criterion. However, due to the limitation of the method, they only concentrated on comparing the use of active power and line current as input signals and did not make an effort to analyze the possibility of using bus voltage and bus frequency as input signals of the damping controller. Similar analysis of applying SVC to enhance the damping using the equal area criterion was proposed by Zhou in [30]. Zhou also proposed a discontinuous SVC control approach in which the change of SVC reactive power output at discrete points is determined by the power deviation on a transmission line.

Optimal control and adaptive control strategies were also employed in the design of damping controllers for FACTS. In [31] & [32], Smith et al presented two enhanced

LQ adaptive SVC controllers which only use local network information to damp oscillations. These control strategies have shown good performance on simulation of a 3-machine 9-bus system. Son and Park [33] applied the Linear Quadratic Gaussian technique to the design of TCSC damping controller. The optimal Hankel norm approximation technique was used for obtaining a low-order power system model, and a controller was designed based on the reduced-order model. The authors also discussed the application of the Loop Transfer Recovery technique to reserve the robustness of the designed damping controller. The 3-machine 9-bus system was again used here to verify the performance of the control strategy. Even though those methods showed good results on a 3-machine 9-bus system, due to the matrix size problem, they were not applied to higher order systems.

Field test results for TCSC in commercial operation were reported in [34], [35]. In [34], Gama presented the project which supported the task of locating and designing a TCSC to damp the North-South low frequency inter-area mode. In [35], the authors presented the result of a joint research project which aims at investigating the feasibility of installing a combination of conventional series capacitors and TCSC at a main transmission line connecting northern area of Taiwan and Central area of Taiwan. The damping controller design was based on a conventional root locus method.

Intelligent control strategies have also been applied to damping controller design for FACTS devices. Hsu and Luor [36] designed a PI controller for TCSC with the gain of the PI controller tuned online by a neural network. The proposed controller was tested on a one machine infinite bus system and it demonstrated by simulation better damping performance over fixed parameter PI controller over a wide range of operating conditions.

Mok, Ni and Wu [37] proposed a fuzzy damping controller for UPFC. The scaling factors of the fuzzy controller were optimized by GA. Simulation results for a two area system showed that the fuzzy damping controller performs better than a conventional transfer function based damping controller. In [38], Dash, Mishra and Panda presented a hybrid fuzzy logic proportional plus conventional integral controller for FACTS devices in a 3-machine power system. The controller used an incremental fuzzy logic controller in place of the proportional term in a conventional PI controller and provides a wide variation of controller gains in a nonlinear manner. Simulation results of the 3 machine system validate the effectiveness of the new control strategy in enhancing the damping of oscillations.

Research on the possible damping effect of UPFC, the most versatile FACTS device, has also been conducted during the recent years. Besides the works in [37, 38], Dong, Zhang, and Crow [39] proposed a PI based approach for the dynamic control of UPFC. With this new control strategy, the active and reactive power flow control was achieved as well as the damping of system oscillations. In [40], the authors tested two damping schemes for the UPFC: one is voltage modulation in voltage control of the shunt element and the other is power modulation in constant power control of the series element. A cascade lead-lag transfer function was used for the supplementary control. In [41], a fuzzy logic based damping controller for UPFC was developed, and the effectiveness of this fuzzy controller was demonstrated in the simulation results of a two area four machine system. The authors expanded their work in [42], where two fuzzy logic schemes were used to design a UPFC damping controller. One is based on Mamdani inference engine and the other uses the Takagi-Sugeno engine to compute the controller

output. Simulation was also performed on a two-area-four-machine system and the results for the system with two different fuzzy logic damping controllers were compared.

However, so far, the proper modeling of UPFC for both steady-state power flow and dynamic behavior analysis is not readily available. Unlike the SVC and TCSC, which are simply considered as variable reactance from a power system viewpoint, the UPFC is like an ideal synchronous machine that can exchange both real power and reactive power with the power system to achieve simultaneous control of load flow and bus voltage. Therefore, the UPFC brought many new issues on steady state power flow calculation, the dynamic modeling of UPFC control, and transient simulation. Studies on these topics have been conducted for better understanding the impact of UPFC on the behavior of power systems. In [44], a comprehensive load flow model is proposed, which can be incorporated into an existing Newton-Raphson load flow model. In [48], a detailed modeling of UPFC based on power electronics switching functions is proposed and simulated with EMTP. But the modeling did not include the most important part of the UPFC which is the converter control. In [49], a decoupled control strategy based on [45] is proposed and the UPFC behavior is simulated within a short-time frame. The study mainly concerns the internal control and dynamics of UPFC. The interface of UPFC with the power system, however, is not considered in this paper. In [50], a detailed power flow and transient stability model is proposed. While the model is validated by comparing the results with the results for EMTP models, it is very complicated and not easy to apply in a transient simulation program. In [44], a power frequency model for UPFC is suggested and four control strategies for UPFC are discussed. A method to include the UPFC into the power system transient simulation is also proposed. But the

iteration schemes for the transient simulation only guarantee linear convergence. In [51], a Newton-type current injection model of UPFC is proposed mainly to improve the iteration convergence for the transient simulation process. The Jacobian matrix used at each time step is of very large dimension, however. Industry planning and operation experience about UPFC were also presented in [43, 46, 47, 52, 53]

Objective of This Dissertation and Organization of Remaining Chapters

As can be seen from the reviews there are many devices (PSS and various FACTS devices) that can help the damping of power system oscillations, and there are also many different control methods for the damping controller design. The objective of this thesis is to design advanced PSS and supplementary controllers for various FACTS devices to enhance the damping of power system oscillations. An intelligent control strategy which combines the fuzzy logic control and the neural network was applied to the PSS design. The proposed PSS improved the damping of power system oscillations, comparing with the conventional PSS. However, the same control strategy was not satisfactory for the FACTS damping controller design. The main reason is that FACTS devices do not involve electromechanical oscillations directly. Instead, they affect the power system oscillation by modifying power system network parameters. Therefore, it is difficult to derive the sufficient and complete fuzzy control rules. Another approach was then proposed to design damping controllers for all FACTS devices, and this systematic approach can be used in a power system of any size. First, the low order transfer function between a power system variable and a damping controller signal was obtained by use of a PRONY method [57] in the form of residue and eigenvalue couples.

By comparing the residues in those transfer functions which are associated with the same eigenvalues that are of interest, proper control input can was selected. Then a damping controller was designed using the root locus method. And a best (or close to best) controller gain was chosen for different loading conditions. The controller gain can be adjusted online based on the operating conditions, and better damping effects can be achieved compared to those obtained using a fixed gain controller.

The following pages are organized into four chapters. Chapter 2 describes the design of neuro-fuzzy adaptive stabilizers, which have a fuzzy logic design base and use neural network to adjust the fuzzy logic parameters. The systematic approach of damping controller design for both SVC and TCSC is presented in Chapter 3. In Chapter 4, much effort is put on power flow and transient stability modeling development for UPFC. The transient stability model includes the UPFC converter control and dynamics. The method for interfacing UPFC with power systems for the dynamic simulation is also proposed, and the fundamental operating constraints of the UPFC are considered in the modeling and simulation. An approach similar to that used in Chapter 3 is applied to design UPFC damping controllers. Chapter 5 is the conclusion.

CHAPTER 2

APPLICATION OF INTELLIGENT CONTROL TO PSS DESIGN

Introduction

As mentioned in Chapter 1, high-gain-continuously-acting automatic voltage regulators help improve the dynamic limits of power systems. They also introduce negative damping, and consequently make the system unstable, especially in large, weakly coupled systems. To overcome this problem, a supplementary stabilizing signal is introduced in the excitation system. Power System Stabilizers (PSSs) provide this supplementary stabilizing signal and are widely used to suppress the generator electromechanical oscillations and enhance the overall stability of power systems. A conventional PSS is based on the use of a transfer function designed for a linear model representing the generator at a certain operating point [1, 59]. Conventional PSSs are widely used and have improved the stability of power systems. However, because a conventional PSS is designed for a particular operating point for which the linearized transfer function model is obtained, it often does not provide satisfactory results over a wide range of operating conditions. Power systems are highly nonlinear, and random disturbances like load changes and time-varying operating conditions make precise modeling of large power systems in real time very difficult. It is this nonlinearity and imprecision in modeling that lead our attention to fuzzy logic control, which is a powerful tool in controlling systems which are not precisely characterized.

The design of an adaptive neural-fuzzy inference system [65] based PSS (ANFIS PSS)

combined the physical perspectives of the power system oscillations, system identification, and the intelligent control theories (more specifically, fuzzy logic and neural network.) It uses the post-disturbance value of the electrical power and speed deviation (obtained on line) as inputs, and the heuristic fuzzy control rules are based on the understanding of physical aspects of the power system oscillations. A 3rd order auto regression moving average (ARMA) model is used for the generating system. The recursive least square (RLS) method with a variable forgetting factor is used to obtain the coefficient vector of the generating system model [60]. The ANFIS PSS uses a zero order Sugeno-type fuzzy logic controller [61] whose membership functions and consequences are also tuned on-line by use of a neural network. The detailed description of the proposed ANFIS PSS is given in the following sections. Simulation results for a one-machine-infinite-bus system and two multi-machine systems are presented later to show the effectiveness of the proposed method.

ANFIS PSS Design

The System Structure

The proposed controller, whose structure is shown in Fig. 2-1, consists of two subsystems, the identifier for the generator and the ANFIS PSS. The parameters of the identifier are updated based on the error between the estimated generator speed deviation ($\Delta\hat{\omega}$) and its actual value ($\Delta\omega$), while the parameters of the ANFIS PSS are tuned by back-propagating the error signal between $\Delta\hat{\omega}$ and its desired value $\Delta\omega_d$.

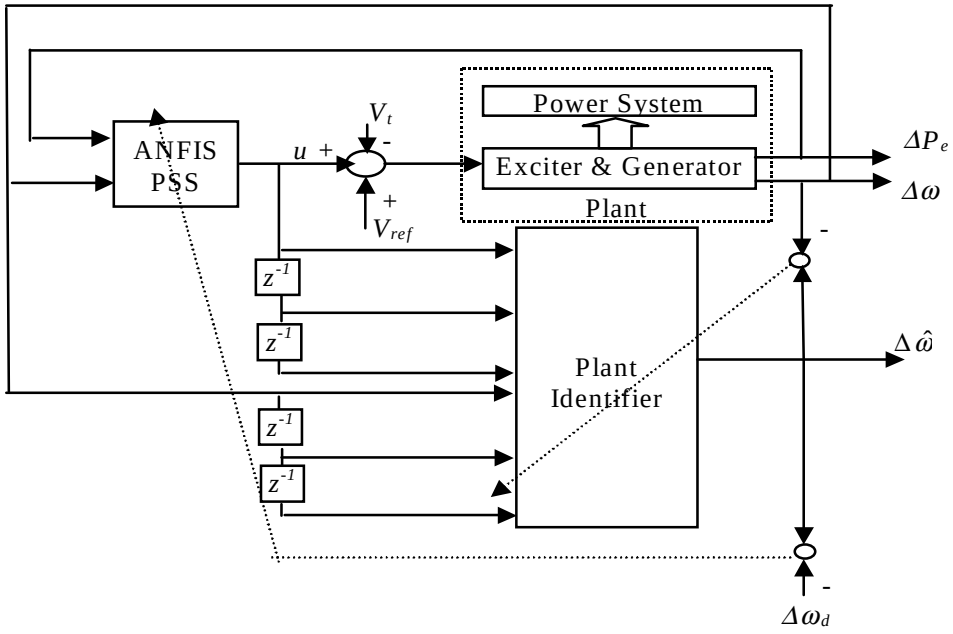

Fig. 2-1 Structure of the study system

The Plant Identifier

The plant identifier is very important for successful tuning of the PSS. Fast parameter tracking ability is needed especially for time-varying systems. The RLS method with a variable forgetting factor is used since it is shown to be very efficient in this case [60]. The forgetting factor is a time varying parameter that enables faster convergence of the RLS algorithm, thus improving its tracking ability. Under large disturbances (large initial estimated error), a small value is chosen for the forgetting factor to increase the identifier sensitivity (and quickly reduce the error in the estimated model parameters.) When these parameters converge to their new values and the prediction improves, the forgetting factor returns to a value close to unity. The identifier is a 3rd order ARMA model of the form:

$$\Delta\omega(t) = \phi^T(t-1)\hat{\theta}(t-1) + e(t) \tag{2-1}$$

where,

$\phi^T(t-1) = [-\Delta\omega(t-1), -\Delta\omega(t-2), -\Delta\omega(t-3), u(t-1), u(t-2), u(t-3)]$

$\hat{\theta} = [\theta_1, \theta_2, \theta_3, \theta_4, \theta_5, \theta_6]^T$ is initially a randomly chosen constant vector and $e(t)$ is the identified error.

The coefficient vector θ can be updated using the following steps [60]:

1) Prediction: $$\hat{x}(t) = \phi^T(t-1)\hat{\theta}(t-1) \quad (2\text{-}2)$$

2) Error: $$e(t) = x(t) - \hat{x}(t) \quad (2\text{-}3)$$

3) Forgetting factor: $$\rho(t) = \min\{\rho_0\rho(t-1) + (1-\rho_0), 1 - e^2(t)/\Sigma_0\}$$

$$0 < \rho_0 < 1 \;\; ; \rho_{\min} < \rho(t) < \rho_{\max} \quad (2\text{-}4)$$

4) Gain: $$K(t) = P(t-1)\phi(t-1)/(\rho(t) + \phi^T(t-1)P(t-1)\phi(t-1)) \quad (2\text{-}5)$$

5) Update: $$\hat{\theta}(t) = \hat{\theta}(t-1) + K(t)e(t) \quad (2\text{-}6)$$

6) Covariance: $$P(t) = [1 - K(t)\phi^T(t-1)]P(t-1)/\rho(t) \quad (2\text{-}7)$$

where, $P(t)$ is the covariance matrix and $\rho(t)$ is the forgetting factor – a time varying parameter that enables faster convergence of the above algorithm, thus improving its tracking ability especially under a large disturbance. Its minimum value is set to get smooth parameter identification, and its maximum value is set to make the identifier more sensitive to system changes under steady-state operation. ρ_0 is the initial value of the forgetting factor, set to be 0.99 in this study. In (2-4), Σ_0 is a constant and can be chosen by the method proposed in [60]. $P(0)$ is equal to some large number times the identity matrix.

Fuzzy logic Based ANFIS PSS

A zero-order Sugeno-type fuzzy controller [61] with 49 rules is used for the ANFIS PSS whose block diagram is given in Fig. 2-2. The inputs to the PSS are speed and electrical power, which are passed through a washout filter to eliminate any existing dc offset. The first scaling block maps the real input to the normalized input space in which the membership functions are defined. The second scaling block is used to map the output of the fuzzy inference system to the real output needed. The fuzzy inference system consists of the fuzzification block, rule table block and Sugeno defuzzification block.

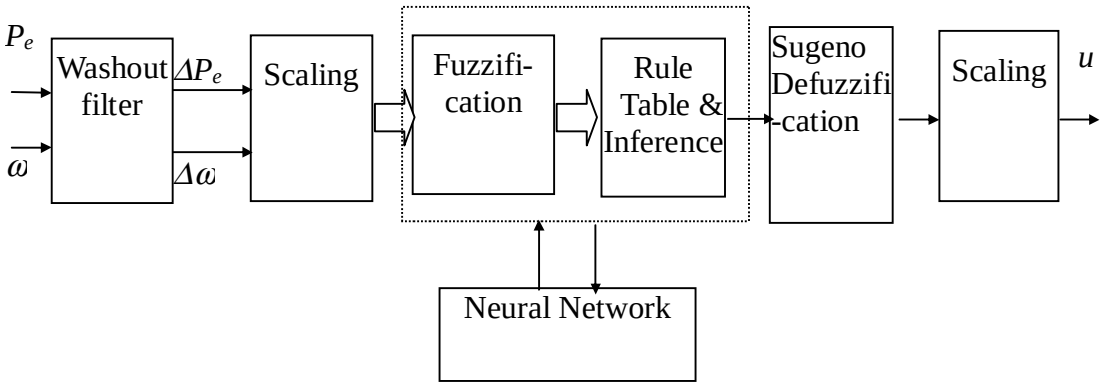

Fig. 2-2 Block diagram of ANFIS PSS model

The fuzzy control rule design is based on the understanding of the role and effect of the controller, which is obtained by experience. The rules are built using the generator accelerating power (P_{acc}=shaft mechanical power (P_m) – generator electrical power (P_e)) and speed deviation ($\Delta\omega$) as control variables, as shown in Table 2-1. In practice it is difficult to measure P_m, and in addition, due to the slow governor response (relative to the exciter response), P_m is assumed constant from one sample to the next. Therefore,

$\Delta P_m = P_m - P_{m_0}$ is assumed to be zero, whereas $\Delta P_e = P_e - P_{e_0}$ can change from sample to sample. P_{m_0} and P_{e_0} are the steady-state value of P_m and P_e, respectively and $P_{m_0} = P_{e_0}$. As a result, $P_{acc} = P_m - P_e \approx -\Delta P_e$ is used in the development of the rule table.

The control rules are of the form: IF $\Delta\omega$ is A_i AND P_{acc} is B_i, THEN $u = k_i$. A_i, B_i are the fuzzy sets representing some linguistic terms, and k_i is a crisp value. The membership function for each linguistic term is of the form:

$$\mu_{A_i^j} = \exp(-(x_j - c_i^j)^2 / 2\sigma_i^{j\,2}) \tag{2-8}$$

where x_j is the jth input, A_i^j represents the ith linguistic term related to the jth input and c_i^j, σ_i^j are the centers and spreads of the membership function related to A_i^j, which are adjustable by the neural network block of the ANFIS. The linguistic terms used for the membership function are LP (large positive), MP (medium positive), SP (small positive), ZE (zero), SN (small negative), MN (medium negative), and LN (large negative). The centers of the membership functions are initially distributed evenly along the normalized input space.

The firing strength of each rule is calculated using the minimum function, which represents the AND operation.

The rule table is shown in Table 2-1. As seen in this table, an example rule is: IF $\Delta\omega$ is ZE and P_{acc} is MP, THEN u = 0.66, where u is the initial value of the output of each rule (fuzzy consequence) used by the neural network. Since the fuzzy rules are established by some experience (i.e., by an experienced control designer), the initial parameter values of the ANFIS will be reasonable. The speed of adaptation of the

ANFIS PSS is therefore dependent on the values obtained from Table 1, which are functions of the PSS control variables (P_{acc} and $\Delta\omega$) obtained on line.

Table 2-1 Rule matrix

		P_{acc} ($\approx$ -ΔP_e)						
		LP	MP	SP	ZE	SN	MN	LN
$\Delta\omega$	LP	1.0	1.0	1.0	1.0	0.66	0.33	0.0
	MP	1.0	1.0	0.66	0.66	0.33	0.0	-0.33
	SP	1.0	0.66	0.33	0.33	0.0	-0.33	-0.66
	ZE	0.66	0.66	0.33	0.0	-0.33	-0.66	-0.66
	SN	0.66	0.33	0.0	-0.33	-0.33	-0.66	-1.0
	MN	0.33	0.0	-0.33	-0.66	-0.66	-1.0	-1.0
	LN	0.0	-0.33	-0.66	-1.0	-1.0	-1.0	-1.0

The Sugeno defuzzification algorithm [61] is used to obtain a crisp (normalized) PSS output signal. After the firing strength of each rule is obtained, the output of the fuzzy inference system can be obtained by the operation of the weighted average of the form:

$$r = \frac{\sum_{i=1}^{N} r_i \cdot w_i}{\sum_{j=1}^{N} w_j} = \sum_{i=1}^{N} r_i \cdot \overline{w}_i \tag{2-9}$$

where

$$\overline{w_i} = \frac{w_i}{\sum_{j=1}^{N} w_j} \tag{2-10}$$

where, r_i is the output of the ith rule, N is the number of rules, and $\overline{w}_i$ is the normalized firing strength of the ith rule.

Neural Network Representation of Fuzzy Logic Based PSS

The fuzzy logic-based controller can be made adaptive by being represented in a feed forward neural network form, as shown in Fig. 2-3. In this figure, K_1, K_2 and K_3 are the

input and output scaling factors, respectively. This network consists of four layers, with each layer representing a specific part in the ANFIS controller. The node functions in the first layer represent the Gaussian membership function given by equation (2-8). In the second layer, the firing strength of each rule is calculated. The third layer calculates the normalized firing strength of each rule given by equation (2-10), and the fourth layer combines the output of all rules to get the overall output of the controller using the Sugeno defuzzification technique given by equation (2-9).

There are two sets of parameters needed to be adjusted for the ANFIS PSS; one set contains the scaling factors for the input and output of the PSS that are outside the fuzzy inference system, and the other set is the membership function parameters and consequence parameters. Experience shows that the scaling factors are important in the performance of the fuzzy logic controller [62]. In our proposed controller, the output scaling factor K_3 is determined by the output limits of the PSS. The scaling factors K_1, K_2 are chosen such that the variables x_1, x_2 (Fig. 2-3) are the normalized values of $\Delta\omega$ and ΔP_e, respectively (i.e. $-1 \le x_1, x_2 \le 1$). Therefore, we set K_1, K_2 to be (approximately) the reciprocal of the maximum values of $\Delta\omega$ and ΔP_e respectively, as observed by simulation.

The objective for updating the parameters inside the fuzzy inference system is to minimize the cost function:

$$J = \frac{1}{2} \cdot \Delta\hat{\omega}(t+1)^2 + \frac{\lambda}{2} u(t)^2 \tag{2-11}$$

where $\Delta\hat{\omega}(t+1)$ is the estimated speed deviation at time step t+1, λ is the penalty factor to improve the plant output dynamic characteristics such as overshoot and settling time of

the response curve. The gradient descent method is used to update all the adjustable parameters of fuzzy inference system. Assume α is a parameter in this fuzzy inference system; the learning procedure that implements the gradient descent method is given below [63]:

$$\alpha(t+1) = \alpha(t) - \eta_\alpha \frac{\partial J}{\partial \alpha} \tag{2-12}$$

where η is the learning rate of the parameter α (η_α equals a constant, in this study chosen to be 0.02) and $\frac{\partial J}{\partial \alpha}$ is the gradient which can be calculated by:

$$\frac{\partial J}{\partial \alpha} = \frac{\partial J}{\partial u(t)} \frac{\partial u(t)}{\partial \alpha} = [\Delta\hat{\omega}(t+1) \cdot \frac{\partial \Delta\hat{\omega}(t+1)}{\partial u(t)} + \lambda \cdot u(t)] \cdot \frac{\partial u(t)}{\partial \alpha} \tag{2-13}$$

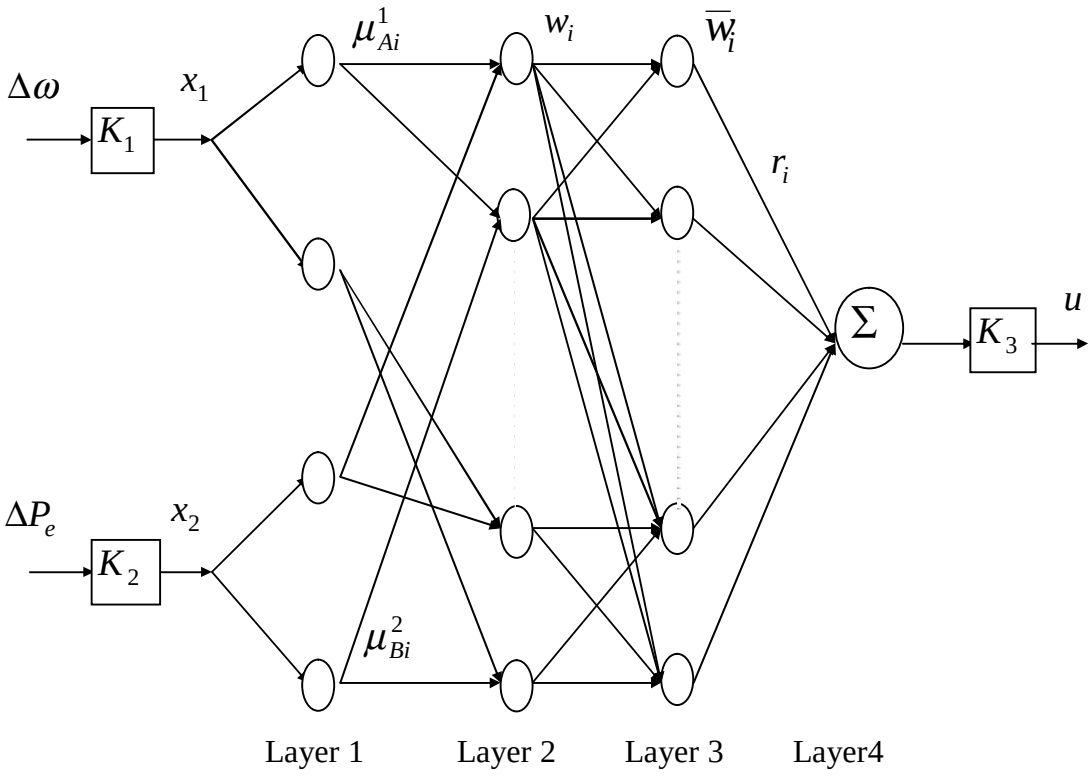

Fig. 2-3 Neural Network Model of the ANFIS

$$\frac{\partial u(t)}{\partial \alpha} = \sum_{O^* \in S} \frac{\partial u(t)}{\partial O^*} \frac{\partial O^*}{\partial \alpha} \tag{2-14}$$

where, $\frac{\partial \Delta \hat{\omega}(t+1)}{\partial u(t)}$ can be obtained by the coefficient vector of the plant model, S is the set of nodes whose outputs depend on α, and O^* is the output of nodes belonging to S.

If the node is the output node of ANFIS, we have

$$\frac{\partial u(t)}{\partial O} = K_3 \tag{2-15}$$

and for an internal node, we have

$$\frac{\partial u(t)}{\partial O_i^k} = K_3 \cdot \sum_{n=1}^{N} \frac{\partial u(t)}{\partial O_n^{k+1}} \cdot \frac{\partial O_n^{k+1}}{\partial O_i^k} \tag{2-16}$$

In equation (2-16), O_i^k is the output of the ith node of the kth layer and N is the number of nodes in the $(k+1)th$ layer. Following the above procedure, the cost function J is minimized in each sampling period. As seen from the above description, there is no need for a desired controller design, and the adjustment of the controller depends only on the performance of the plant.

When back-propagating the error signal through the "min" function, the following method is used: assume $y = \min(x_1, x_2)$, then rewrite y in a differentiable function form [64]:

$$y = \sum_{i=1,2} x_i \cdot \prod_{l \neq i} U(x_l - x_i) \tag{2-17}$$

where, $U(x)$ is the unit step function which equals to 1 for positive x and zero otherwise. Therefore,

$$\partial y / \partial x_i = \prod_{l \neq i} U(x_l - x_i) = \begin{cases} 1; & \text{If } x_i \text{ is minimum} \\ 0; & \text{otherwise} \end{cases} \quad (2\text{-}18)$$

By using the above method to get the partial derivatives of the "min" function, only the parameters of the membership functions that contribute to the control action or decision output are updated and the cost of calculating the gradient is greatly reduced.

On-line Training of ANFIS PSS

The on-line training of the ANFIS PSS consists of the following steps:

1) Sample $\Delta\omega(t)$ and $\Delta P_e(t)$ at time step t.

2) Update the parameter vector $\hat{\theta}(t+1)$ of the identifier.

3) Calculate the estimated speed deviation $\Delta\hat{\omega}(t+1)$, using the ANFIS PSS output $u(t)$ and $\hat{\theta}(t+1)$ obtained in step 2.

4) Update the membership function parameters and consequence parameters of the ANFIS PSS using the estimated speed deviation $\Delta\hat{\omega}(t+1)$ and equations (2-12) through (2-16).

Using this training method, the parameters of the ANFIS PSS are updated based on the performance of the generator (i.e. $\Delta\omega$). The plant identifier is used to get the coefficient vector for the generating system model so that the error signal can be back propagated through the identifier; hence, there is no need for a desired controller.

Simulation Results – ANFIS PSS

To test the performance of the proposed stabilizer, simulation studies were performed on three systems: a one-machine-infinite-bus system; a two-area, 4-machine, 13-bus

system; and a 16-machine, 68-bus system. Six states are used to model each generator: $\Delta\delta$, $\Delta\omega$, $\Delta E'_q$, $\Delta E'_d$, $\Delta\psi_{kd}$, $\Delta\psi_{kq}$ [59]. The sampling period used in all cases was 0.01*sec*. Power System Toolbox [58] has been used for this simulation study.

One-Machine-Infinite-Bus System

A generator is connected to an infinite bus through a transformer and two parallel lines. The generator is equipped with a speed governor and an IEEE type ST3 excitation system. The parameters for this system are given in Appendix A. A three-phase fault was applied at the end of one line under different operating conditions and cleared after 0.05 *sec*. Simulation results are given for two operating conditions (light loading and heavy loading) to evaluate the performance of the ANFIS PSS. A CPSS (with the speed signal used as its input) was also designed at heavy loading (P = 1.0 *pu*) for comparison, using the frequency domain method [1, 59]. The transfer function for the PSS is:

$$H_c(s) = 300 \cdot \frac{s}{10s+1} \cdot \frac{(0.1s+1)^2}{(0.01s+1)^2} \tag{2-19}$$

With the proposed PSS applied, Figs. 2-4 and 2-5 show the generator speed deviation as a function of time, for a light loading condition (P=0.2 *pu*) and a heavy loading condition (P=1.0 *pu*), respectively. For comparison purposes, the generator responses are also shown with no PSS and with a conventional PSS.

A Two-Area, 4-Machine, 13-Bus System

Fig. 2-6 shows a 4-machine, 13-bus system, where the generators are located in two distant areas and there is no infinite bus in the system. The parameters for this system

are given in Appendix A. A three-phase fault was applied at one end of one transmission line and was cleared after 0.05 *sec*. (see Fig. 2-6). When there is no PSS installed, the system goes unstable under heavy loading condition, and there exist multi-mode oscillations, as shown in Fig. 2-7. This figure shows the speed difference between different generators and G1 (chosen as the reference generator) under heavy loading (P_{G2} = 7.0 *pu*, P_{G3} = 7.16 *pu*) with PSSs installed on G2 and G3. Generator responses are also shown, when CPSSs are used, for comparison. All generators in Fig. 2-6 are equipped with governors. G1 and G4 are equipped with IEEE type DC excitation system; G2 uses a simplified excitation system model consisting of a gain and a time constant; and G3 is equipped with an IEEE type ST3 excitation system. First, only one PSS was installed on G2, and the oscillations were damped satisfactorily with the proposed PSS performing better than the CPSS under different loading conditions. Then, two PSSs were installed (one on G2 and one on G3) to investigate their coordination and damping of inter-area oscillations. It was noted that the damping of oscillations was improved when two PSSs were used.

CPSSs (with the speed signal used as their inputs) were also designed at heavy loading condition, given above, for comparison (see Fig. 2-7). The transfer functions for these two PSSs are:

$$H_{c2}(s) = 600 \cdot \frac{s}{20s+1} \cdot \frac{(0.23s+1)^2}{(0.02s+1)^2} \tag{2-20}$$

$$H_{c3}(s) = 600 \cdot \frac{s}{20s+1} \cdot \frac{(0.08s+1)^2}{(0.04s+1)^2} \tag{2-21}$$

The effectiveness of the proposed PSS is clear from the results shown

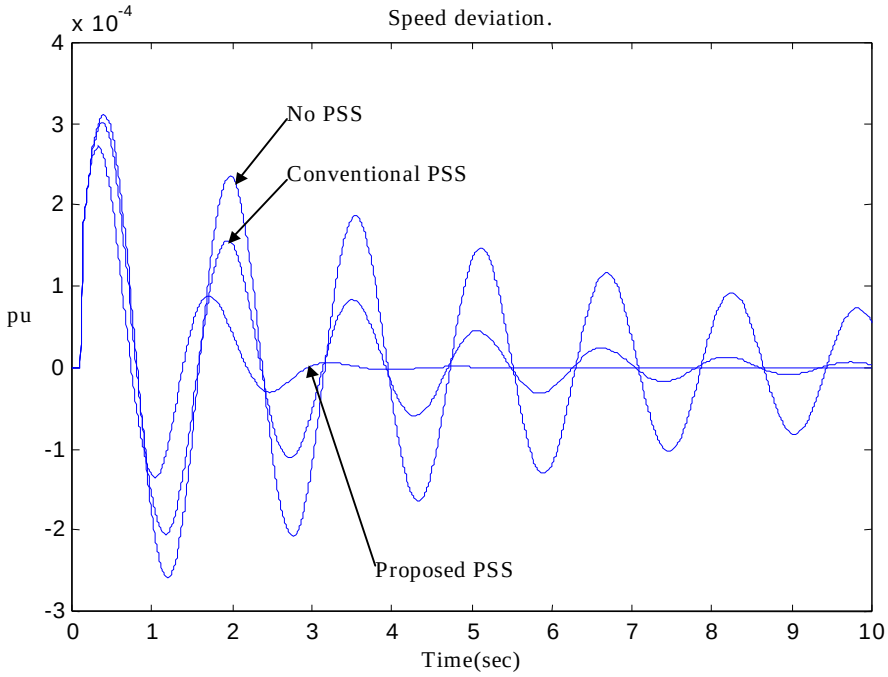

Fig. 2-4 Speed deviation under light loading condition (P = 0.2 pu)

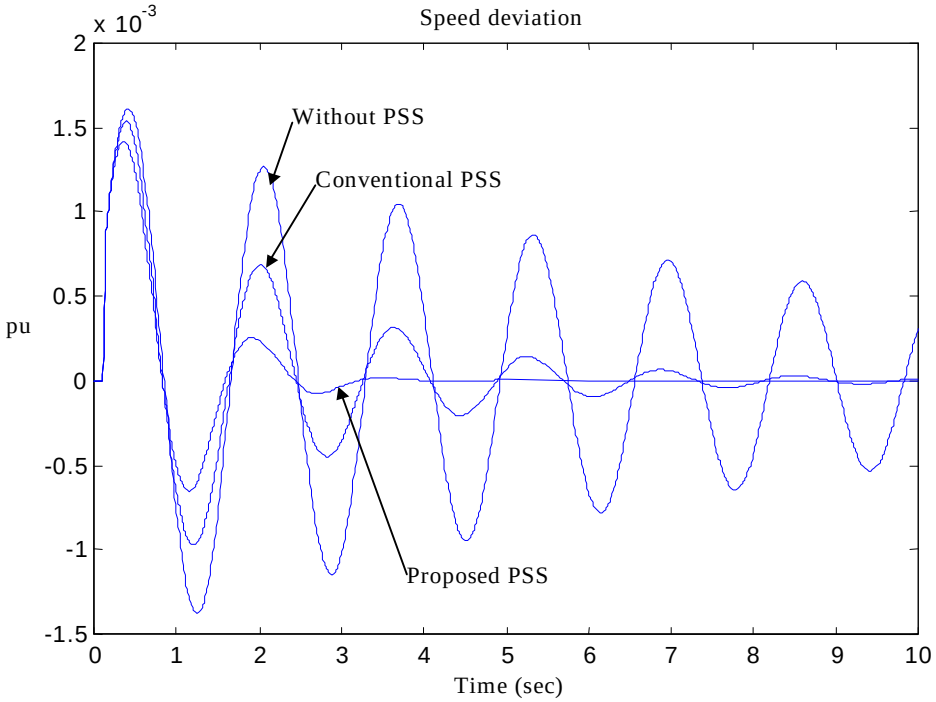

Fig. 2-5 Speed deviation under heavy loading condition (P = 1.0 pu)

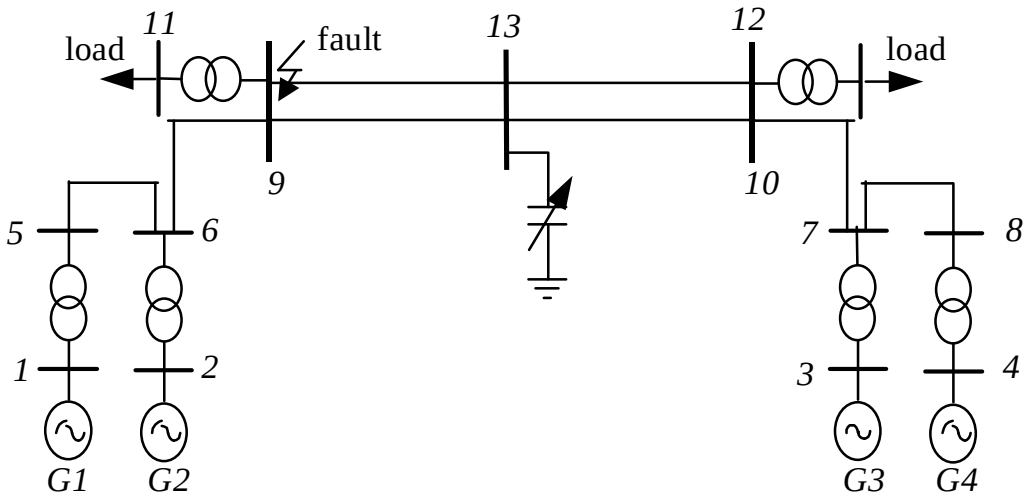

Fig. 2-6 A Two-area system

.

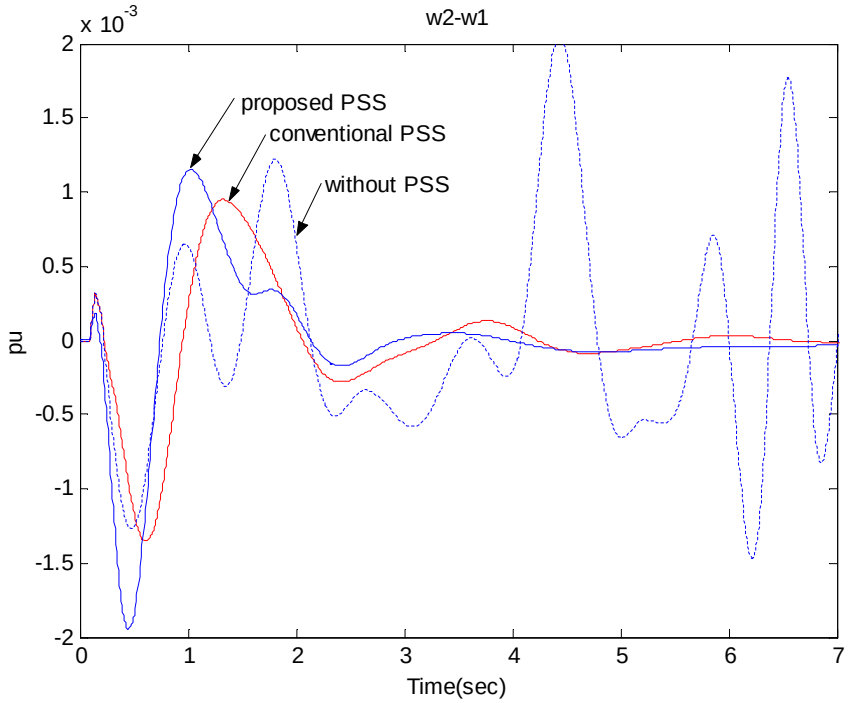

Fig. 2-7 (a)

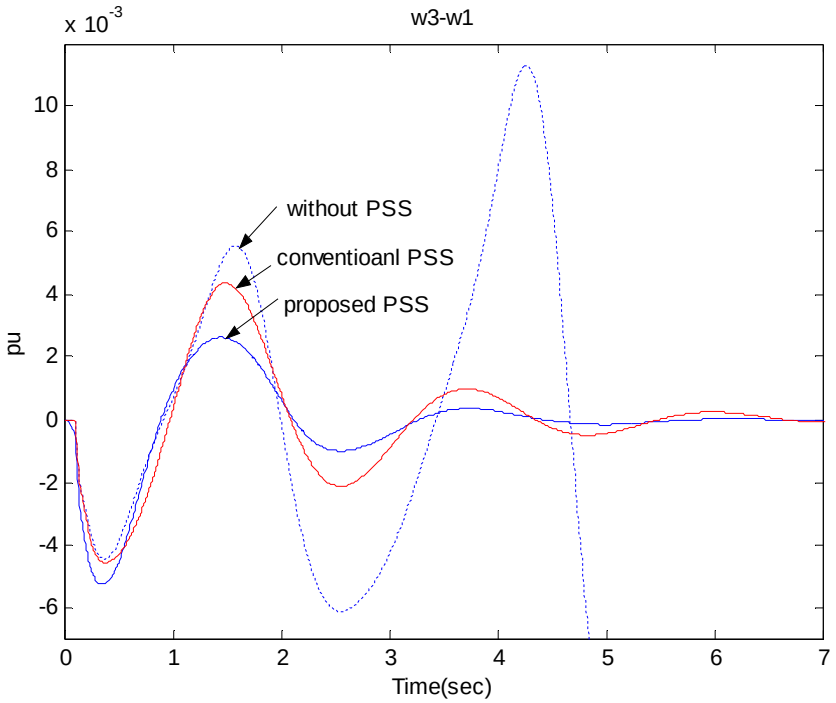

Fig. 2-7 (b)

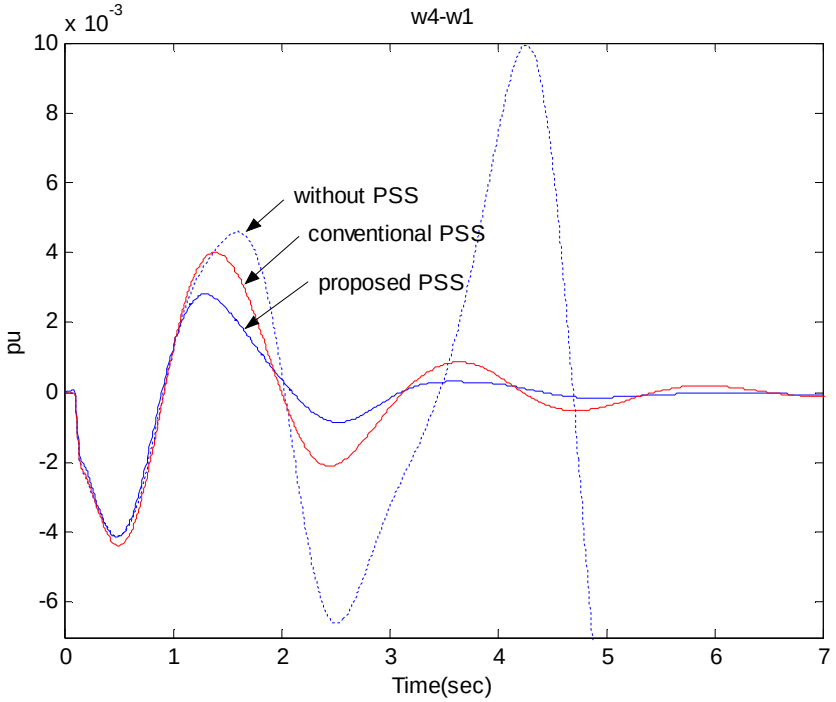

Fig. 2-7 ©

Fig. 2-7 Speed difference between different generators and generator #1

A 16-machine, 68-bus System

This system, shown in Fig. 2-8, is a reduced order model of the New England/New York interconnected system [1]. The parameters of the system can be found in Appendix A. IEEE type DC excitation systems are installed on G1 through G8. G9, on which the ANFIS PSS is installed, is equipped with IEEE type ST3 excitation system. No exciter is used on other generators. Also, none of the generators are equipped with a governor. A three-phase fault was applied on different lines and cleared after 0.05 *sec*. to examine the effectiveness of the proposed PSS. In particular, the fault was applied on two critical lines terminating at bus 1 (line 1-2 and line 1-27, shown bolded in Fig. 2-8.) A conventional stabilizer (speed input PSS) was also designed for G9 at a heavy operating point, $P_{G9} = 8.0$ *pu*. The transfer function for this PSS is

$$H_c(s) = 400 \cdot \frac{s}{10s+1} \cdot \frac{(0.2s+1)^2}{(0.028s+1)^2} \tag{2-22}$$

Figs. 2-9 and 2-10 show the speed deviation of G9 as a function of time, for the three-phase fault applied on the above two critical lines under heavy loading condition given above. The generator responses are also shown when a conventional PSS is applied and when no PSS is applied for comparison. In both cases, the system became unstable when no PSS was used. From these figures, the effectiveness of the proposed neuro-fuzzy stabilizer in damping system oscillations is again clear.

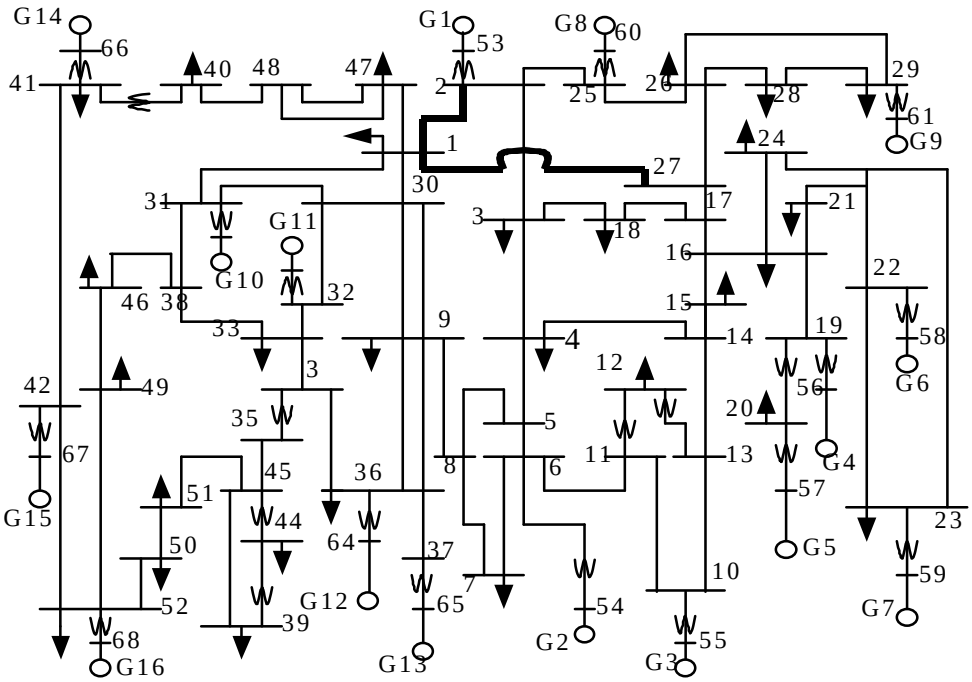

Fig. 2-8 16-machine system

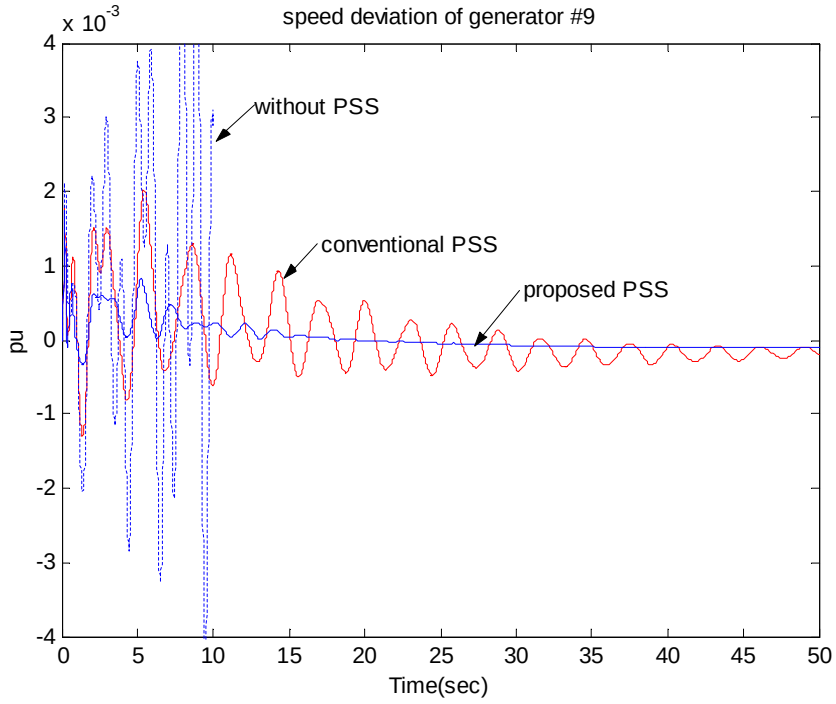

Fig. 2-9 Generator Response for fault applied on line 1-2

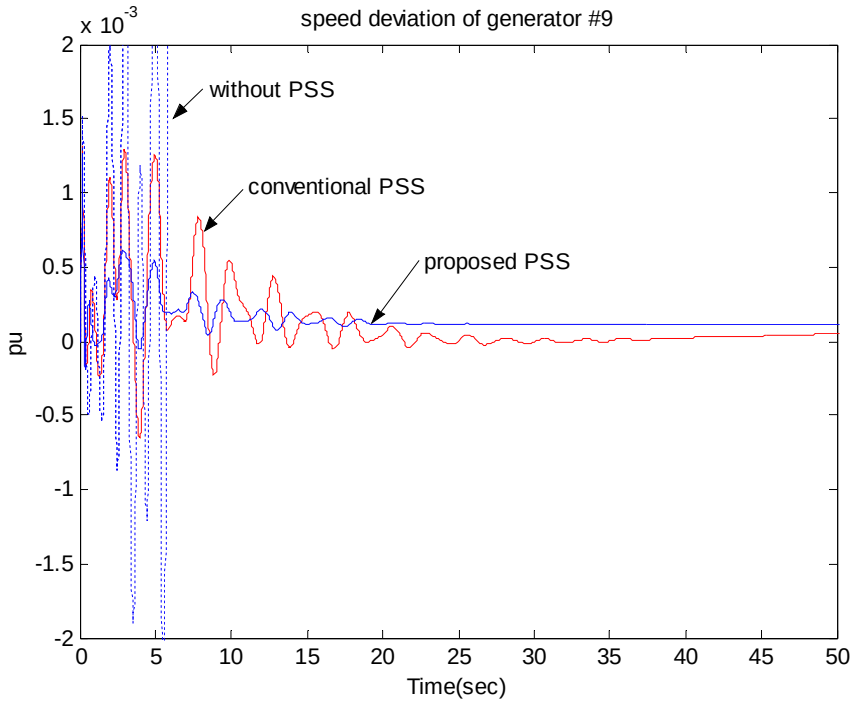

Fig. 2-10 Generator Response for fault applied on line 1-27

ANFIS PSS With Self-Organizing Map

It is observed from the structure of the fuzzy logic based PSS and Fig. 2-3 that the output of the fuzzy inference system is linear with respect to the consequence; and nonlinear with respect to the membership function parameters. Therefore, it is natural to divide the parameters of the fuzzy inference system into two categories, the nonlinear parameters and the linear parameters. The learning algorithm is also divided into two sub-algorithms, the Self Organizing Map (SOM) [63] algorithm for updating the membership function centers and spreads, and the back propagation method for updating the consequence parameters. As seen in the previous section, the centers of the membership functions are initialized evenly distributed in the normalized range –1 to 1, and the initial values of the consequences are set according to Table 2-1. For on-line

training of the ANFIS, the centers of the membership functions should suitably sample the input domain. The SOM algorithm, which is based on organizing the inputs such that mapping of similar inputs result in similar outputs, is used for updating the membership function centers. The computational steps for the SOM algorithm are given below:

1) Compute distances between the input and centers,

$$D_j = \left\| x(k) - C_j(k-1) \right\| , 1 \le \mathrm{j} \le \mathrm{N} \tag{2-22}$$

where *k* is the time step and *N* is the number of centers.

2) Find the winner, i.e. find the index J so that D_J is minimum

$$D_J = \min(D_j(k)), 1 \le \mathrm{j} \le \mathrm{N} \tag{2-23}$$

3) Update centers. For all the centers C_j within a specific neighborhood of C_J, update the centers as:

$$C_j(k) = C_j(k-1) + \eta(k) h_{J,j}(k)(x(k) - C_j(k-1)) \tag{2-34}$$

where, η is the learning rate and $h_{J,j}$ is the neighborhood function. For all the centers C_j outside a specific neighborhood of C_J, update the centers as:

$$C_j(k) = C_j(k-1) \tag{2-35}$$

4) Re-compute the distance and calculate the ANFIS output

$$D_j(k) = \left\| x(k) - C_j(k) \right\| , 1 \le \mathrm{j} \le \mathrm{N} \tag{2-36}$$

The learning rate is a time varying parameter, which starts at an initial value (η_0) close to 0.1 and decreases gradually with increasing time as follows:

$$\eta(k) = \eta_0 \exp(-k/\tau_1) \tag{2-37}$$

where τ_1 is a used for adjusting the learning rate (in this study $\tau_1 = 1000$.)

The typical choice of neighborhood function $h_{J,j}$ is the Gaussian Function.

$$h_{J,j}(k) = \exp(-\frac{(C_J(k-1) - C_j(k-1)^2}{\mu(k)^2}) \tag{2-38}$$

$$\mu(k) = \mu_0 \exp(-k/\tau_2) \tag{2-39}$$

μ_0 is set so that the neighborhood function is initially equal to the membership function, i.e.,

$$\mu_0 = \sqrt{2} \cdot \sigma_0 \tag{2-40}$$

The consequences are updated by the error back propagation method mentioned in the previous section.

The on-line training of this proposed PSS is slightly different from that of the PSS mentioned in previous section. It consists of the following steps:

1) Sample inputs $\Delta\varpi(k), \Delta P_e(k)$ at time step *k*.

2) Update the parameter vector of the identifier.

3) Use the SOM algorithm to update the center and spread of the membership functions.

4) Calculate the ANFIS PSS output and the estimated speed deviation at time step *k+1*.

5) Keep the membership function parameters unchanged and update the consequence parameters by the BP method.

Simulation Results – ANFIS PSS with SOM

To test the performance of the proposed stabilizer, simulation studies were performed on two systems: a one-machine-infinite-bus system and a two-area, 4-machine system.

One-Machine-Infinite-Bus System

Figs. 2-11 and 2-12 show the generator speed deviation as a function of time, for a light loading condition (P=0.2pu) and a heavy loading condition (P=1.0pu), respectively. For comparison purposes, the generator speed deviation responses are also shown in these two figures with no PSS and with a conventional PSS.

A Two-Area, 4-Machine-13-Bus System

The same power system shown in Fig. 2-6 is used here for the simulation. A three-phase fault is applied at one end of the transmission line (shown in Fig. 2-6) and is cleared after 0.05*s*. A stabilizer was designed for generator #2 using the proposed method and the conventional method. Simulation results were obtained for light loading (P_{e2} = 3.12 p.u.) and heavy loading (P_{e2} = 7.0 p.u.) conditions. Figs. 2-13 and 2-14 show the speed deviation response of generator #2 under light loading condition and heavy loading condition, respectively. The speed difference between G3 and G1 at heavy loading condition is also shown in Fig. 2-15 to show the improvement of the inter-area mode. The effectiveness of the proposed PSS in damping the oscillatory modes and its superiority over the conventional PSS is clear. To study the coordination of two PSSs installed in two areas separately to damp the inter-area mode, another stabilizer is installed on generator #3 (in the second area). Figs. 2-16.(a), (b) and (c) show the speed difference between machines 2, 3, 4 and machine 1, respectively, with the proposed PSSs and conventional PSSs installed on machines #2 and #3. In all three cases the superiority of the proposed PSS over the conventional PSS is clear. In particular, the effectiveness of the proposed stabilizer in damping of inter-area modes for machines #3

and #4 can be noted in Figs 2-16.(b) and 2-16.(c).

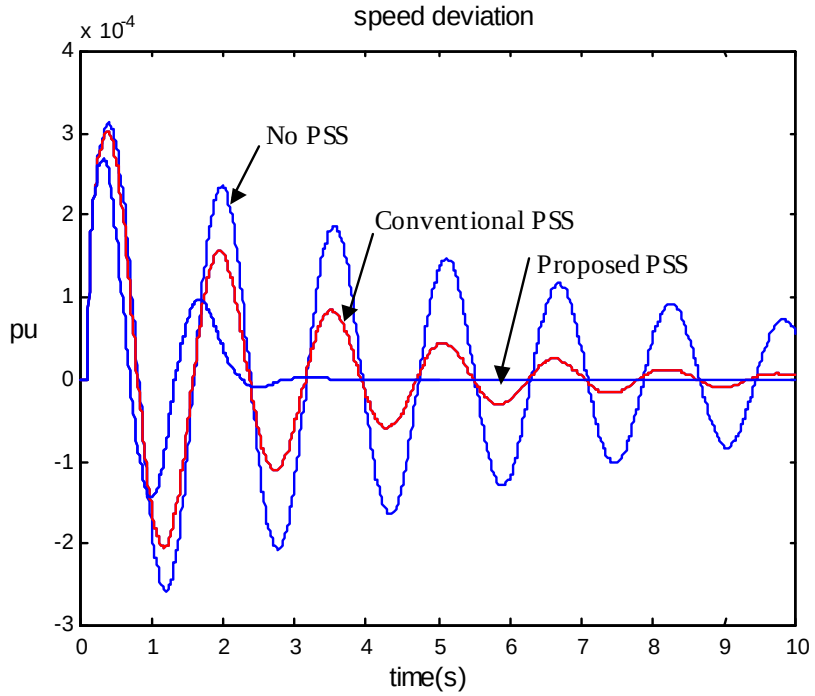

Fig. 2-11 Speed deviation under light loading condition (p=0.2 p.u.)

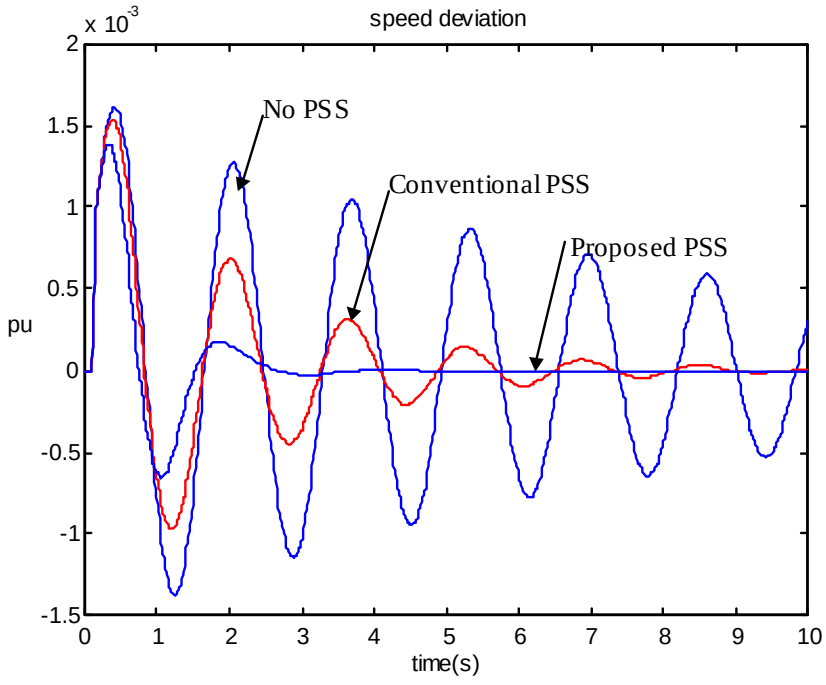

Fig. 2-12 Speed deviation under heavy loading condition (p=1.0 p.u.)

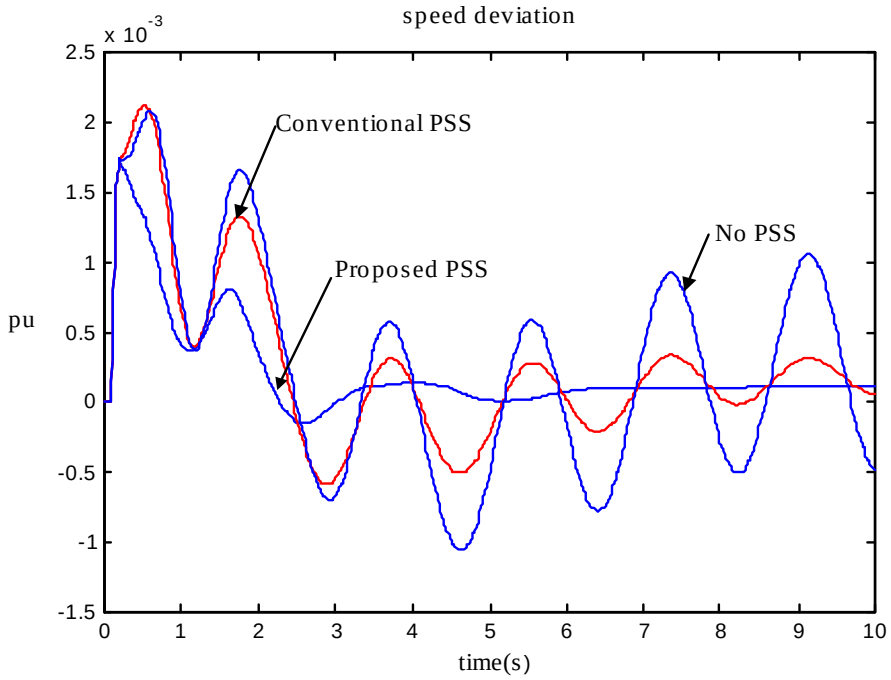

Fig. 2-13 System response under light loading condition (P=3.12pu)

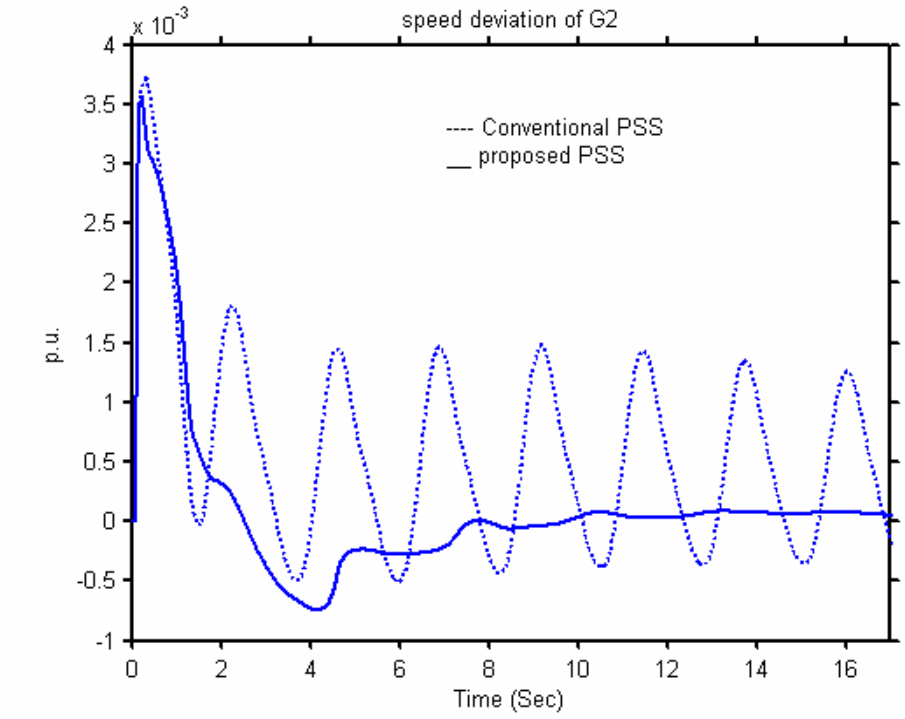

Fig. 2-14 System Response under heavy loading condition (P_{e2}=7.0pu, P_{tran} = 4.0pu)

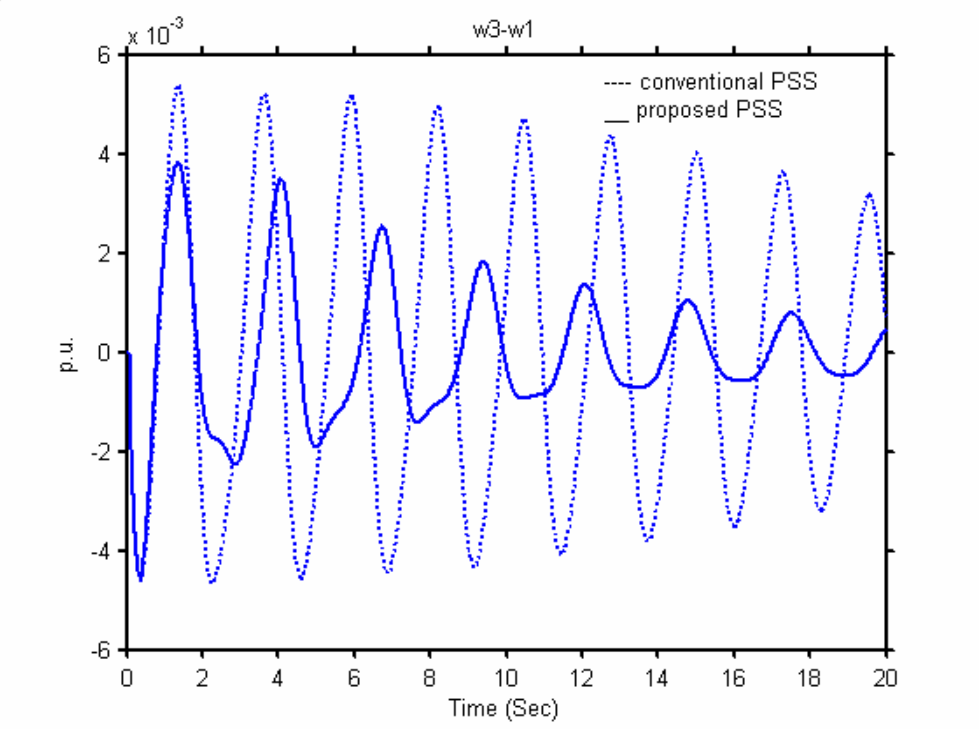

Fig. 2-15 Speed difference of G3 and G1 for heavy loading condition.

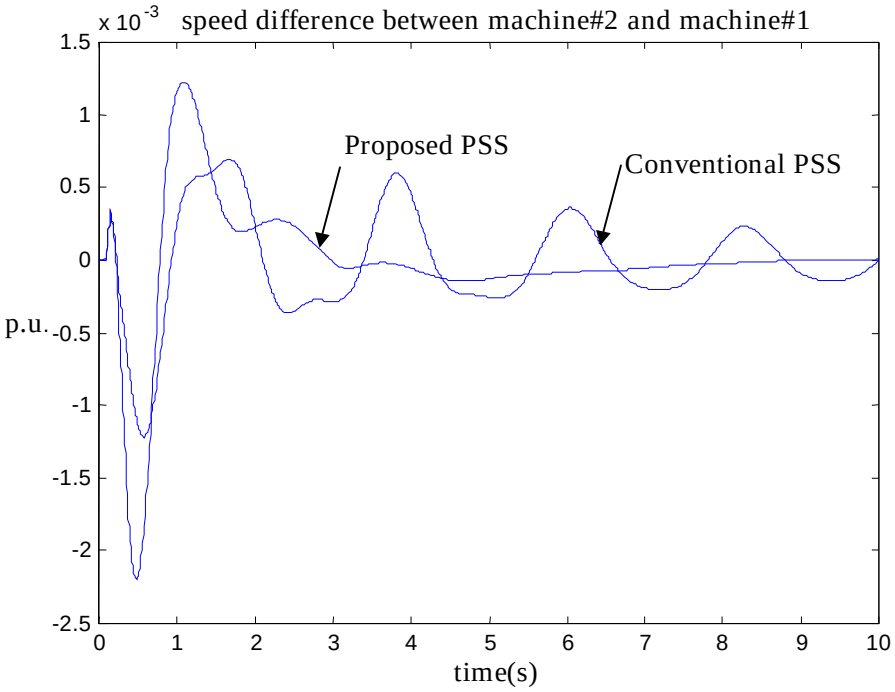

Fig. 2-16 a

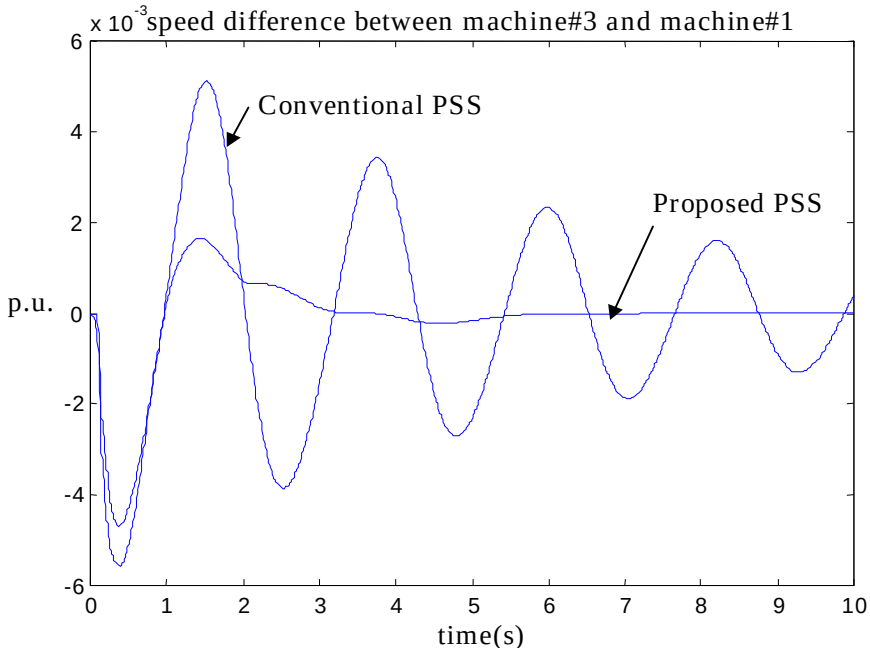

Fig. 2-16 b

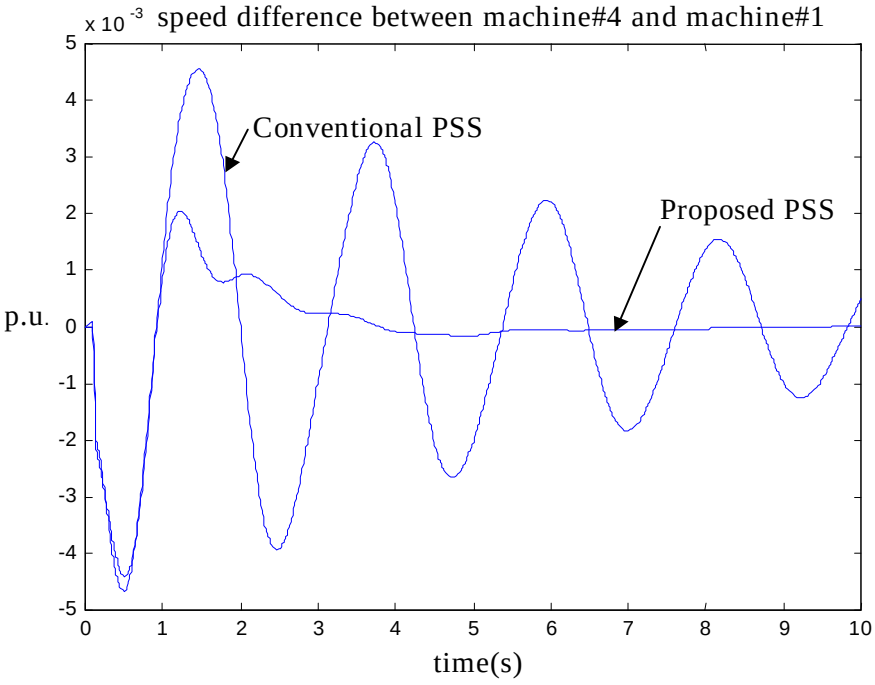

Fig. 2-16 c

Fig. 2-16 System Response under heavy loading condition

A 16-machine, 68-bus System

The same system shown in Fig. 2-8 is used for the demonstration. A three-phase fault was applied on different lines and cleared after 0.05 *sec*. to examine the effectiveness of the proposed PSS. A conventional stabilizer (speed input PSS) was also designed for G9 at a heavy operating point, P_{G9} = 8.0 *pu*. First, a three-phase fault is applied on line 29-28 (shown bold) and cleared after 0.05 sec. Fig. 2-17 shows the speed deviation of G9 as a function of time for the above fault under this heavy operating condition. Next, a three-phase fault was applied on one of the critical lines of the system connecting two of the system areas (line 1-2, shown bolded in Fig. 2-8.) Fig. 2-18 shows the speed response of G9 for this fault. The generator response is also shown when a conventional PSS is applied for comparison. The system became unstable when no PSS was used. From figures 2-17 and 2-18, the effectiveness of the proposed neuro-fuzzy stabilizer in damping system oscillations is again clear.

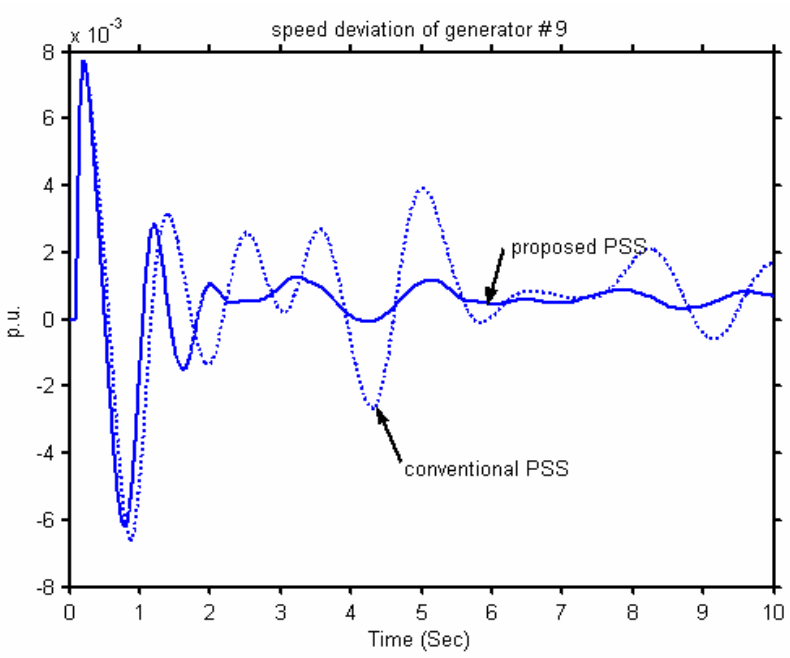

Fig. 2-17 Speed deviation of generator # 9 for fault applied on line 29-28

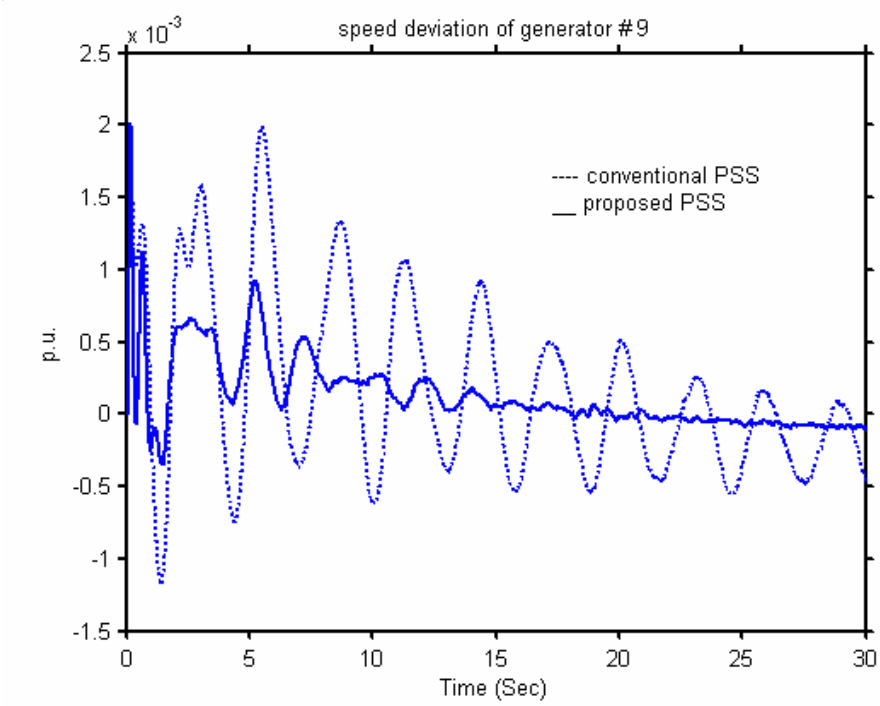

Fig. 2-18 Speed deviation of generator # 9 for fault applied on line 1-2

CHAPTER 3

CONTROLLER DESIGN FOR SVC AND TCSC TO ENHANCE DAMPING OF POWER SYSTEM OSCILLATIONS

Introduction

Even though PSSs are widely used to suppress the generator electromechanical oscillations and enhance the overall stability of power systems, it is noticed that sometimes it is difficult to effectively damp inter-area oscillatory modes using PSSs alone, especially when they are acting through slow acting dc exciters [1]. Continuous advances in power electronic technologies have made the application of FACTS devices very popular in power systems. Most FACTS devices are installed on transmission lines far away from any generator and their purposes are mainly for reasons other than increasing the damping of low frequency oscillations. However, FACTS devices are very expensive and a supplementary controller may be designed for each device to increase the damping of certain electromechanical oscillatory modes (inter-area modes), while meeting the primary goal of the device. Since electronic devices are not directly involved with electromechanical oscillations and the generator signals are not available locally, the damping controller design is not as straightforward as those of the PSS. In this chapter, the damping controller design for both SVC and TCSC is described. SVC and TCSC are FACTS devices that electronically switch capacitors or reactors so that their impedance or succeptance can be controlled. Fig. 3-1 shows the simplified schemes for the SVC and TCSC. The SVC and TCSC consist of a series compensating

capacitor shunted by a Thyristor-Controlled Reactor (TCR), which cancels the effective compensating capacitance of the capacitor. Both SVC and TCSC can be essentially considered as continuously variable impedance with a fixed capacitance and a variable reactance connected in parallel. The SVC is connected in shunt with the transmission line for reactive power support and the TCSC is connected in series with the transmission line to transfer more power on the transmission line.

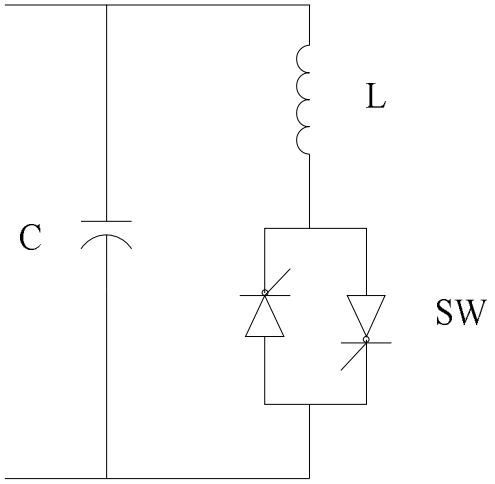

Fig. 3-1 Simplified schemes of SVC and TCSC

Fig. 3-2 (a) shows the block diagram for the SVC with control loop, where V_t is the SVC bus voltage, B_{svc} is the succeptance, and *svc_sig* is the added modulation signal for damping control. Fig. 3-2 (b) shows the block diagram for the TCSC with control loop, where *tcsc_sig* is the added modulation signal of TCSC for damping control, ΔB_{tcsc} is the change of succeptance of the TCSC. In both figures y is a power system variable that contains the low frequency oscillation information and is used as the damping controller input.

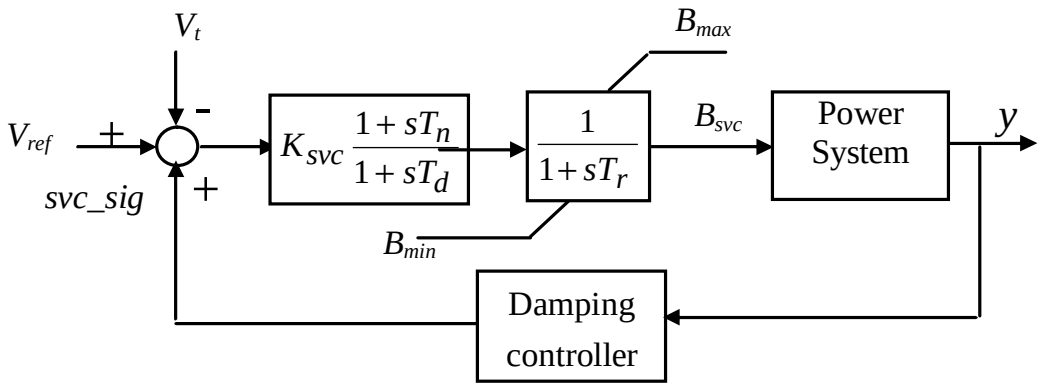

(a)

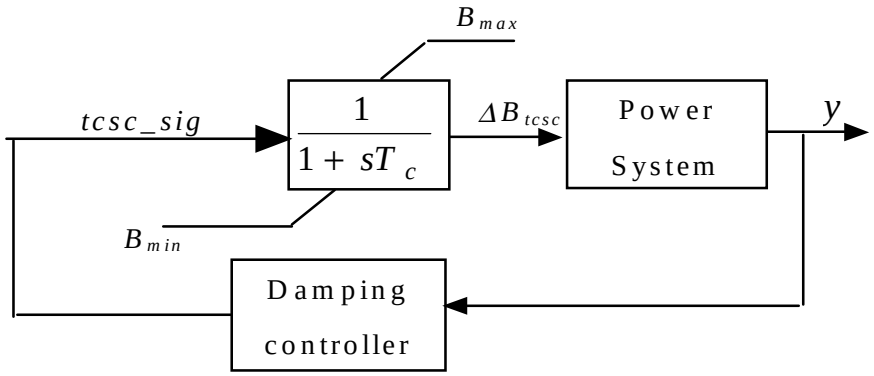

(b)

Fig. 3-2 Block Diagram of SVC and TCSC

The damping controller design is treated as a general control problem, where a mathematical model is obtained for the system and analyzed. Fig. 3-3 shows the block diagram of the closed loop system from a control viewpoint for Fig.3-2, where Δy is control input signal deviation from its steady-state value (obtained by passing y through a washout filter), $G(s)$ represents the plant model (which is the open loop transfer function between Δy and reference input), and $H(s)$ is the transfer function of the damping controller.

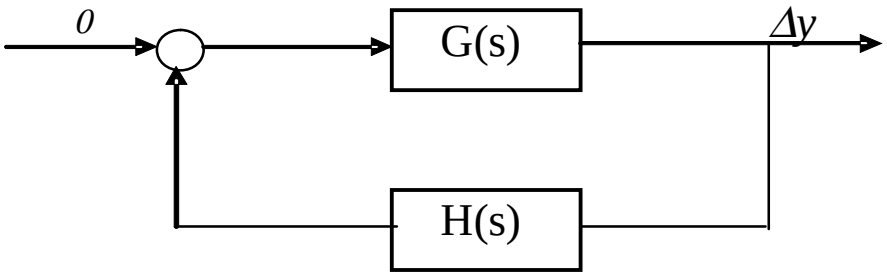

Fig. 3-3 Close Loop Control Diagram

The reduced order model of the system is obtained by the PRONY method because of its simplicity and proven effectiveness [57, 66, 67]. Based on the system characteristics, an appropriate supplementary controller is designed for the FACTS using the residue and the root-locus methods. The transfer function of the SVC or TCSC controller can be determined by analyzing the sensitivity of controller parameters with respect to the mode of interest [68]. However, the gain of the controller which may lead to satisfactory damping of the mode of interest still has to be carefully determined. The root locus plot is used to obtain this controller gain, which is later optimized according to the loading condition on the transmission line. Since FACTS devices are usually installed on a transmission line, generator signals (e.g., generator speed) are not available locally. To avoid the communication problems like time delay and unreliability, local power system network signals are preferred as the input to the damping controller. Possible choices include transmission line active power (P_{tran}), line current (I), SVC bus frequency (f) and SVC bus voltage (V). A systematic approach is proposed to select the most effective input signal to the damping controller and design a controller which works for different operating conditions. A typical two area system is used to illustrate the process of damping controller design. Simulations are performed for a 4-machine 13-bus system

and a 16-machine 68-bus system to demonstrate the effectiveness of the damping controller.

Power System Model Reduction

The order of the transfer function for real power systems can be very large (it could mean thousands for a large power system.) In addition, most of the modes of a power system cannot be observed by any one signal (such as line power or current), and only a very small number of modes are of interest. To obtain a low-order plant model without losing the essential mode, the PRONY method is used.

PRONY Method

PRONY analysis is a technique of analyzing signals to determine mode, damping, phase and magnitude information contained in the signal. It fits an output signal $y(t)$ to a weighted sum of exponential terms of the form

$$y(t) = \sum_{i=1}^{n+1} B_i e^{\lambda_i t} \tag{3-1}$$

in a least-square-error sense, where B_i is the signal residue associated with the mode λ_i. PRONY analysis does not identify the system transfer function directly. However, a reduced order system transfer function can be obtained in the form

$$G(s) = \frac{Y(s)}{I(s)} = \sum_{i=1}^{n} \frac{R_i}{s - \lambda_i} \tag{3-2}$$

The input signal $I(s)$ is a finite summation of delayed signals with the same characteristic eigenvalue in the form

$$I(s) = \frac{c_0 + c_1 e^{-sD_1} + c_2 e^{-sD_2} + \mathrm{L}\ c_k e^{-sD_k}}{s - \lambda_{n+1}} \tag{3-3}$$

where $D_i < D_{i+1}$, and R_i is the residue associated with the identified mode λ_i. The above approach will be used to obtain the reduced order model of the power systems for the purpose of controller design.

Model Validation

In order to properly show the model validation scheme and later for the process of damping controller design, the two-area-four-machine system (shown in Fig. 3-4) is used for the analysis. The power transfer range on the transmission lines is from -3 p.u. to 5 p.u.

The PRONY method was used to obtain the open loop transfer functions ($G(s)$ in Fig. 3-3) between control input signals and the voltage reference for several different operating conditions. A low-amplitude square-wave pulse is used as the PRONY input signal. The transfer function between transmission line current magnitude and V_{ref} is used as an example to show the effectiveness of the PRONY method. Low order models were obtained at three operating conditions: P_{tran} = 4.0 p.u. (nominal/heavy), 1.0 p.u.(light) and -3.0 p.u (opposite power transfer direction). A pulse input was applied to the three identified low order systems, and their time responses were compared with those of the actual system. The bode plot of the transfer function of the identified low order model was also compared with those of the actual system model. Figs. 3-5 and 3-6 show the line (12-13) current time and frequency (amplitude and phase) responses for the heavy loading condition, respectively. It is clear from these figures that the responses of the identified model match well with those of the actual system. Very good

matches of both the time domain and frequency domain responses between the identified and the actual system transfer functions were also obtained at other operating conditions.

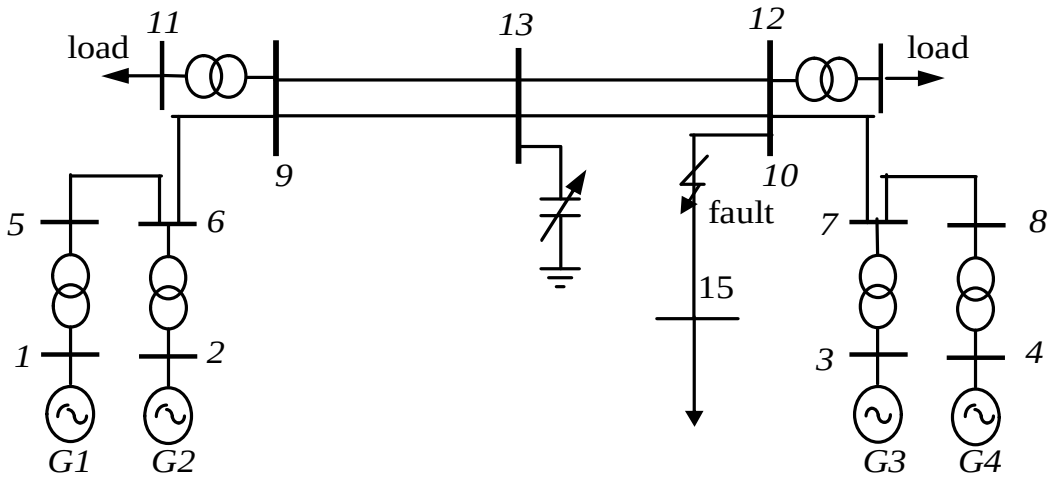

(a) Two area system with SVC

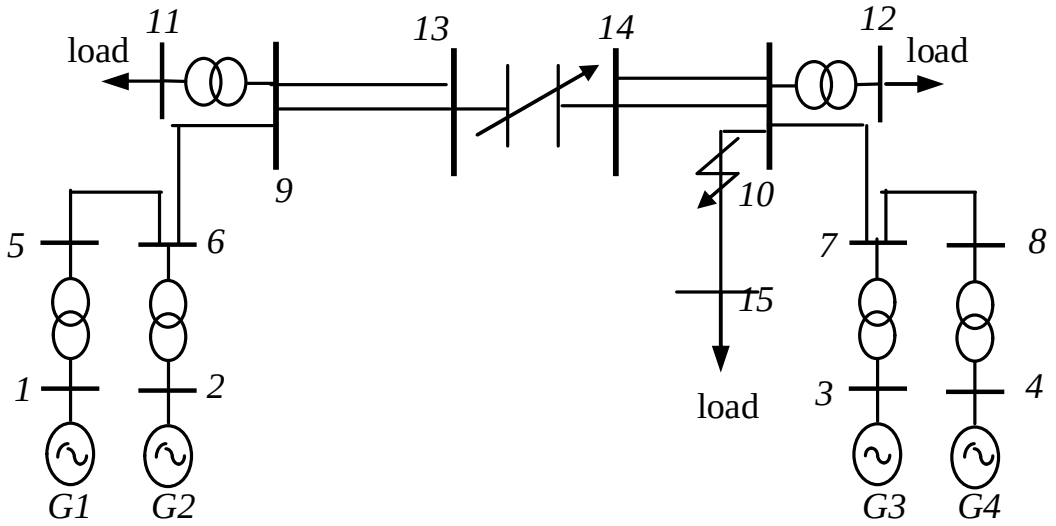

(b) Two area system with TCSC

Fig. 3-4 The two-area-four-machine system with different FACTS devices

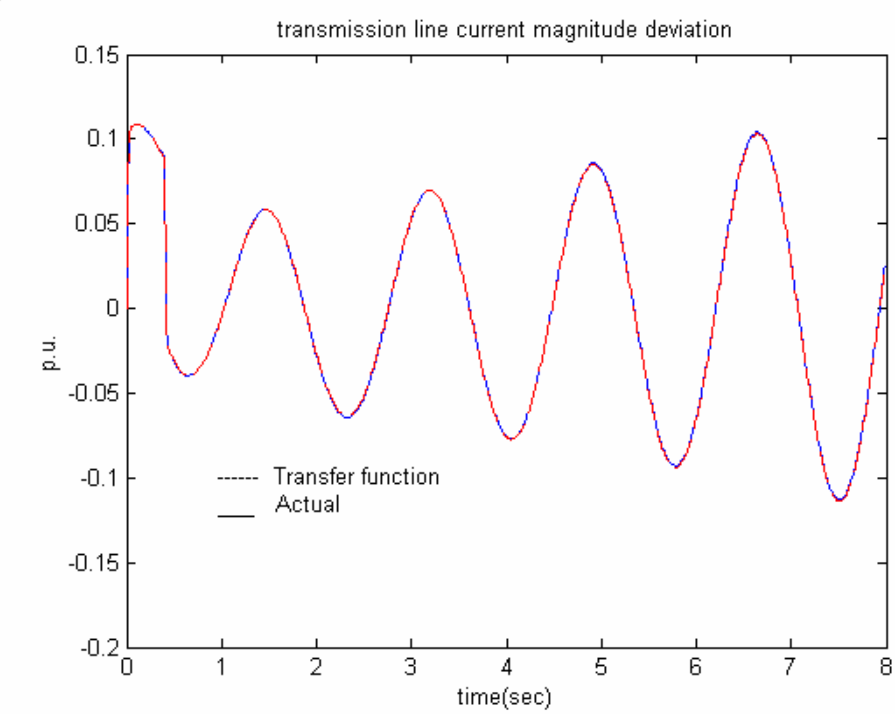

Fig. 3-5 Transfer function output versus actual output at P_{tran} = 4.0 pu

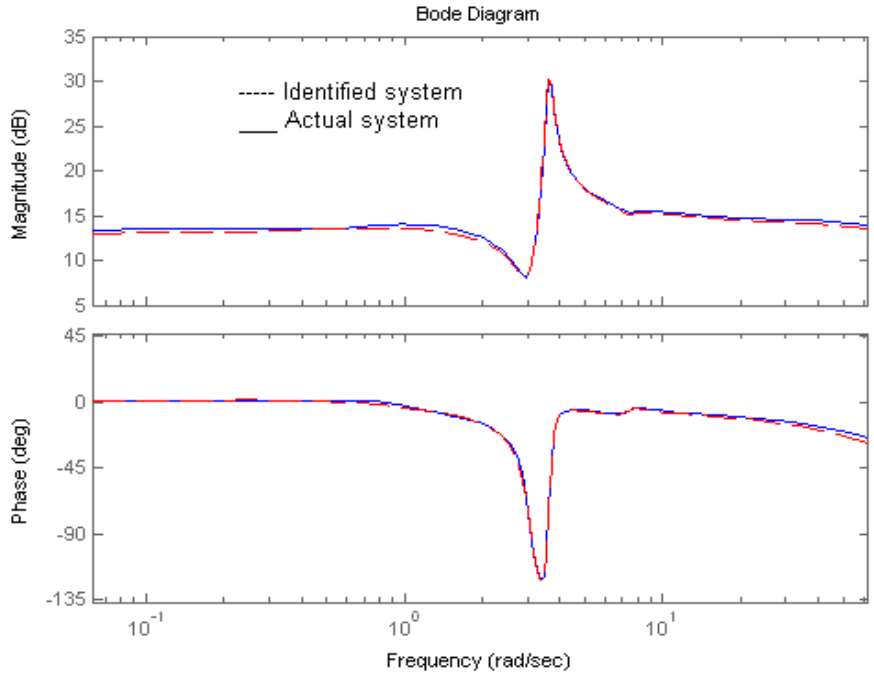

Fig. 3-6 Bode plot of identified system versus actual system at P_{tran} = 4.0 pu

Damping Controller Design

There are a few considerations that must be thought through when designing the supplementary damping controller for SVC and TCSC. 1) The damping controller must be designed so as not to detract from the main purpose of FACTS devices such as voltage control. 2) The supplementary damping controller should be able to provide positive damping for all the operating conditions, including the opposite power flow direction.

Selection of control input

The local signals transmission line power P_{tran}, line current I_m, bus voltage V, and bus frequency f were considered as candidate input signals to the controller (H(s)). Tables 3-1 and 3-2 show the identified inter-area mode and residue of $G(s)$ for these candidate control input signals at different operating conditions for the system with a SVC and a TCSC, respectively.

Table 3-1 Identified inter-area mode and residue of the system with SVC at different operating conditions.

P_{tran} (pu)	Inter-area Mode	Residue of G(s) using different control input			
		P_{tran}	I_m	f	V
4.0	0.11 +j3.64	$4.21\angle 99^o$	$3.45\angle 98^o$	$0.36\angle 38^o$	$0.03\angle -49^o$
2.0	0.034 +j3.83	$2.49\angle 100^o$	$1.36\angle 99^o$	$0.06\angle 46^o$	$0.0016\angle -49^o$
-2.0	-0.075+j3.93	$2.22\angle -99^o$	$2.06\angle 82^o$	$0.07\angle 40^o$	$0.002\angle -111^o$
-3.0	-0.080+j3.90	$3.30\angle -90^o$	$3.44\angle 90^o$	$0.14\angle 47^o$	$0.02\angle -57^o$

Table 3-2 Identified inter-area mode and residue of the system with TCSC at different operating conditions.

P_{tran} (pu)	Inter-area Mode	Residue of G(s) using different control input			
		P_{tran}	I_m	V	f
4.0	0.25 +j3.18	0.032 $\angle$-100^o	0.039 $\angle$-98^o	0.0058 $\angle$95^o	0.018 $\angle$-131^o
2.0	0.077+j3.65	0.019 $\angle$-115^o	0.024 $\angle$-100^o	0.0016 $\angle$90^o	0.004 $\angle$-44^o
-2.0	-0.71+j3.77	0.030 $\angle$79^o	0.031 $\angle$-101^o	0.0010 $\angle$78^o	0.015 $\angle$178^o
-3.0	-0.069+j3.62	0.042 $\angle$80^o	0.047 $\angle$-100^o	0.0022 $\angle$86^o	0.023 $\angle$-172^o

For the damping controller to be robust, it is expected that the transfer function of the damping controller be able to provide sufficient phase compensation at all the operating conditions. The angles of the residues are compared. From Table 3-1, it can be seen that for the SVC damping controller, when P_{tran} is used as the control input signal, the angle of the residue associated with the inter-area mode changed about 180^o when power transfer changed direction. This indicates that the sign of the modulation control signal has to be adapted with the direction of power transfer, which is not an easy task. Also, it was noticed that the angles of the residues in the last column of Table 1 vary a lot at different operating conditions. On the other hand, when I_m or f is used as control input signal, the vectors of the residue point in the same direction for all the operating conditions. Moreover, from the frequency response of the transfer function between the line current magnitude and voltage reference (Fig. 3-6), it can be seen that the system is very sensitive around the inter-area mode frequency; since there are large spikes in both the gain and phase plot of the system transfer function around the inter-area mode frequency range. Therefore, it is concluded that I_m and f are both good choices as

control input signal among the four choices considered. The same analysis was performed for Table 2. It can be seen from this table that both V and I_m are good candidates as the damping controller input for TCSC damping controller. This is because the residue vectors for different operating conditions point in the same direction when these two quantities are used as the controller input signal, as was the case for SVC controller design. In this study, I_m was used as the input signal to the damping controller of SVC and V was used as the input signal to the damping controller of TCSC. Also, it is noticed from both tables that the magnitude of the residue associated with the inter-area mode gets smaller when the magnitude of the power transfer through the transmission line is reduced. The magnitudes of residues are indicative of how far their corresponding eigenvalue can be moved through feedback. This indicates that the SVC damping controller would be more effective for damping oscillations at high levels of power transfer. Therefore the controller design was performed for the heavy (nominal) operating condition.

Phase compensation

Controller design was aimed at moving the loci of the inter-area modes to the left half of the complex plane. A brief description of this design is as follows. Suppose the reduced order plant model $G(s)$ can be expressed in terms of residues and eigenvalues as:

$$G(s) = \sum_{i=1}^{k} \frac{R_i}{(s - \lambda_i)} \tag{3-4}$$

where R_i/λ_i is the residue/eigenvalue associated with the ith mode. Depending on whether the feedback in the block diagram of Fig. 3-2 is positive or negative feedback, the eigenvalue sensitivity of the closed loop system shown in Fig. 3-2 can be expressed

by:

$$\frac{\partial \lambda_i}{\partial K} = \pm R_i \frac{\partial (K \cdot H(\lambda_i))}{\partial K} = \pm R_i H(\lambda_i) \tag{3-5}$$

Considering very small changes of feedback gain (ΔK) and eigenvalue ($\Delta\lambda$), (3-5) can be written as

$$\Delta \lambda_i = \pm R_i H(\lambda_i) \cdot \Delta K \tag{3-6}$$

Therefore, the effect of the controller transfer function in the feedback path is to modify the sensitivity of the eigenvalue of the original system by the value of the controller transfer function evaluated at the original eigenvalue. Let α be the angle of the residue of the inter-area mode and ϕ be the desired phase compensation of the controller, then according to (3-6)

$$\alpha - \pi + \phi = (2n+1)\pi \quad \text{or} \quad \phi = -\alpha + 2n\pi \qquad (\text{n} = 0, \pm 1, \pm 2, \text{L}) \tag{3-7}$$

The controller designed is made up of washout filter and lead-lag blocks, with the following transfer function:

$$H(s) = k \frac{sT_w}{1+sT_w} \left(\frac{1+sT_1}{1+sT_2}\right)^n \tag{3-8}$$

T_w is the time constant of a washout filter and its value can be taken as a number between 1 and 20 *sec*. Values of T_1 and T_2 can be determined by the method proposed in [69]. Since the limit of phase compensation of the lead-lag block is about 60^o [69], the number of the lead-lag blocks (n) can be determined by taking the nearest larger number of $\phi/60$, where ϕ is the required phase compensation of the controller at the inter-area frequency range. Suppose the controller is a lag controller, the steps to determine T_1 and T_2 are as follows:

$$c = \frac{1+\sin(\phi / n)}{1-\sin(\phi / n)} \tag{3-9}$$

$$T_1 = \frac{1}{\omega \cdot \sqrt{c}} \tag{3-10}$$

$$T_2 = c \cdot T_1 \tag{3-11}$$

Gain adjusting

The next step in the controller design is to obtain the gain. Equation (3-6) is based on the eigenvalue sensitivity for small signal stability analysis and it is only accurate for a very small value of K. Therefore, it is necessary to perform the root locus analysis to carefully choose the gain K which can provide the best possible damping of the inter-area mode. Since the controller design was based on a reduced order simplified power system, transient simulations are performed afterwards to check the performance of the controller and retune the gain K if necessary. This methodology is done for nominal operating condition, where the magnitude of the residue of the transfer function (G(s)) associated with the oscillatory mode of interest is the largest. Since the magnitude of the residue associated with the inter-area mode gets smaller when the magnitude of the power transfer through the transmission line is reduced, it is possible that better damping effects can be achieved at the other operating conditions other than nominal by adjusting the controller gain according to the operating condition. A sensitivity analysis is carried out to determine an optimal value of the controller gain which will result in maximum damping at one specific operating condition. A performance measure, which is the quantitative measure of the system deflection away from the steady state position, is proposed for the sensitivity analysis. The performance measure is

$$CF = \frac{1}{N}\sum_{i=1}^{N}(P_{line}(i) - P_{ss})^2 \qquad (3\text{-}12)$$

where N is the iteration number at simulation time, P_{line} is the transmission line power. Subscript *ss* represents steady state. The optimal controller gain is chosen so that the performance measure is minimized. For the two-area system studied, the power transfer range is about –3 pu to 5 pu, and the controller gains at several typical operating conditions between this range are determined in this way. The controller gains at other operating conditions can be determined by interpolation. Therefore, rather than using one fixed gain controller for all operating conditions, the controller gain can be adjusted on-line according to the steady state value of the power transferred on the transmission line, which can be obtained by filtering the power signal through a high-pass filter.

Simulation Results

To test the performance of the proposed FACTS controller, simulation studies were performed on a two-area, 4-machine, 13-bus system and a reduced order New York/ New England system [1]. Six states are used to model each generator in the power system: $\Delta\delta$, $\Delta\omega$, $\Delta E'_q$, $\Delta E'_d$, $\Delta\psi_{kd}$, $\Delta\psi_{kq}$. The sampling period used in all cases was 0.01*sec*.

Two-area, 4-machine, 13-bus system

System with SVC. Four operating conditions (P_{tran} = 4.0 *pu*, 2.0 *pu*, and -2.0*pu*, -3.0 *pu*, respectively) were considered. The required phase compensation at the inter-area oscillation frequency for all the operating conditions is about -100^o. Table 3-3 shows the important identified modes and corresponding residues of G(s) at the nominal operating condition. The controller designed is

$$H(s) = k \cdot \frac{20s}{1+20s} \frac{(1+0.10s)^2}{(1+0.75s)^2} \tag{3-13}$$

The transfer function obtained using the PRONY method was used as the feed forward term (G(s)), and the SVC damping controller as the feedback term. Fig. 3-7 shows the important parts of the root locus in the upper half of the s-plane for a nominal operating condition (P_{tran}=4pu). In this figure, mode 1 is the inter-area mode which was unstable initially and has a fair amount of damping added to it as k increases. Mode 2 is a local mode detected by the PRONY method and is barely influenced by the controller since the magnitude of the residue associated with this mode is small (see Table 3-3). Mode 3 is the mode introduced to the system by adding a controller, which has a good damping ratio. Similar root-locus analyses were performed on the system under different operating conditions, and similar observations were made from the root-locus plots. However, as the level of loading was reduced, the amount of damping improvement that can be made to the inter-area mode was reduced, as shown in the root locus plot of Fig.3-8 given for the light loading condition (P_{tran}=1.0 *pu*). Initially, an open-loop pole of the identified transfer function related to the inter-area mode (mode 1) to be damped is very close to a zero near the imaginary axis in the right half plane, and the designed controller barely moves the pole to the left half-plane. Therefore the controller design was carried out for heavy operating condition, where best possible damping ratio can be achieved at gain k=0.9, as shown in Fig. 3-7. Simulation studies were performed to verify the root locus analysis. First a small disturbance (pulse signal) was applied to the SVC voltage reference. The current magnitude in line 12-13 and SVC bus voltage responses to this disturbance under nominal operating conditions (with and without SVC

controller) are shown in Figs. 3-9 and 3-10. It is clear from this figure that the SVC controller improves the small signal stability of the system, hence increasing the system's steady-state power transfer capability. It is also noted from the SVC bus voltage response that the SVC controller helps improve the voltage stability. The SVC bus voltage oscillation is unstable without the SVC controller but stable at steady-state with the SVC controller. Similar results were obtained for other operating conditions ($P_{tran} = 2.0\,pu$ and $P_{tran} = -3.0\,pu$) as shown in the line current responses given in Figs. 3-11 and 3-12. Then a three-phase fault is applied on line 13-15 and was cleared by removing the faulted line after 0.05 *sec*. There is 50 MW of load at bus 15, which is lost following fault clearance, as shown in Fig. 3-3. A limit of ± 0.1 *pu* was applied to the SVC control output (svc_sig). Fig. 3-13 shows the power transferred on the tie-line at nominal operating condition. It was noticed from both the root locus analysis and controller performance calculation that at most operating conditions the cost function slightly improves for different controller gains. This is verified by the simulation results. The power transfers on the tie-line at two other operating conditions (P = 2.0 pu and P = -3.0 pu) for three cases (without damping controller (DC), with fixed gain DC and with varying gain DC) are shown in Figs. 3-14 and 3-15. It can be seen that the system responses with a varying gain damping controller slightly improves the damping compared to a fixed gain SVC damping controller.

System with TCSC Similar analysis and design procedures used for SVC were also carried out for the damping controller design for TCSC. The TCSC has a $40\% \pm 10\%$ compensation of the reactance of the transmission line. Table 3-3 shows the important identified oscillatory modes and corresponding residues of G(s) at the nominal operating

condition. The transfer function of the controller is

$$H(s) = k \cdot \frac{20s}{1+20s} \frac{(1+0.755s)^2}{(1+0.129s)^2} \tag{3-14}$$

First an active load increase is applied at bus 11. Figs. 3-16 and 3-17 show the power system response with and without TCSC damping controller at the nominal operating condition. Figs. 3-18 and 3-19 show the system response at opposite power transfer condition (*P=-3p.u.*). It is clear from these figures that the TCSC damping controller improves the small signal stability of the system, hence increasing the system's steady-state power transfer capability. The system responses to the same three-phase fault at 3 different operating conditions are shown in Figs. 3-20, 3-21 and 3-22, respectively. The varying controller gain strategy was also applied to the controller design. It is noticed that in general, the varying gain strategy improved the damping of the system oscillations, especially at the light loading condition.

Table 3-3 Identified Modes and residues of the system at nominal operating condition

	Mode #	Mode	Residue
System with SVC	1 (inter-area)	0.1125 +3.6370i	-0.4910 +3.3867i
	2 (local)	-0.7287 +7.3875	-0.3745 +0.1137i
System with TCSC	1 (inter-area)	0.23+3.20i	-1.459e-4+3.105e-3i
	2 (local)	-0.46 +6.39i	1.878e-5-2.858e-6i

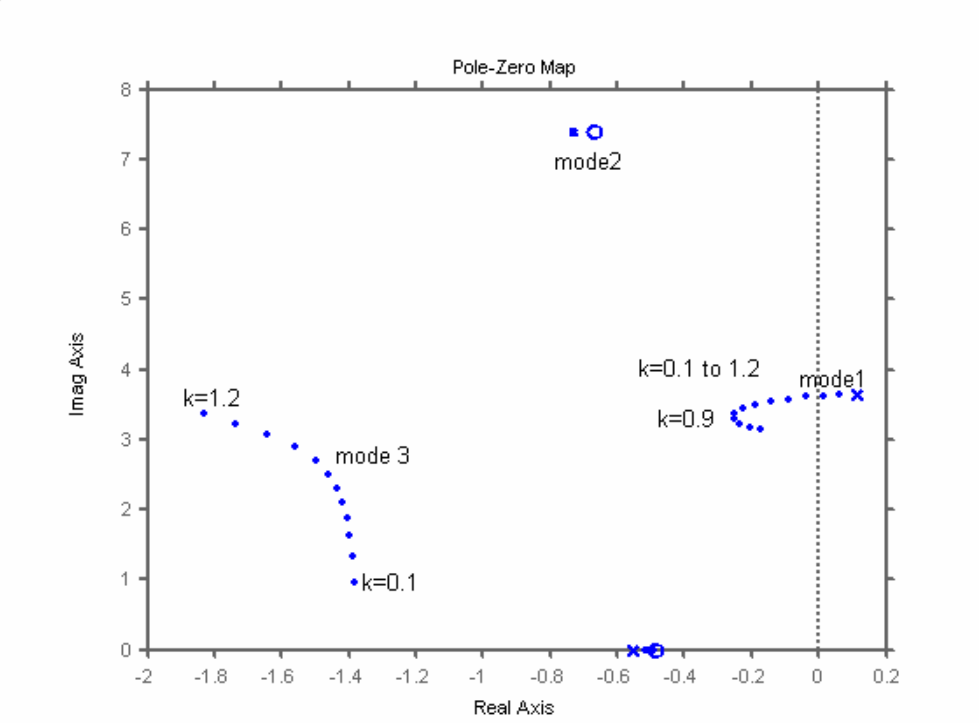

Fig. 3-7 Root locus plot for the SVC controller design at nominal operating point

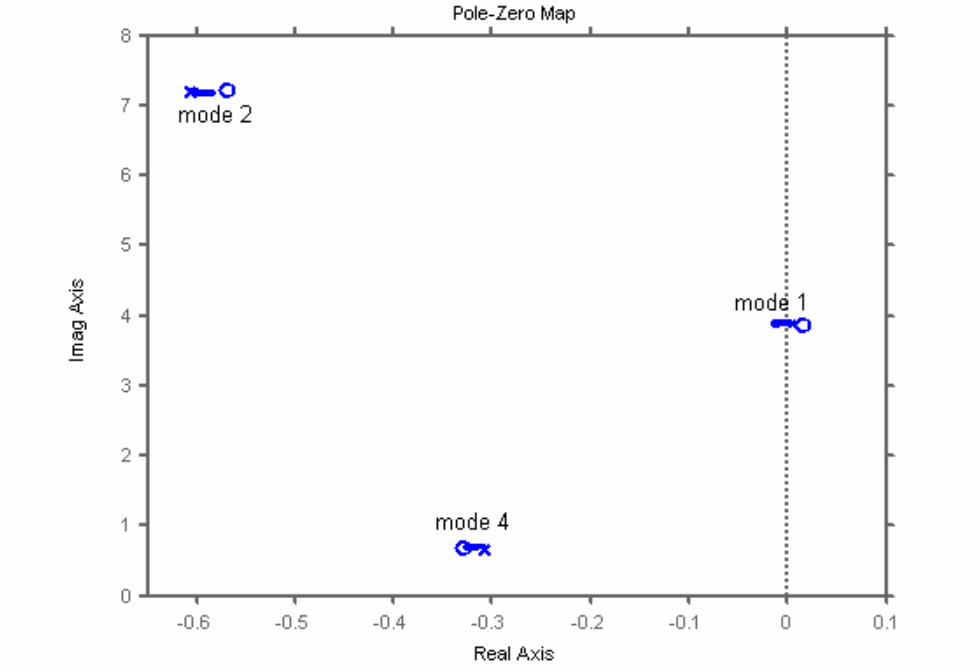

Fig. 3-8 Root locus plot for the SVC controller design at light operating point

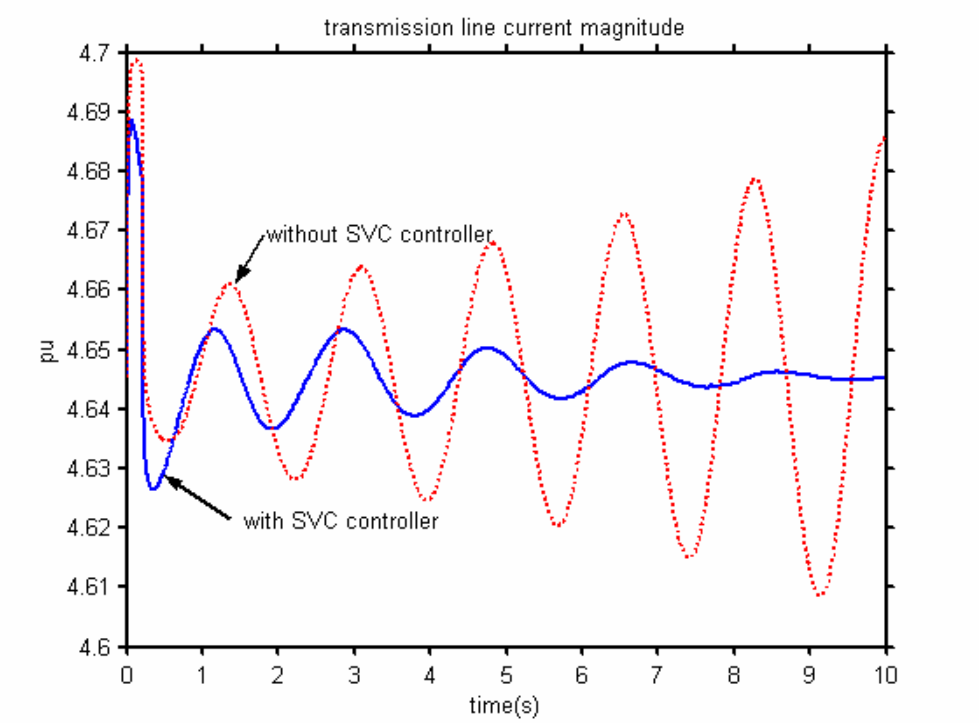

Fig. 3-9 Line current for small disturbance at nominal operating condition

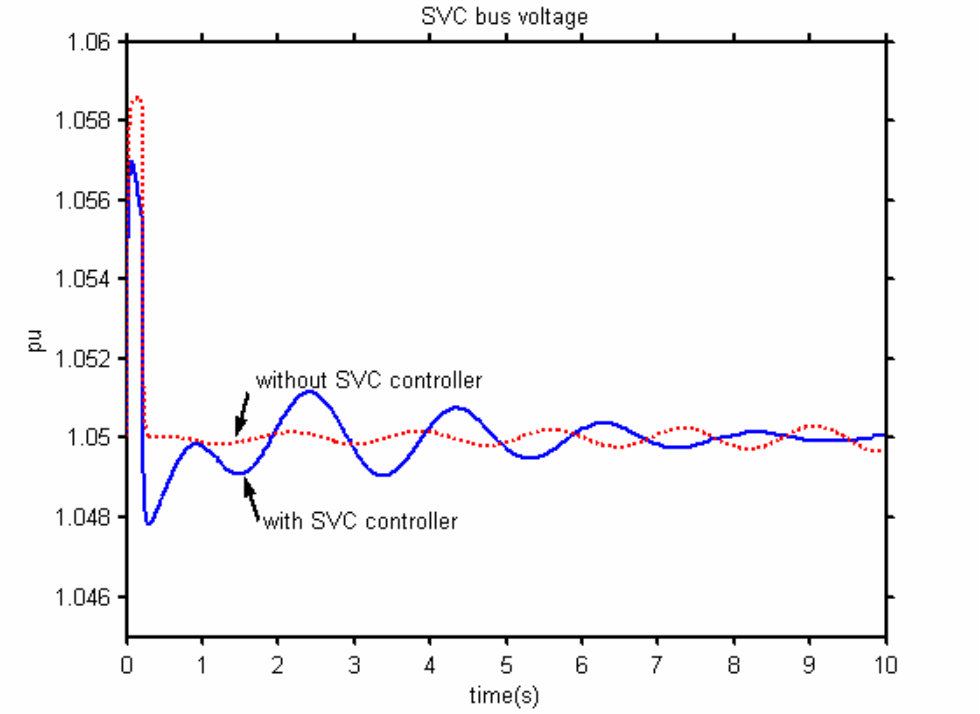

Fig. 3-10 SVC bus voltage for small disturbance at nominal operating condition

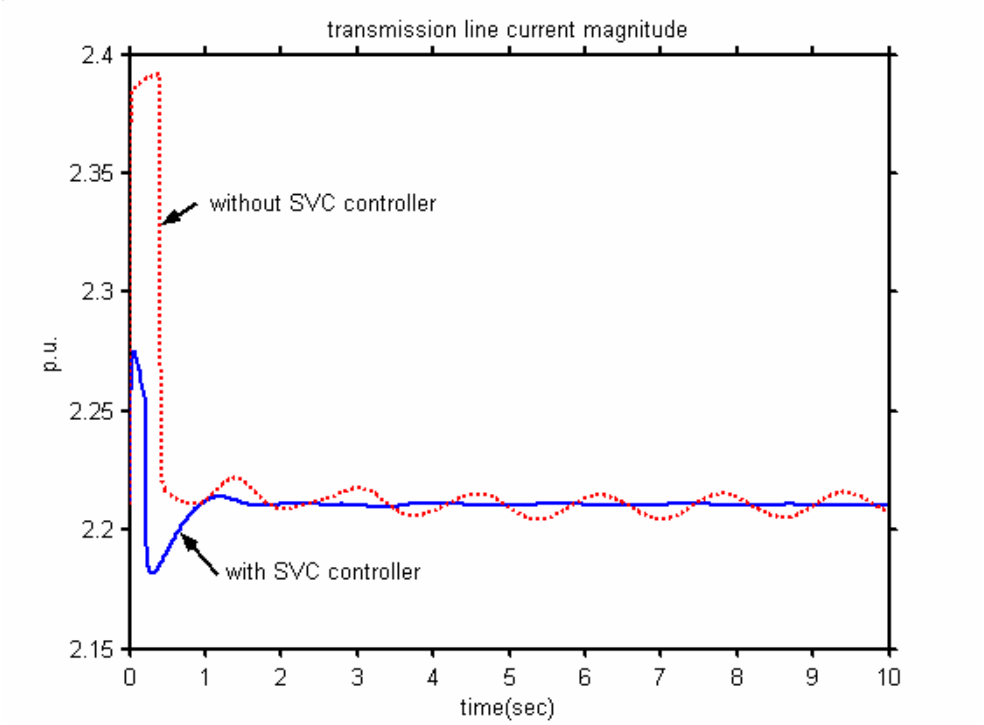

Fig. 3-11 Line current for small disturbance at light operating condition (SVC case)

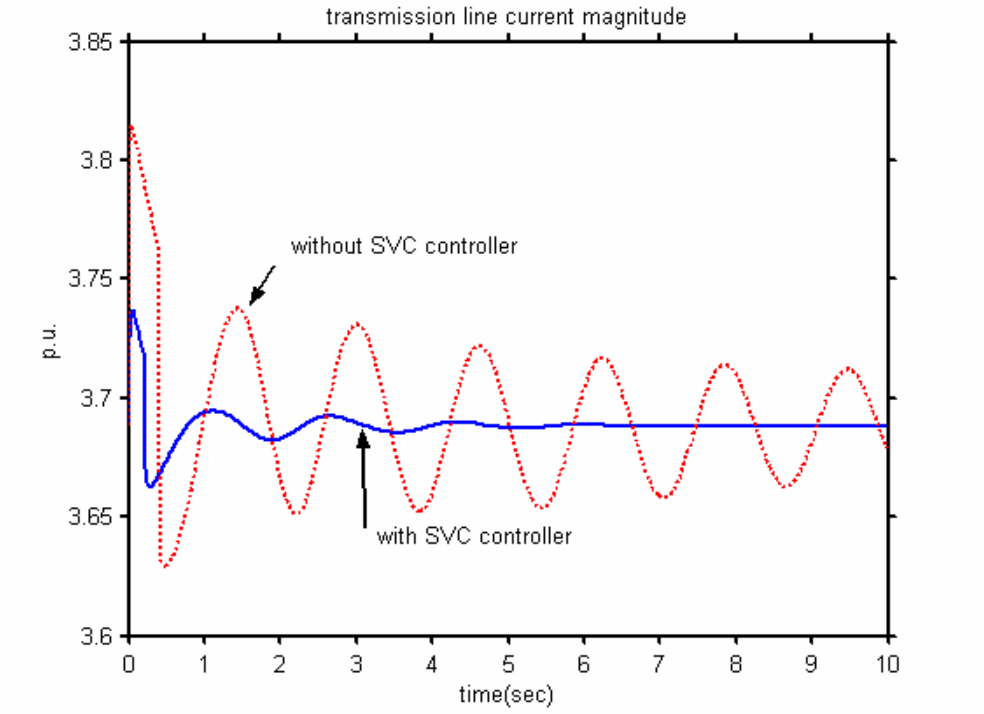

Fig. 3-12 Line current for small disturbance for opposite power transfer condition (TCSC case)

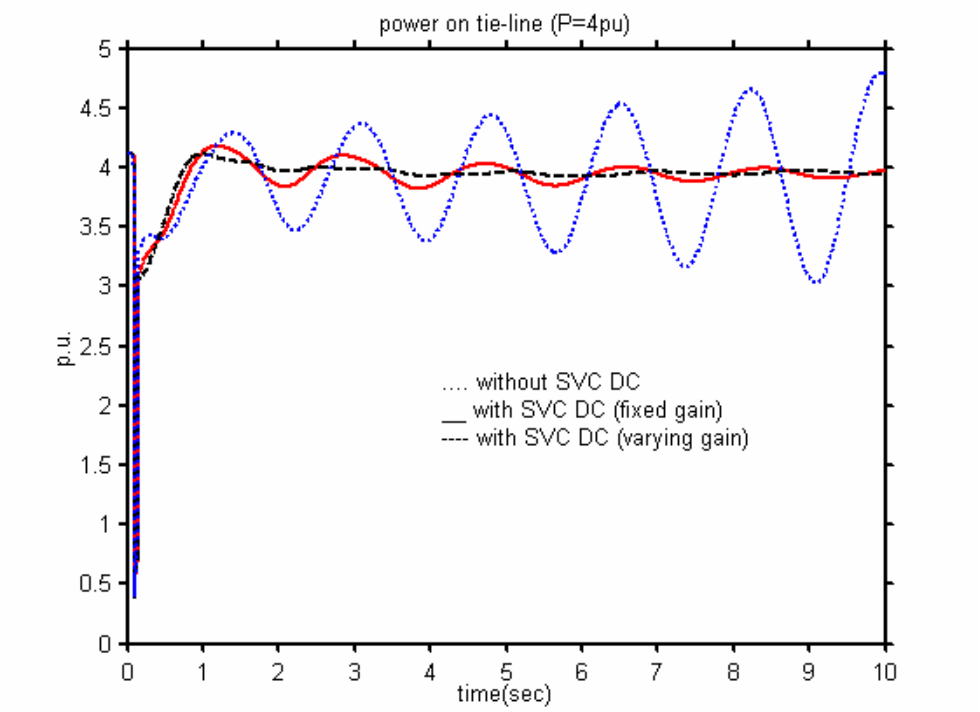

Fig. 3-13 Power on tie-line for fault at nominal operating condition

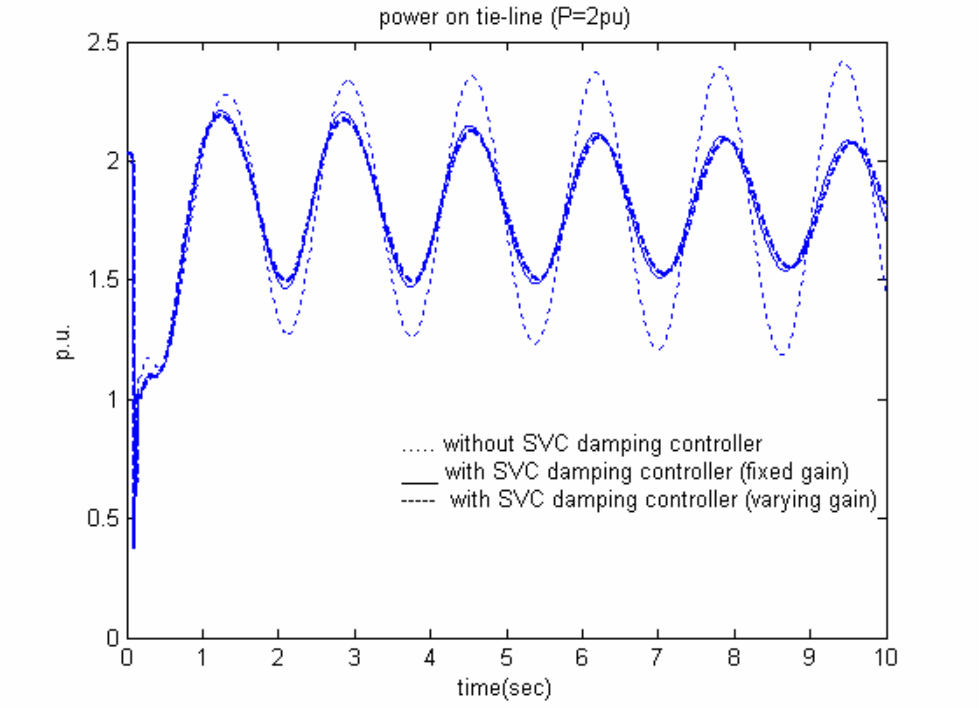

Fig. 3-14 Power on tie-line for fault at light operating condition

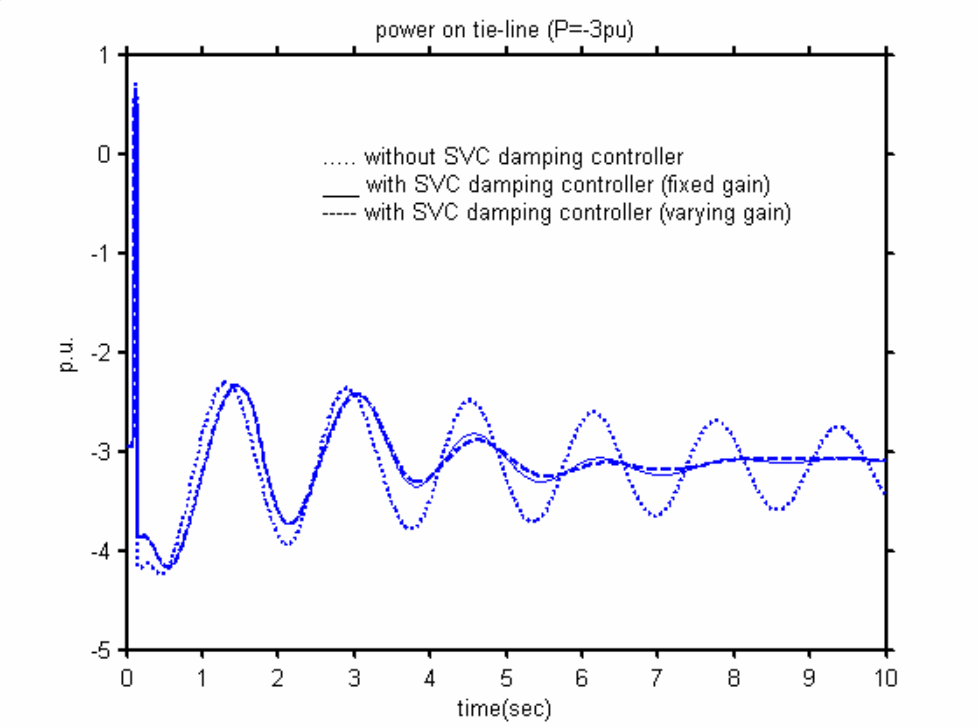

Fig. 3-15 Power on tie-line for fault for opposite power transfer direction

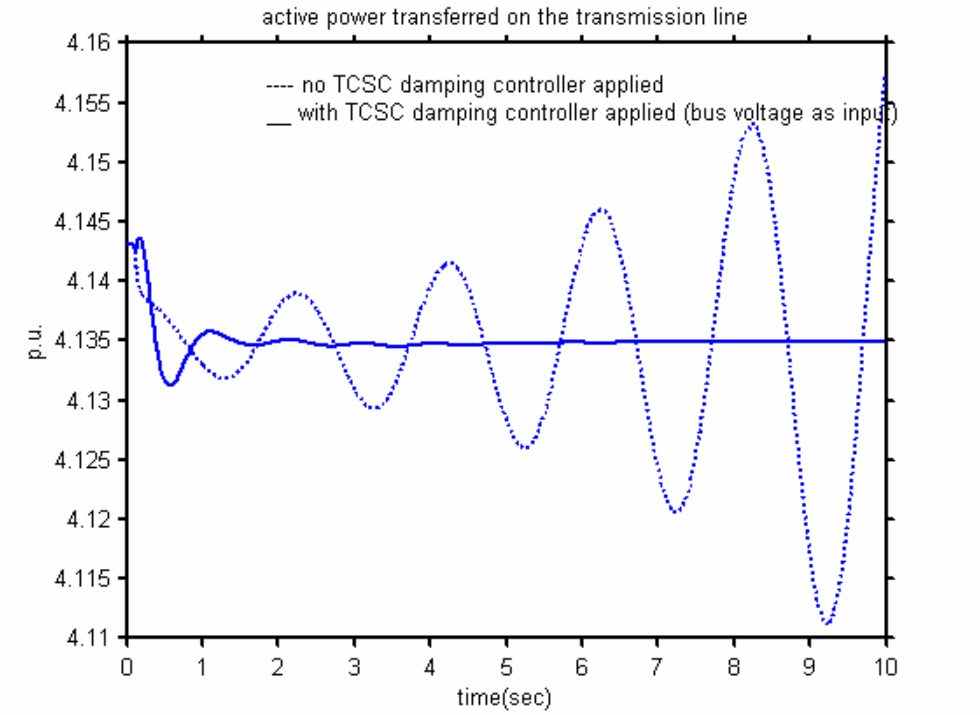

Fig. 3-16 Power on tie line for load change at nominal operating condition

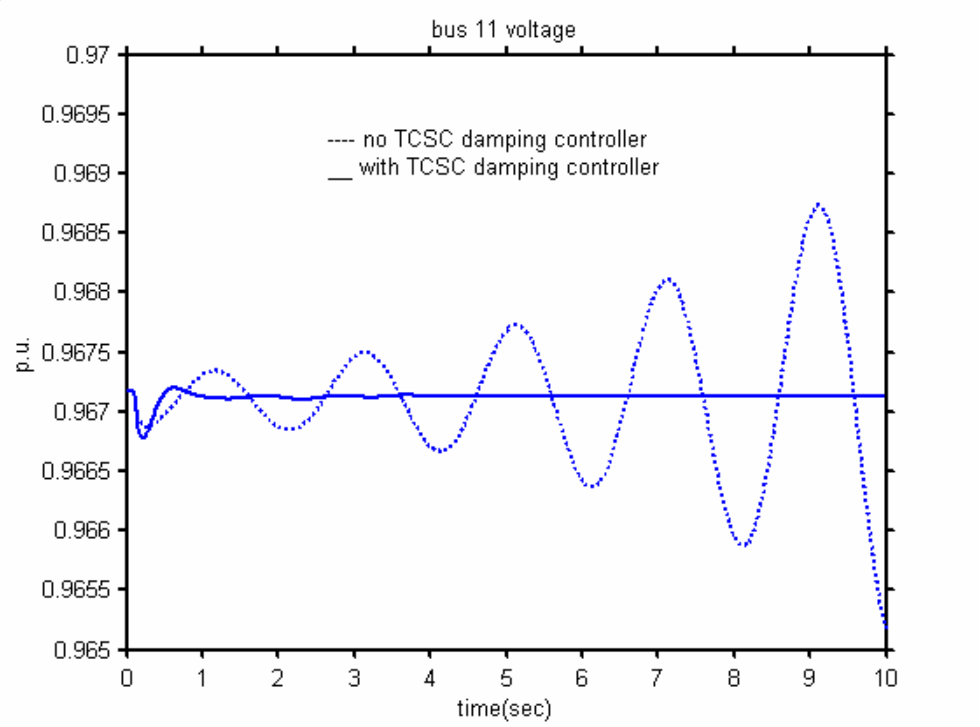

Fig. 3-17 Voltage of bus 14 for load change at nominal operating condition

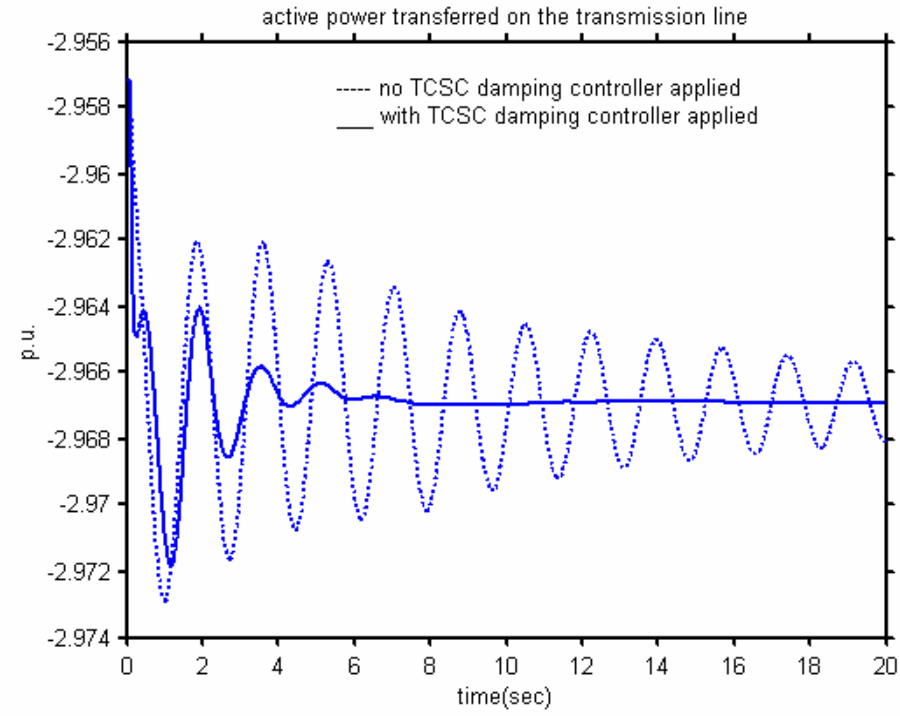

Fig. 3-18 Power on tie line for load change for opposite power transfer direction

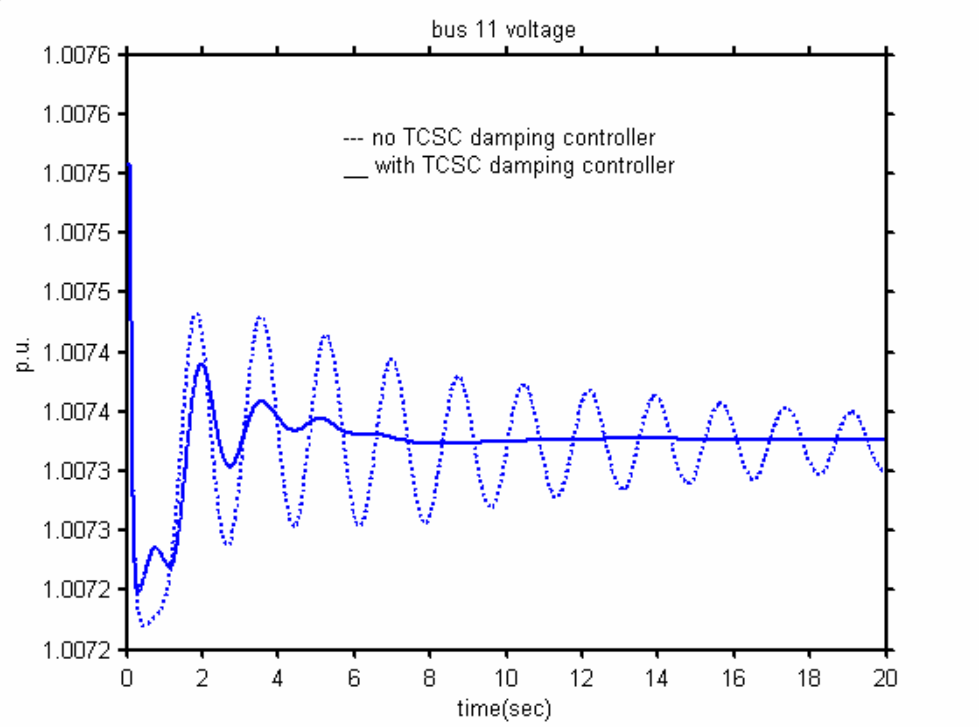

Fig. 3-19 Voltage of bus 14 for load change for opposite power transfer direction

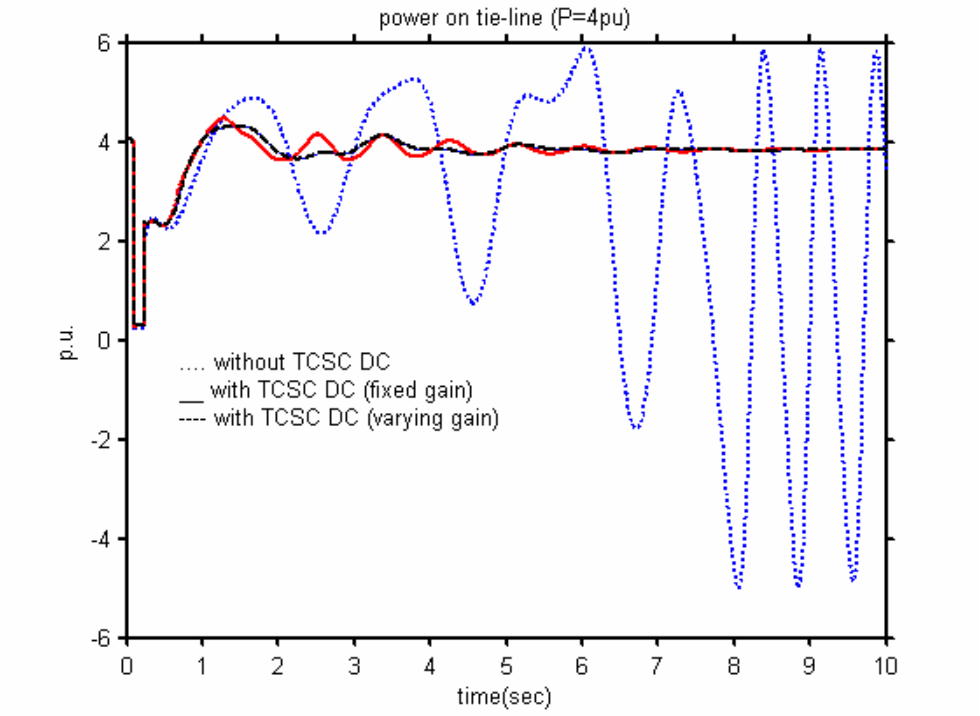

Fig. 3-20 Power on tie-line for fault at nominal operating condition

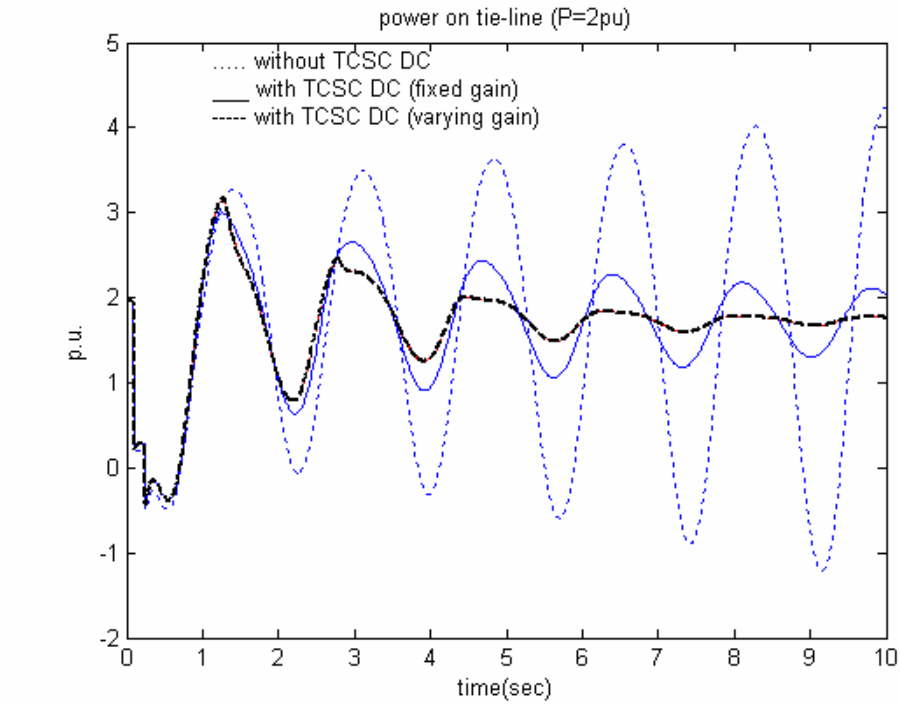

Fig. 3-21 Power on tie-line for fault at light operating condition

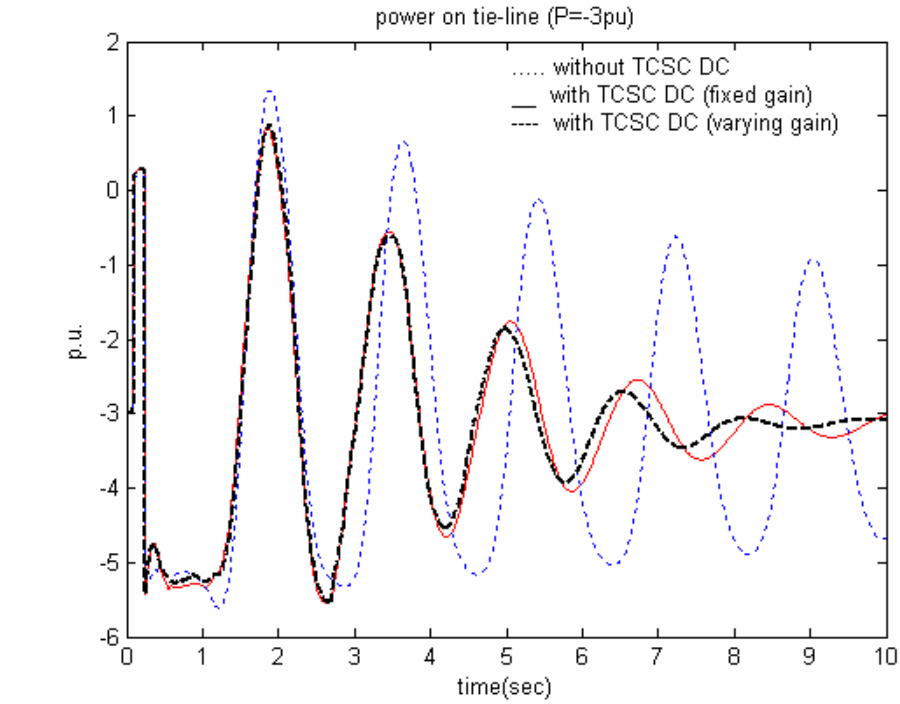

Fig. 3-22 Power on tie-line for fault for opposite power transfer direction

A 16-machine, 68-bus system

This system is shown in Fig. 3-23. A power system stabilizer was installed on G9. Major inter-area tie lines are shown bold. First the performance of the SVC damping controller is investigated. An SVC was installed at bus 50 (in area 3) since the voltage oscillation at this bus was greatest without the SVC. It is noticed from the PRONY identification results that all the modes with fairly large residues are inter-area modes. The residues for other modes are very small, meaning that those modes are either poorly controllable or poorly observable. A damping controller was designed based on the methodology proposed, and the transfer function designed for the damping controller is shown in (3-15). The fixed gain controller was designed for the nominal operating condition.

$$H(s) = K \frac{20s}{1+20s} \frac{(1+0.14s)^2}{(1+0.69s)^2} \tag{3-15}$$

Time domain simulations were carried out to investigate the effectiveness of the designed controller under severe disturbance. A three-phase fault was applied on line 1-2 (tie line between area 5 and area 1, at bus 1) and cleared after 0.05 *sec*. by removing the faulted line. The power transfers on the tie-line at two other operating conditions (nominal and light power transfer) for three cases (without DC, with fixed gain DC and with varying gain DC) are shown in Figs. 3-24 and 3-25, respectively. Next the SVC is removed and a TCSC is installed on line 50-51 to investigate the performance of the TCSC damping controller. The same fault is applied to the system and the system responses to this fault for same two operating conditions are shown in Figs. 3-26 and 3-27, respectively. It can be seen that the varying gain strategy can improve the damping to

some extent at light tie-line power transfer condition.

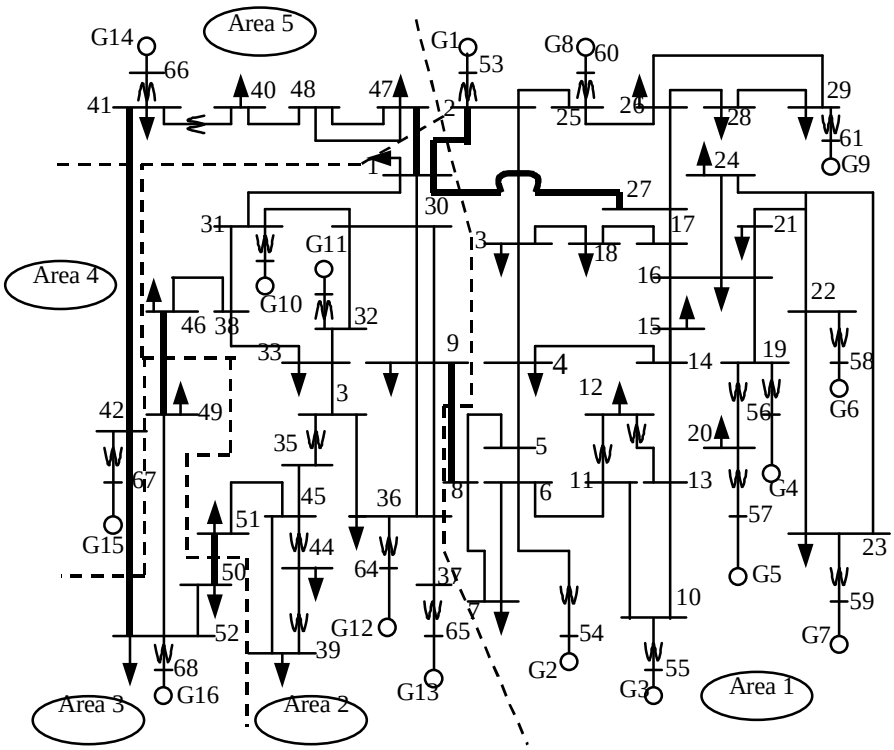

Fig. 3-23 16-machine. 68-bus system

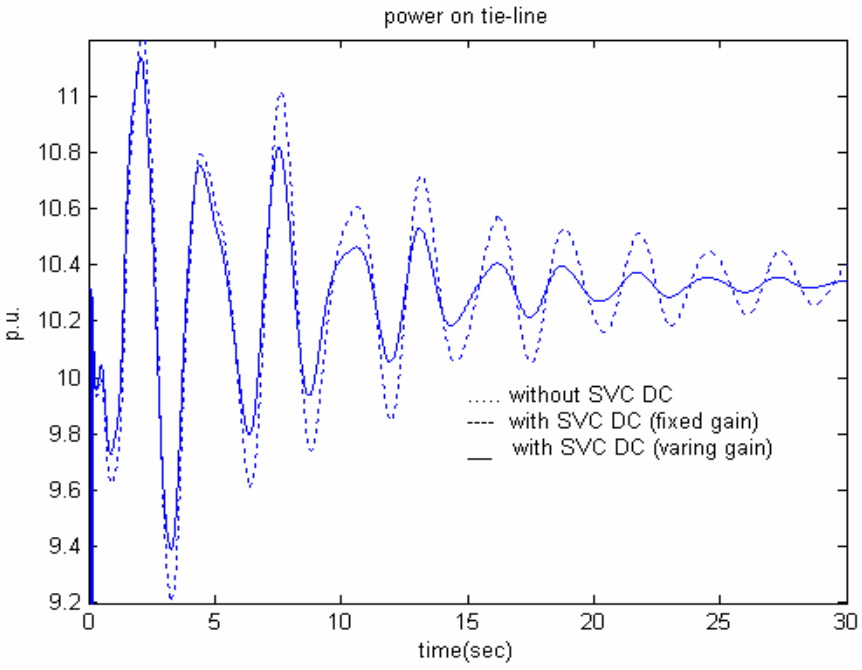

Fig. 3-24 Power on line 50-51 at nominal operating condition

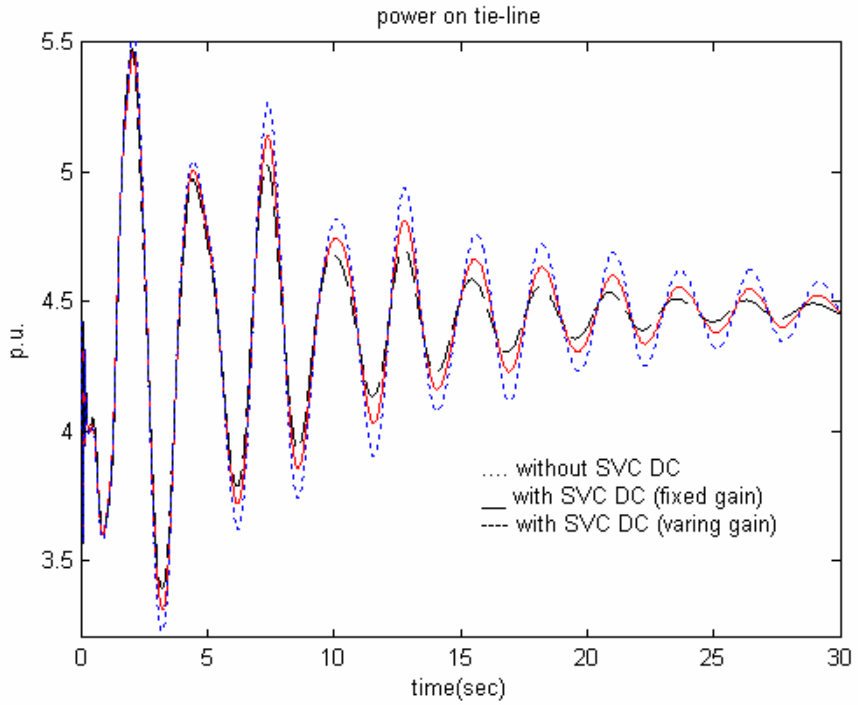

Fig. 3-25 Power on line 50-51 at light power transfer condition

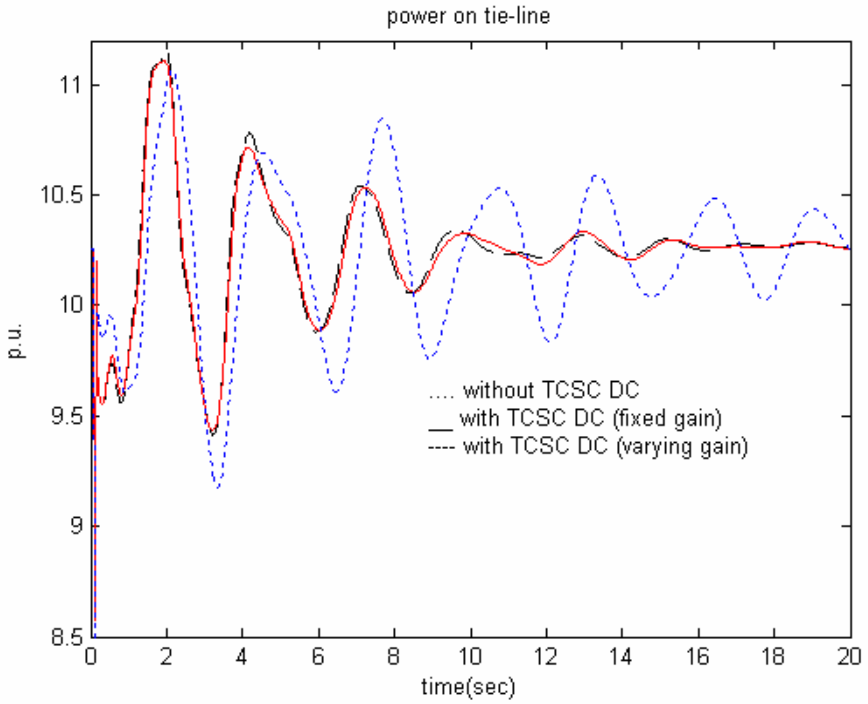

Fig. 3-26 Power on line 50-51 at nominal operating condition

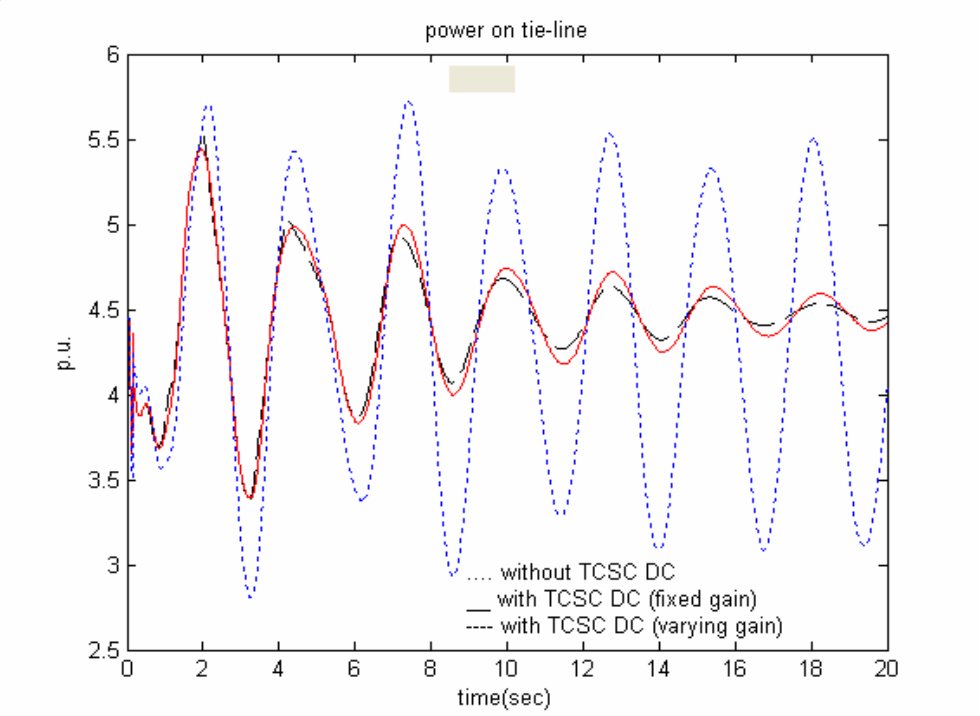

Fig. 3-27 Power on line 50-51 at light power transfer condition

CHAPTER 4

MODELING AND DAMPING CONTROLLER DESIGN FOR UPFC

Introduction

With increasing power system loading requirement, some transmission lines are running close to their full capacities. This causes little operation flexibility and controllability for contingency outages and abnormal system conditions. FACTS devices can provide feasible solutions to reinforce the transmission systems to better utilize the existing power systems. As demonstrated in the previous chapter, the SVC and TCSC can increase the steady-state transfer capability of transmission lines and improve power system stability to some extent. These FACTS devices act individually on one of the three transmission line operating parameters (voltage for the SVC, impedance for the TCSC) which determine the transmitted power. The unified power flow controller (UPFC) is a special FACTS device that was devised for real-time control and dynamic compensation of ac-transmission systems, providing multifunctional flexibility [56]. The UPFC has control over all the parameters (voltage, impedance and phase angle) affecting power flow on the transmission line. It is capable of controlling the real and reactive power on the transmission line and the bus voltage simultaneously and independently. However, the modeling of a UPFC is very complex compared to the modeling of the SVC and TCSC and is not available in the transient simulation software used for the study. SVC and TCSC are composed of a thyristor-controlled reactor or capacitor and they are normally modeled as a variable impedance connected in shunt or series with the transmission line. A UPFC, in contrast, is composed of self-commuted,

voltage-sourced switching converters that can realize rapidly controllable static synchronous voltage sources. A UPFC is like an ideal synchronous machine that can exchange both real power and reactive power with the power system. It automatically generates or absorbs the exchanged reactive power without the need of capacitors or reactors. But the exchanged real power should be either generated or absorbed by the power system.

In this chapter, a model of a UPFC which is suitable for both steady state analysis and dynamic stability analysis of power systems is developed. This model includes both converter control and internal dynamics of the UPFC and is able to demonstrate the unique characteristics of the UPFC for controlling power flow and bus voltage independently. A Newton-raphson iteration process based on a reduced network is also developed to interface the UPFC with power systems for the time-domain simulation. Practical operating constraints are included in the modeling and simulation. A damping controller is also designed for the UPFC using PRONY and root locus methods, as used for SVC and TCSC. Simulations are performed on a two area system for three cases: reference change, load change, and three phase fault.

Simplified UPFC Model

The UPFC structure is shown in Fig. 4-1 [56]. It consists of two voltage-sourced inverters (a shunt converter and a series inverter) which are operated from a common dc link provided by a dc storage capacitor. Both converters can exchange reactive power freely with the transmission system. The real power demand of the series converter is converted back into dc power on the dc link and this dc power has to be either provided

or absorbed by the shunt converter. The series converter will be responsible for the main function of the UPFC to control the power flow on the transmission line by injecting a synchronous voltage source with controllable magnitude and angle. The shunt converter will provide both controllable shunt reactive power to control the voltage of the sending end bus and real power to meet the dc power requirement. For modeling and simulation purpose, these two converters are modeled as a shunt connected synchronous voltage source (SVS) and a series connected SVS. The shunt and series coupling transformers are represented by their resistance and leakage reactance. The schematic diagram of the UPFC model is shown in Fig. 4-2. In this figure, V_{vr} and V_{cr} represent the shunt and series connected SVS, I_{vr} and I_{cr} are the currents through the two converters, and Z_{vr} and Z_{cr} represent the impedances for the coupling transformers. Buses k and m are the sending and receiving buses; lines 1-k and m-2 are part of the transmission line.

There are different functional control modes for the UPFC such as direct voltage injection mode, bus voltage regulation and control mode, line impedance compensation mode, phase angel regulation mode and automatic power flow control mode [56]. This dissertation only concerns the automatic power flow control mode of the series converter since this operating mode can fully utilize the capabilities of the UPFC. And the shunt converter is used in the automatic voltage control mode. In the power flow control mode, power flow out of the UPFC (i.e. P and Q on line m-2 in Fig. 4-2) and the sending end bus voltage (V_k) are supposed to be maintained at their references.

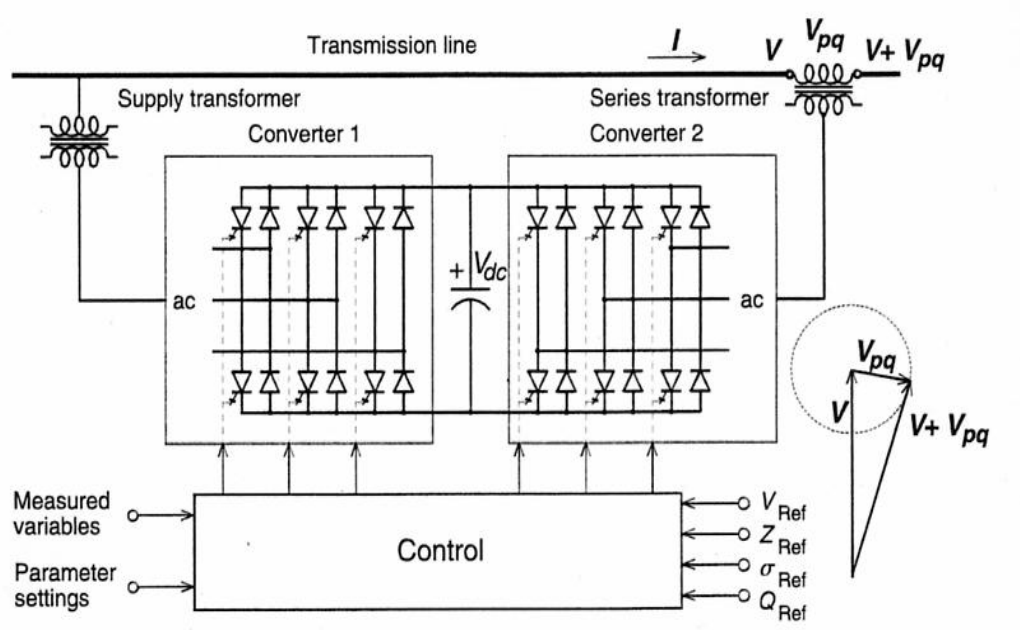

Fig. 4-1 UPFC Structure

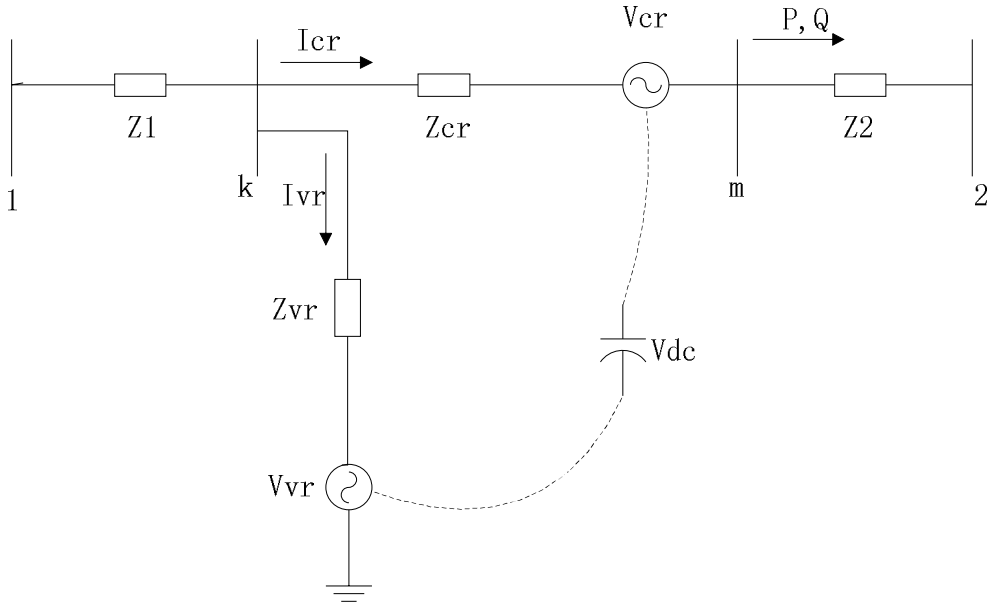

Fig. 4-2 Schematic diagram of UPFC model

Power Flow Calculation

When a UPFC is included in a power system, power flow calculation has to be modified to include the special features of the UPFC [44]. These features are:

1) The real and reactive power flows out of the receiving end bus equal the real and reactive power references.

2) Real power balance is kept for the dc link capacitor, i.e. the real power exchange of the series converter with the power system is either supplied or absorbed by the shunt converter.

The above features can be represented in the equations shown in (4-1)-(4-3)

$$P = P_{ref} \tag{4-1}$$

$$Q = Q_{ref} \tag{4-2}$$

$$P_{dc} = real(V_{vr} \cdot I_{vr} + V_{cr} \cdot I_{cr}) = 0 \tag{4-3}$$

These equations will be used in the power flow calculation as the added criteria. The unknowns related to the UPFC are two voltage sources (V_{vr} and V_{cr}) and two UPFC bus voltages (V_k and V_m) except the magnitude of V_k since the UPFC controls the sending end bus voltage to the reference level. These unknowns can be represented in a vector form $X_2 = [\Delta\theta_k \;\; \Delta V_m / V_m \;\; \theta_m \;\; \Delta V_{vr} / V_{vr} \;\; \theta_{vr} \;\; \Delta V_{cr} / V_{cr} \;\; \theta_{cr}]^T$, where θ represents the angle of a voltage variable. The power mismatch criteria related to the UPFC are represented as $g(X) = [\Delta P_k \;\; \Delta P_m \;\; \Delta Q_k \;\; \Delta Q_m \;\; \Delta P_{dc} \;\; \Delta P \;\; \Delta Q]^T$, where, ΔP_k , ΔP_m , ΔQ_k and ΔQ_m are the real and reactive power mismatches at UPFC buses k and m, ΔP_{dc} is the power mismatch at the UPFC DC link capacitor, and ΔP and ΔQ are the

power flow mismatches on transmission line m-2.

Combining with the rest of the power network, the expanded power flow equations are written as

$$\begin{bmatrix} f(X) \\ g(X) \end{bmatrix} = J_{new} \cdot \begin{bmatrix} X_1 \\ X_2 \end{bmatrix} = \begin{bmatrix} J_{11} & J_{12} \\ J_{21} & J_{22} \end{bmatrix} \cdot \begin{bmatrix} X_1 \\ X_2 \end{bmatrix} \tag{4-4}$$

where $X = [X_1^{\mathrm{T}} \;\; X_2^{T}]^{T}$, X_1 represents the variable vector for buses other than UPFC buses, and J_{new} is the new Jacobian matrix. $f(X)$ represents power mismatch for buses other than UPFC buses and $g(X)$ is defined above. In equation (4-4), the elements of the partition matrices J_{11}, J_{12} and J_{21} have the same form as the original Jacobian matrix, and the elements of J_{22} need to be defined. It is noticeable that at the two UPFC buses, the current injection and power calculation at the UPFC buses should include the elements of UPFC voltage sources. With reference to Fig. 4-2, the current injections at the two UPFC buses are

$$\begin{bmatrix} I_k \\ I_m \end{bmatrix} = \begin{bmatrix} Y_{1k} & Y_{kk} & Y_{km} & Y_{km} & Y_{VR} & 0 \\ 0 & Y_{mk} & Y_{mm} & -Y_{mk} & 0 & Y_{2m} \end{bmatrix} \begin{bmatrix} V_1 \\ V_k \\ V_m \\ V_{cr} \\ V_{vr} \\ V_2 \end{bmatrix} \tag{4-5}$$

where $Y_{kk} = y_{CR} + y_{VR} + y_1$, $Y_{mm} = y_{CR} + y_2$, $Y_{km} = -y_{CR}$, $Y_{VR} = -y_{VR}$, $Y_{1k} = -y_1$, $Y_{2m} = -y_2$ and $y_1 = \frac{1}{Z_1}$, $y_2 = \frac{1}{Z_2}$, $y_{cr} = \frac{1}{Z_{cr}}$, $y_{vr} = \frac{1}{Z_{vr}}$

Define $G_1 + jB_1 = y_1$, $G_2 + jB_2 = y_2$, $G_{cr} + jB_{cr} = y_{cr}$ and $G_{vr} + jB_{vr} = y_{vr}$

The equations used in [44] for power injection calculation at the two UPFC buses have

been modified and written below:

$$\begin{aligned} P_k &= real(V_k I_k{}^*) \\ &= V_k{}^2(G_{cr}+G_{vr}+G_1) - V_k V_m[G_{cr}\cos(\theta_k-\theta_m)+B_{cr}\sin(\theta_k-\theta_m)] \\ &\quad - V_k V_{cr}[G_{cr}\cos(\theta_k-\theta_{cr})+B_{cr}\sin(\theta_k-\theta_{cr})] \\ &\quad - V_k V_{vr}[G_{vr}\cos(\theta_k-\theta_{vr})+B_{vr}\sin(\theta_k-\theta_{vr})] \\ &\quad - V_k V_1[G_1\cos(\theta_k-\theta_1)+B_1\sin(\theta_k-\theta_1)] \end{aligned} \tag{4-6}$$

$$\begin{aligned} Q_k &= imag(V_k I_k{}^*) \\ &= V_k{}^2(-B_{cr}-B_{vr}-B_1) + V_k V_m[-G_{cr}\sin(\theta_k-\theta_m)+B_{cr}\cos(\theta_k-\theta_m)] \\ &\quad + V_k V_{cr}[-G_{cr}\sin(\theta_k-\theta_{cr})+B_{cr}\cos(\theta_k-\theta_{cr})] \\ &\quad + V_k V_{vr}[-G_{vr}\sin(\theta_k-\theta_{vr})+B_{vr}\cos(\theta_k-\theta_{vr})] \\ &\quad + V_k V_1[-G_1\sin(\theta_k-\theta_1)+B_1\cos(\theta_k-\theta_1)] \end{aligned} \tag{4-7}$$

$$\begin{aligned} P_m &= real(V_m I_m{}^*) \\ &= V_m{}^2(G_{cr}+G_2) + V_m V_{cr}[G_{cr}\cos(\theta_m-\theta_{cr})+B_{cr}\sin(\theta_m-\theta_{cr})] \\ &\quad + V_k V_m[-G_{cr}\cos(\theta_m-\theta_k)-B_{cr}\sin(\theta_m-\theta_k)] \\ &\quad + V_m V_2[-G_2\cos(\theta_m-\theta_2)-B_2\sin(\theta_m-\theta_2)] \end{aligned} \tag{4-8}$$

$$\begin{aligned} Q_m &= imag(V_k I_k{}^*) \\ &= -V_m{}^2(B_{cr}+B_1) + V_k V_m[-G_{cr}\sin(\theta_m-\theta_k)+B_{cr}\cos(\theta_m-\theta_k)] \\ &\quad + V_k V_{cr}[G_{cr}\sin(\theta_m-\theta_{cr})-B_{cr}\cos(\theta_m-\theta_{cr})] \\ &\quad + V_m V_2[-G_2\sin(\theta_m-\theta_2)+B_2\cos(\theta_m-\theta_2)] \end{aligned} \tag{4-9}$$

The power flow out of the receiving end bus can be calculated as

$$\begin{aligned} P &= real(V_m I_{cr}{}^*) \\ &= V_k V_m[G_{cr}\cos(\theta_m-\theta_k)+B_{cr}\sin(\theta_m-\theta_k)] \\ &\quad - V_m V_{cr}[G_{cr}\cos(\theta_m-\theta_{cr})+B_{cr}\sin(\theta_m-\theta_{cr})] - V_m{}^2 G_{cr} \end{aligned} \tag{4-10}$$

$$\begin{aligned} Q &= imag(V_m I_{cr}{}^*) \\ &= V_k V_m[G_{cr}\sin(\theta_m-\theta_k)-B_{cr}\cos(\theta_m-\theta_k)] \\ &\quad - V_m V_{cr}[G_{cr}\sin(\theta_m-\theta_{cr})-B_{cr}\cos(\theta_m-\theta_{cr})] + V_m{}^2 B_{cr} \end{aligned} \tag{4-11}$$

The real power balance on the DC capacitor is

$$
\begin{aligned}
P_{upfc} &= real(V_{vr} \cdot I_{vr} - V_{cr} \cdot I_{cr}) \\
&= -V_{cr}{}^2 G_{cr} - V_{vr}{}^2 G_{vr} + V_{cr} V_k [G_{cr} \cos(\theta_{cr} - \theta_k) + B_{cr} \sin(\theta_{cr} - \theta_k)] \\
&\quad - V_{cr} V_m [G_{cr} \cos(\theta_{cr} - \theta_m) + B_{cr} \sin(\theta_{cr} - \theta_m)] \\
&\quad + V_{vr} V_k [G_{vr} \cos(\theta_{vr} - \theta_k) + B_{vr} \sin(\theta_{vr} - \theta_k)]
\end{aligned} . \qquad (4\text{-}12)
$$

Let us expand the part of the equation (4-4) that is associated with J_{22} in details, as shown in equation (4-13)

$$
\begin{bmatrix} \Delta P_k \\ \Delta P_m \\ \Delta Q_k \\ \Delta Q_m \\ \Delta P_{dc} \\ \Delta P \\ \Delta Q \end{bmatrix} = \begin{bmatrix} N_{11} & N_{12} & N_{13} & N_{14} & N_{15} & N_{16} & N_{17} \\ N_{21} & N_{22} & N_{23} & N_{24} & N_{25} & N_{26} & N_{27} \\ N_{31} & N_{32} & N_{33} & N_{34} & N_{35} & N_{36} & N_{37} \\ N_{41} & N_{42} & N_{43} & N_{44} & N_{45} & N_{46} & N_{47} \\ N_{51} & N_{52} & N_{53} & N_{54} & N_{55} & N_{56} & N_{57} \\ N_{61} & N_{62} & N_{63} & N_{64} & N_{65} & N_{66} & N_{67} \\ N_{71} & N_{72} & N_{73} & N_{74} & N_{75} & N_{76} & N_{77} \end{bmatrix} \begin{bmatrix} \Delta\theta_k \\ \Delta V_m / V_m \\ \theta_m \\ \Delta V_{vr} / V_{vr} \\ \theta_{vr} \\ \Delta V_{cr} / V_{cr} \\ \theta_{cr} \end{bmatrix} + C . \qquad (4\text{-}13)
$$

The elements of J_{22} can be obtained from the partial derivative calculations of (4-6) – (4-12) and the results are attached in Appendix B

Modeling of UPFC Control and Dynamics

The primary function of the UPFC is to manage power flow on the transmission lines. This function is accomplished by the injection of an ac compensating voltage source with varying magnitude and angle. With proper converter control, this series connected voltage source (V_{cr}) can vary rapidly and continuously to meet the requirement of fast tracking of the power reference. As mentioned in [56], the series converter responds directly and independently to the demand for series voltage injection and changes in series voltage can be affected instantaneously.

The control of the UPFC series converter is based upon the vector control approach proposed for the static VAR compensator in [45]. Instead of considering electrical

variables in a phasor form, the vector, which is a representation of a set of three instantaneous phase variables that sum to zero, is used. An extended Park's transformation [45, 48] is used to change the electrical variables in the abc reference frame into a synchronous rotating (d-q-0) reference. The advantage of this transformation is that the controllable electrical variables are now dc values. Take the series path of the UPFC shown in Fig. 4-2 as an example. Suppose in a three-phase balanced system, an electrical variable is represented as $x_a = |x_a| \cos(\omega t + \gamma_0)$. The extended Park's transformation uses the receiving end bus voltage V_m as a rotating reference, i.e. the d-axis of the new co-ordinate system is always coincident with the instantaneous voltage vector and the q-axis is always in quadrature with it, as shown in Fig. 4-3. Let $v_{ma} = |v_m| \cos(\omega t + \alpha_0)$, and the extended Park's transformation matrix is given by

$$P = \begin{bmatrix} \cos\beta & \cos(\beta - 2/3\pi) & \cos(\beta + 2/3\pi) \\ -\sin\beta & -\sin(\beta - 2/3\pi) & -\sin(\beta + 2/3\pi) \\ 1/\sqrt{2} & 1/\sqrt{2} & 1/\sqrt{2} \end{bmatrix} \tag{4-14}$$

Then

$$\begin{bmatrix} x_d \\ x_q \\ x_0 \end{bmatrix} = \frac{2}{3} \cdot P \cdot \begin{bmatrix} x_a \\ x_b \\ x_c \end{bmatrix} = \begin{bmatrix} |x_a| \cos(\beta - \gamma) \\ |x_a| \sin(\beta - \gamma) \\ 0 \end{bmatrix} \tag{4-15}$$

If x represents i_{cr}, then the real and reactive power out of the UPFC are calculated as

$$P_{3phase} = \frac{3}{2} |v_m| \cdot |i_{cr}| \cos(\beta - \gamma) = \frac{3}{2} |v_m| \cdot i_{crd} \tag{4-16}$$

$$Q_{3phase} = \frac{3}{2} |v_m| \cdot |i_m| \sin(\beta - \gamma) = \frac{3}{2} |v_m| \cdot i_{crq} \tag{4-17}$$

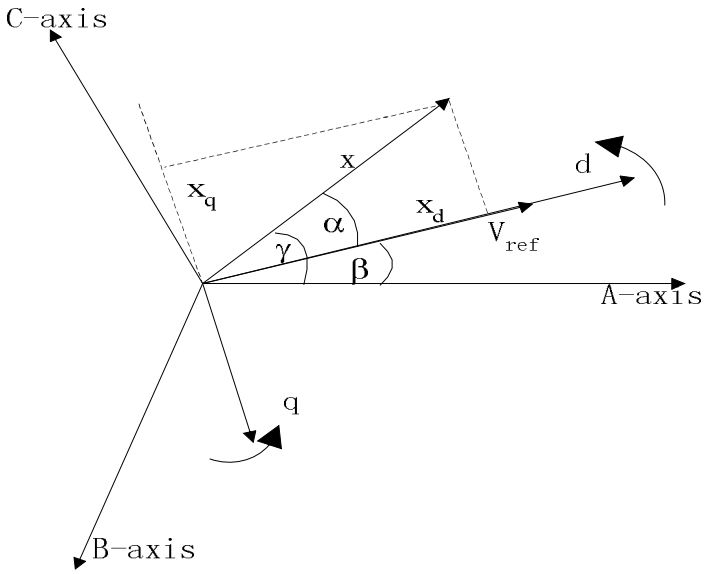

Fig. 4-3 Extended Park's Transformation

From the above two equations, it can be seen that control of the power and the reactive power can be obtained by controlling the real and reactive components of the line current (i_{crd} and i_{crq}), separately. It also can be seen from Fig. 4-3 that

$$\alpha = \tan^{-1}\left(\frac{-x_q}{x_d}\right) \tag{4-18}$$

The circuit equations for the series path of UPFC in Fig. 4-2 in per unit can be written as follows:

$$\frac{d}{dt}\begin{bmatrix} i_{cra} \\ i_{crb} \\ i_{crc} \end{bmatrix} = \begin{bmatrix} -\frac{R_{cr}\omega_b}{L_{cr}} & 0 & 0 \\ 0 & -\frac{R_{cr}\omega_b}{L_{cr}} & 0 \\ 0 & 0 & -\frac{R_{cr}\omega_b}{L_{cr}} \end{bmatrix} \begin{bmatrix} i_{cra} \\ i_{crb} \\ i_{crc} \end{bmatrix} + \frac{\omega_b}{L} \begin{bmatrix} v_{ka} - v_{ma} - v_{cra} \\ v_{kb} - v_{mb} - v_{crb} \\ v_{kc} - v_{mc} - v_{crc} \end{bmatrix} \tag{4-19}$$

By performing extended Park's transformation to (10) using V_m as the reference, the

circuit equations in the rotating reference frame are

$$\frac{d}{dt}\begin{bmatrix} i_{crd} \\ i_{crq} \end{bmatrix} = \begin{bmatrix} -\omega_b \frac{R}{L} & \omega \\ -\omega & -\omega_b \frac{R}{L} \end{bmatrix} \begin{bmatrix} i_{crd} \\ i_{crq} \end{bmatrix} + \frac{\omega_b}{L} \begin{bmatrix} v_{kd} - v_{md} - v_{crd} \\ v_{kq} - v_{mq} - v_{crq} \end{bmatrix} \tag{4-20}$$

where $v_{md} = |v_m|$, $v_{mq} = 0$ and the other variables can be calculated using (4-15).

Controlling the series inverter voltage vector as:

$$v_{crd} = v_{kd} - |v_m| + L \cdot i_{crq} - L \cdot x_1 \tag{4-21}$$

$$v_{crq} = v_{kq} - L \cdot i_{crd} - L \cdot x_2 \tag{4-22}$$

then

$$\frac{d}{dt}\begin{bmatrix} i_{crd} \\ i_{crq} \end{bmatrix} = \begin{bmatrix} -\omega_b \frac{R}{L} & 0 \\ 0 & -\omega_b \frac{R}{L} \end{bmatrix} \begin{bmatrix} i_{crd} \\ i_{crq} \end{bmatrix} + \begin{bmatrix} x_1 \\ x_2 \end{bmatrix} \tag{4-23}$$

According to (4-23), a decoupled control of the currents, and thus the power, is achieved since i_{crd} and i_{crq} are only responding to x_1 and x_2 respectively.

Let

$$x_1 = (K_p + \frac{K_i}{s})(i_{crd\_ref} - i_{crd}) \tag{4-24}$$

$$x_2 = (K_p + \frac{K_i}{s})(i_{crq\_ref} - i_{crq}) \tag{4-25}$$

Substitution of both (4-24) and (4-25) into (4-23) yields the closed loop transfer function between the currents and their references, which is

$$\frac{i_{crd/q}}{i_{crd/q\_ref}} = \frac{K_p s + K_i}{s^2 + (\omega_b \frac{R}{L} + K_p)s + K_i} \tag{4-26}$$

By choosing K_p and K_i, $i_{crd/q}$ will be able to track i_{crd/q_ref} in the desired way. The

current reference can be calculated easily from (4-16) and (4-17).

The control block diagram is depicted in Fig. 4-4. In this figure, superscript "*" represents the reference value and "SF" represents a smoothing filter.

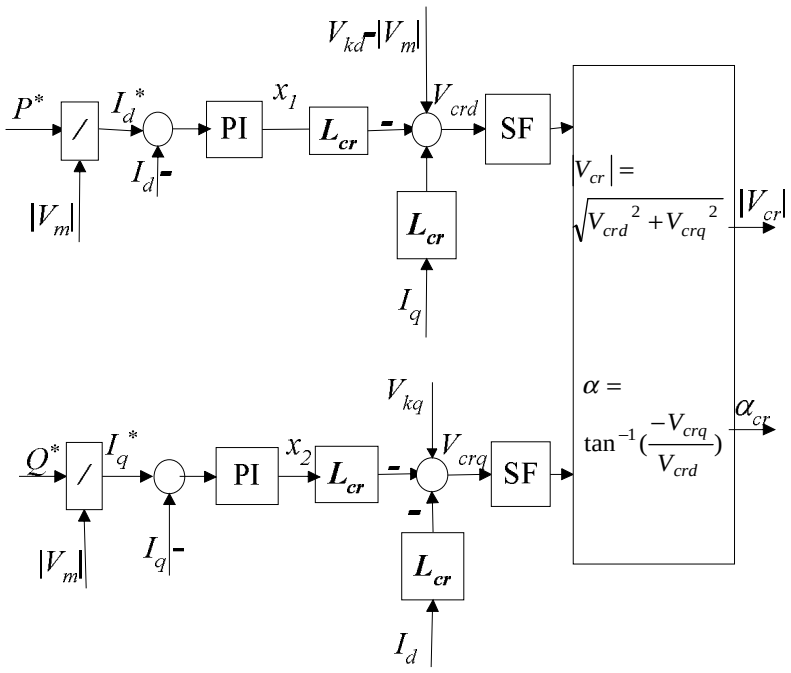

Fig. 4-4 Block Diagram for series converter control

Optionally, the shunt converter may provide reactive power to control the voltage magnitude at the UPFC's sending end bus. If a constant dc terminal voltage is required, the shunt converter also needs to generate or absorb real power to the dc terminal as demanded by the series converter. In contrast to the series converter, the shunt converter operates under a closed-loop current control structure whereby the shunt real and reactive power components are controlled independently [56]. Therefore, the control strategy of the shunt converter will be different from that of the series converter. The d-axis and the q-axis current control loops are separate from each other. Since the real and reactive power references for the shunt converter are not readily available, the

shunt converter current references are generated by the outer control loops which are responsible for the voltage control. Inner feedback control loops are used to regulate the converter currents by adjusting the corresponding converter voltage elements. The control block diagram for the shunt converter is shown in Fig. 4-5. The d-q decomposition is performed with reference to sending end bus voltage V_k. As seen in this figure, the d-axis current will be regulated by the q-axis voltage and the q-axis current will be regulated by the d-axis voltage. For the voltage control loop, a slope setting can be introduced (set values for K_{s1} and K_{s2}) to allow the terminal voltages to vary in proportion with the compensating currents. If the dc capacitor voltage is allowed to vary according to the prevailing shunt compensation demand to reduce the converter losses and harmonics [56], then the upper part of Fig. 4-5 will control the angle α directly instead of V_{vrd} so that the shunt converter may keep a constant maximum voltage modulation ratio between the converter output voltage and the dc-capacitor voltage. In this case the shunt converter of UPFC will operate like a Static Var Compensator [48].

The dynamics on the dc capacitor can be derived easily from the power balance equation. The power unbalance on the dc capacitor will cause the voltage variation as shown in (4-27)

$$CV_{dc}\frac{dV_{dc}}{dt} = real(V_{vr}\cdot I_{vr}^{\ *} + V_{cr}\cdot I_{cr}^{\ *}) \tag{4-27}$$

The overall block diagram of the UPFC control and the interface with power system is shown in Fig. 4-6.

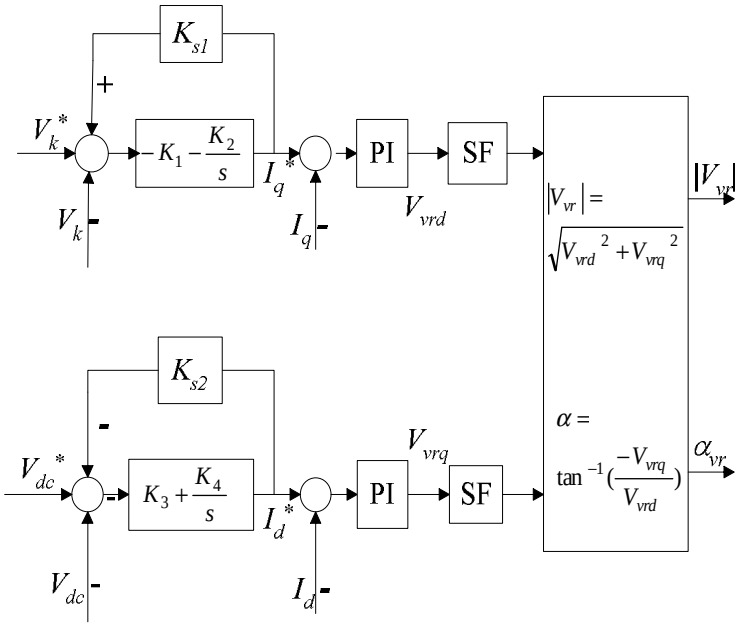

Fig. 4-5 Block Diagram for shunt converter control

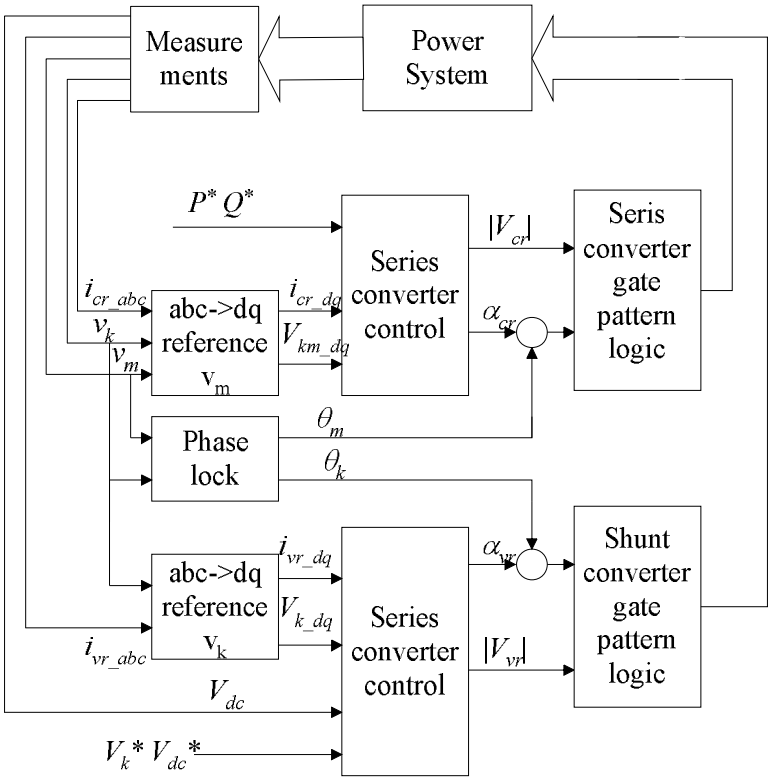

Fig. 4-6 Overall structure of UPFC control and interface with power system

Time domain Simulation of the Power System with UPFC

The previous section elaborated on the series and shunt converter control blocks shown in Fig. 4-6. In this section, the interface of UPFC with the power system for time domain simulation is discussed.

Power System Reduction in Transient Simulation

In transient stability analysis, in order to simplify the system analysis, it is a common practice to reduce the system to the generator internal nodes. First, the original system network is expanded to include both the generator internal nodes and the loads so that current injections at all the buses in the expanded network, except for the generator internal nodes, are all zeros. The constant impedance loads are represented as the equivalent admittance calculated from the pre-fault load-flow values $Y_1 = (P_{load} - jQ_{load})/V^2$. The generators are modeled as a voltage source behind the direct-axis transient reactance. The original system admittance matrix is modified to include both the load admittance and the generator transient reactance and these values will be added to the diagonal elements of the admittance matrix. Self admittance matrix for generator internal nodes and mutual admittance matrices between the generator buses and the generator internal nodes for the extended system are also created. The current injection equations for all the nodes of the extended system can be written as

$$\begin{bmatrix} 0 \\ I_g \end{bmatrix} = \begin{bmatrix} Y_{bus}^{n} & Y_{12} \\ Y_{21} & Y_{22} \end{bmatrix} \begin{bmatrix} V \\ E \end{bmatrix} \tag{4-28}$$

where

$Y_{bus}{}^{n}$ is the modified admittance matrix for the original system

Y_{12} and Y_{21} are the mutual admittance matrices between the generator buses and the generator internal nodes

Y_{22} is the self admittance matrix for generator internal nodes

V is the voltage vector of the original system buses

E is the internal voltage vector of the generators

I_g represents the current injection vector into the generator internal nodes.

Elimination of V from the above equation (Kron reduction) will lead to the admittance matrix of the reduced system

$$Y_{red} = Y_{22} - Y_{21} \cdot Y_{bus}^{n\ -1} \cdot Y_{12} \tag{4-29}$$

and the reduced system equation is

$$I_g = Y_{red} \cdot E \tag{4-30}$$

Using (4-28), the load bus voltages can be written as

$$V = Y_{bus}^{n\ -1} Y_{12} \cdot E \tag{4-31}$$

Power System Reduction When UPFC is Included

When a UPFC is included in the power system, the above system reduction method is adopted with some modifications. We want to include the UPFC buses in the reduced system. The system network is first divided into two parts: a system without UPFC and UPFC only as shown in Fig. 4-7. The Kron reduction is performed on the system without UPFC and this sub-system is reduced to the generator internal nodes and the UPFC sending and receiving end buses. The system equations can be written as

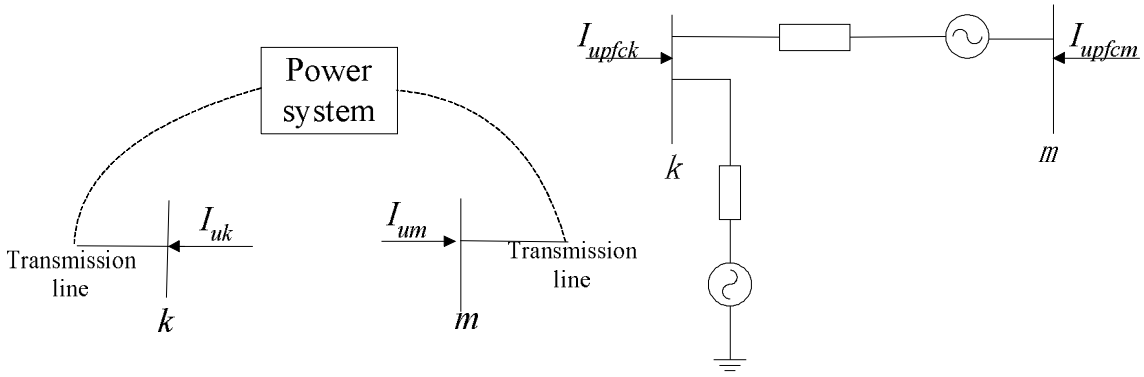

Fig. 4-7 System Division

$$\begin{bmatrix} 0 \\ I_u \\ I_g \end{bmatrix} = \begin{bmatrix} Y_{11} & Y_{12} & Y_{13} \\ Y_{21} & Y_{22} & Y_{23} \\ Y_{31} & Y_{32} & Y_{33} \end{bmatrix} \begin{bmatrix} V \\ V_u \\ E \end{bmatrix} \tag{4-32}$$

where

V is the voltage vector of the original system bus except for the UPFC buses

E is the internal voltage vector of the generators

V_u is the UPFC bus voltage vector, $V_u = [V_k, V_m]^T$

I_u is the current injection vector at UPFC buses, $I_u = [I_{uk}, I_{um}]^T$

I_g is the current injection vector into the generator internal nodes.

By eliminating V from (4-32), the equations of the reduced system can be obtained as

$$\begin{aligned} I_u &= (Y_{22} - Y_{21}Y_{11}^{-1}Y_{12})V_u + (Y_{23} - Y_{21}Y_{11}^{-1}Y_{13})E \\ &= Y_{uu}V_u + Y_{ue}E \end{aligned} \tag{4-33}$$

$$I_g = (Y_{32} - Y_{31}Y_{11}^{-1}Y_{12})V_u + (Y_{33} - Y_{31}Y_{11}^{-1}Y_{13})E \tag{4-34}$$

and the load bus voltages can be calculated as

$$V = -Y_{11}^{-1}Y_{12} \cdot V_u - Y_{11}^{-1}Y_{13}E \tag{4-35}$$

Newton-Raphson Iteration to Calculate Bus Voltages

While considering the UPFC diagram shown in the right part of Fig. 4-7, the current injection at the UPFC buses can also be calculated as

$$\begin{bmatrix} I_{upfck} \\ I_{upfcm} \end{bmatrix} = \begin{bmatrix} y_{cr} + y_{vr} & -y_{cr} & -y_{vr} & -y_{cr} \\ -y_{cr} & y_{cr} & 0 & y_{cr} \end{bmatrix} \begin{bmatrix} V_k \\ V_m \\ V_{vr} \\ V_{cr} \end{bmatrix} \tag{4-36}$$

where V_{vr} and V_{cr} are related with V_k and V_m by

$$V_{vr} = |V_{vr}| \cdot \exp(j(\theta_k + \alpha_{vr})) \tag{4-37}$$

$$V_{cr} = |V_{cr}| \cdot \exp(j(\theta_m + \alpha_{cr})) \tag{4-38}$$

where α_{cr} and α_{vr} are already defined in Fig. 4-4 and Fig. 4-5, respectively, and θ_k and θ_m are the angles of V_k and V_m.

Let

$$I_{upfc} = \begin{bmatrix} I_{upfck} \\ I_{upfcm} \end{bmatrix}, \theta_u = \begin{bmatrix} \theta_k \\ \theta_m \end{bmatrix}, \alpha = \begin{bmatrix} \alpha_{vr} \\ \alpha_{cr} \end{bmatrix} \text{ and } V_{upfc} = \begin{bmatrix} V_{vr} \\ V_{cr} \end{bmatrix}$$

then

$$V_{upfc} = |V_{upfc}| \bullet \exp(j(\theta_u + \alpha)) \tag{4-39}$$

$$I_{upfc} = \begin{bmatrix} Y_{u1} & Y_{u2} \end{bmatrix} \cdot \begin{bmatrix} V_u \\ V_{upfc} \end{bmatrix} \tag{4-40}$$

where "$\bullet$" indicates vector dot product.

Given that

$$I_{upfc} + I_u = 0 \tag{4-41}$$

The combination of (4-33), (4-39) and (4-40) will yield

$$I_{upfc} + I_u = (Y_{uu} - Y_{u1})V_u - Y_{u2} \mid V_{upfc} \mid \bullet \exp(\, j(\theta_u + \alpha)) + Y_{ue}E = 0 \qquad (4\text{-}42)$$

(4-42) is a non-linear function and the unknowns are V_u including magnitude $|V_u|$ and phase θ_u. The current balance is used as the criteria, and the Newton-Raphson algorithm is chosen for the iteration process due to its quadratic convergence characteristics. The iteration process is demonstrated in the following sets of equations. At each step the current balance $I_{upfc}+I_u$ is calculated and the variation of the voltage variables is calculated by

$$\begin{bmatrix} real(I_{upfc} + I_u) \\ imag(I_{upfc} + I_u) \end{bmatrix} = \begin{bmatrix} N & P \\ Q & R \end{bmatrix} \cdot \begin{bmatrix} \Delta \mid V_u \mid \\ \Delta\theta_u \end{bmatrix} \qquad (4\text{-}43)$$

$$\begin{bmatrix} \Delta \mid V_u \mid \\ \Delta\theta_u \end{bmatrix} = J_{upfc}^{-1} \cdot \begin{bmatrix} real(I_{upfc} + I_u) \\ imag(I_{upfc} + I_u) \end{bmatrix} \qquad (4\text{-}44)$$

The voltage variables are updated by

$$\begin{bmatrix} |V_u|^{new} \\ \theta_u^{new} \end{bmatrix} = \begin{bmatrix} |V_u|^{old} \\ \theta_u^{old} \end{bmatrix} - \begin{bmatrix} \Delta \mid V_u \mid \\ \Delta\theta_u \end{bmatrix} \qquad (4\text{-}45)$$

where $J_{upfc} = \begin{bmatrix} N & P \\ Q & R \end{bmatrix}$ is the Jacobian matrix and the dimension of J_{upfc} is $2n \times 2n$, where n is the number of UPFCs in the power system. Obviously the order of the Jacobian matrix is not large and the calculation burden is well controlled.

Then the elements in this Jacobian Matrix are calculated as follows.

$$\begin{aligned} N &= \frac{\partial real(I_{upfc} + I_u)}{\partial |V_u|} \\ &= B\_r \cdot diag(\cos(\theta_u)) - B\_i \cdot diag(\sin(\theta_u)) \end{aligned} \qquad (4\text{-}46)$$

$$Q = \frac{\partial imag(I_{upfc} + I_u)}{\partial |V_u|} = B\_r \cdot diag(\sin(\theta_u)) + B\_i \cdot diag(\cos(\theta_u)) \tag{4-47}$$

$$\begin{aligned} P &= \frac{\partial real(I_{upfc} + I_u)}{\partial \theta_u} \\ &= -B\_r \cdot diag(|V_u|) \cdot diag(\sin(\theta_u)) - B\_i \cdot diag(|V_u|) \cdot diag(\cos(\theta_u)) \\ &\quad + Y_{u2\_r} \cdot diag(|V_{upfc}|) \cdot diag(\sin(\theta_u + \alpha)) \\ &\quad + Y_{u2\_i} \cdot diag(|V_{upfc}|) \cdot diag(\cos(\theta_u + \alpha)) \end{aligned} \tag{4-48}$$

$$\begin{aligned} R &= \frac{\partial imag(I_{upfc} + I_u)}{\partial \theta_u} \\ &= B\_r \cdot diag(|V_u|) \cdot diag(\cos(\theta_u)) - B\_i \cdot diag(|V_u|) \cdot diag(\sin(\theta_u)) \\ &\quad - Y_{u2\_r} \cdot diag(|V_{upfc}|) \cdot diag(\cos(\theta_u + \alpha)) \\ &\quad + Y_{u2\_i} \cdot diag(|V_{upfc}|) \cdot diag(\sin(\theta_u + \alpha)) \end{aligned} \tag{4-49}$$

where $B = Y_{uu} - Y_{u1}$, $B\_r = real(B)$, $B\_i = imag(B)$, $Y_{u2\_r} = real(Y_{u2})$, and $Y_{u2\_i} = imag(Y_{u2})$.

After the UPFC bus voltages are obtained, the load bus voltages can be calculated using (4-35).

It is feasible to expand the reduced system equations and the associated Jacobian matrix following the same strategy when the system has load buses other than constant impedance loads. The reduced system equations can be extended to include those buses. A similar Newton-Raphson iteration process can be taken to calculate the voltage of UPFC buses and those load buses.

Modeling of Fundamental Operating Constraints

Some practical operating constraints need to be considered for the modeling of UPFC

converter control. The magnitude of the series and shunt injected voltages is limited by their voltage rating. Each converter has a nominal current rating at which level it can operate continuously. Also, since in most cases the UPFC is located in a substation, the receiving end bus will be on the outgoing line side of the equipment. The UPFC has an intrinsic ability to raise or lower the magnitude of the receiving end bus voltage by a large fraction [53]. In order not to put too much voltage stress on the line, proper limits will be imposed on the allowable magnitude of the receiving end bus voltage (for example, 20% or less). These constraints will affect the achievable magnitude and phase of the two voltage sources. Referring to Fig. 4-2, these constrains can be represented as $|V_{cr}| < V_{cr\_r}$, $|V_{vr}| < V_{vr\_r}$, $|I_{vr}| < I_{vr\_r}$ and $|I_{cr}| < I_{cr\_r}$, $V_{m\_\min} < |V_m| < V_{m\_\max}$, where subscript *r* represents the rating.

Applying Voltage Limits To Converters

Setting the voltage magnitude limits for the converters is straightforward. These limits can be applied to the simulation by adding hard limits to the control output $|V_{cr}|$ and $|V_{vr}|$ in Figs. 3 and 4, respectively.

Applying Current Limit To Shunt Converter

For the shunt inverter current, as can be seen from Fig. 4-5, I_{vrd} is related to the power balance between the two converters, no limit will be imposed on I_{vrd}. This gives the priority to the constant V_{dc} control and leaves the remaining capability of the shunt converter for sending end bus voltage control [54]. Therefore, limits will be imposed to both I_{vrq}^{*} and I_{vrq}, as shown in equation 35.

$$I_{vrq\_l} \text{ and } I_{vrq\_l}{}^{*} = \sqrt{I_{vr\_r}{}^{2} - I_{vrd}{}^{2}} \tag{4-50}$$

Ignoring the resistance of the coupling transformer, the current equation of the shunt path of the UPFC is

$$V_{k\_abc} - I_{vr\_abc} \cdot (jX_{cr\_abc}) = V_{vr\_abc} \tag{4-51}$$

Applying extended Park's transform to the above equation using V_k as the reference, the decomposed current equations are

$$|V_k| - I_{vr\_q} \cdot X_{vr} = V_{vr\_d} \tag{4-52}$$

$$I_{vr\_d} \cdot X_{vr} = V_{vr\_q} \tag{4-53}$$

To make $|I_{vr\_q}| < I_{vrq\_l}$, proper limits should be imposed on V_{vr_d}. From equation (4-52), the following limits for V_{vr_d} can be derived.

$$|V_k| - I_{vrq\_l} \cdot X_{vr} < V_{vr\_d} < |V_k| + I_{vrq\_l} \cdot X_{vr} \tag{4-54}$$

Applying Current Limit To Series Converter

A similar procedure can be applied to solve the series converter current constraint. The current equation of the series path of the UPFC is

$$V_k - V_{cr} - jI_{cr} \cdot X_{cr} = V_m \tag{4-55}$$

The decomposed current equations for the series path of the UPFC (using V_m as the reference) are

$$V_{kd} - |V_m| - I_{crq} \cdot X_{cr} = V_{crd} \tag{4-56}$$

$$V_{kq} + I_{crd} \cdot X_{cr} = V_{crq} \tag{4-57}$$

It can be seen from the above two equations that V_{cr_d} and V_{cr_q} are on a circle, which

has the center $(V_{k\_d} - |V_m|, V_{k\_q})$ and the radius $|I_{cr}| \cdot X_{cr}$, i.e.,

$$(V_{crd} + |V_m| - V_{kd})^2 + (V_{crq} - V_{kq})^2 = |I_{cr}|^2 \cdot {X_{cr}}^2 \tag{4-58}$$

If we let the left part of equation (4-58) be smaller than ${I_{cr\_r}}^2 \cdot {X_{cr}}^2$, the series converter current constraint can be achieved. But in simulation, it is found that the series converter current is actually well defined within the limit when the proper voltage limit is imposed on the injected series voltage.

Applying Voltage Limits to the Receiving End Bus

The voltage constraints and the current constraints for the converters correspond to the physical limitation of the UPFC. But this receiving end bus voltage limitation is an operating problem. The relationship between the receiving end bus voltage and the UPFC variables is described in equation (4-55). The diagram of Fig. 4-8 shows this relationship.

One approach to solve this problem is to adjust the angle of V_{cr} so that it is possible that the magnitude of V_m will fall into the allowable range. Let $V = V_k - jI_{cr} \cdot X_{cr}$, and rewrite $V = |V| \cdot \exp(j\theta)$. From (4-55), the magnitude of V_m can be calculated as

$$|V_m| = \sqrt{|V|^2 + |V_{cr}|^2 - 2|V| \cdot |V_{cr}| \cdot \cos(\theta - \theta_{cr})} \tag{4-59}$$

To ensure $V_{m\_\min} < |V_m| < V_{m\_\max}$, from (4-59), the following constraints should be met

$$\cos(\theta - \theta_{cr}) < \frac{|V|^2 + |V_{cr}|^2 - {V_{m\_\min}}^2}{2 \cdot |V| \cdot |V_{cr}|} \tag{4-60}$$

$$\cos(\theta - \theta_{cr}) > \frac{|V|^2 + |V_{cr}|^2 - {V_{m\_\max}}^2}{2 \cdot |V| \cdot |V_{cr}|} \tag{4-61}$$

The allowable range of θ_{cr} can be obtained from the above two equations. Thus the allowable range of α_{cr} can also be obtained since $\alpha_{cr} = \theta_{cr} - \theta_m$.

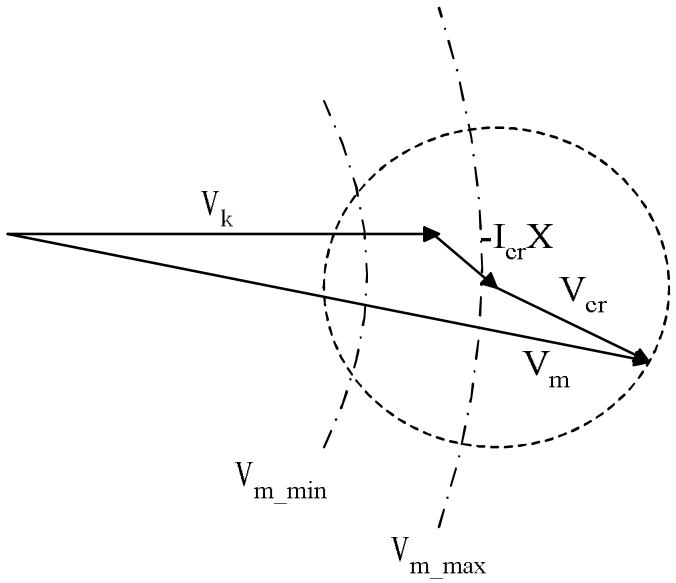

Fig. 4-8 Constraints on V_m

If either equation (4-60) or (4-61) is ill-conditioned, i.e. the right side of (4-60) is smaller than -1 or the right side of (4-61) is larger than 1, an adjustment to the $|V_{cr}|$ should be made. Again from equation(4-59), the following two equations are derived for solving the allowable range of $|V_{cr}|$.

$$|V_{cr}|^2 - 2|V||V_{cr}|\cos(\theta - \theta_{cr}) + |V|^2 - V_{m\_\max}{}^2 \le 0 \qquad (4\text{-}62)$$

$$|V_{cr}|^2 - 2|V||V_{cr}|\cos(\theta - \theta_{cr}) + |V|^2 - V_{m\_\min}{}^2 \ge 0 \qquad (4\text{-}63)$$

Solving UPFC constraints in simulation

All the above constraints given in equations (4-54), (4-58) and (4-60)-(4-63) are derived based on the steady-state circuit equations for UPFC. In transient simulation, however, all the other voltage variables in these equations are also varying. Therefore,

in transient simulation, another iteration loop is introduced to combine these equations together with power flow calculation to solve for the constraint problem. After the power flow calculation is performed, those constraints are checked for violation. If there is some violation, proper adjustment to the UPFC converter control output is made and the new values for the converter control output are used to perform another power flow calculation until no constraints are violated. The flow chart of the process is shown in Fig. 4-9.

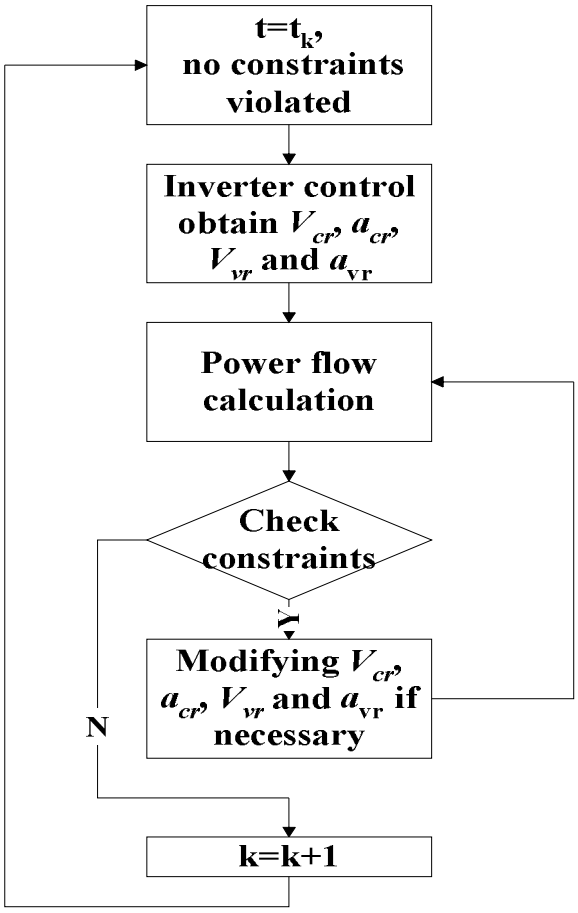

Fig. 4-9 Flow chart for solving the UPFC constraints in transient simulation

Damping Controller Design for UPFC

A supplementary damping controller can be designed to increase the inter-area oscillation damping and keep the system stable. The same method proposed for damping controller design for SVC and TCSC is adopted here. Fig. 4-10 (a) shows the control block diagram for the damping controller design. As seen in this figure, a damping signal is introduced to the voltage or power reference point of the UPFC. y is a power system variable that contains the oscillation information and it is used as the input to the damping controller. The candidates for y are inter-area speed, power on the parallel transmission line and bus voltage. The linearized closed loop system diagram is shown in Fig. 4-10 (b), where Δy is the control input signal deviation from its steady-state value (obtained by passing y through a washout filter), $G(s)$ represents the plant model (which is the open loop transfer function between Δy and ΔV_{ref} or ΔP_{ref}), and $H(s)$ is the transfer function of the damping controller. When the damping signal is added to the power reference or voltage reference, the controlled power flow or bus voltage will have some variations to counteract the oscillation in the power exchange between two areas. In most applications UPFC will be installed in a substation, and V_k will be the substation voltage. In order not to put too much stress on the substation voltage control, we add the damping signal to the power reference point of the UPFC.

The transfer function of G(s) can by obtained by linearizing all the equations associated with the UPFC and its control. However, as seen in the modeling, there are two synchronous rotating systems (with references to be Vk and Vm, respectively) in the UPFC model, the linearization can be somehow difficult. Also, the obtained transfer

function could be of a large order with lots of modes which are either poorly observable or controllable. Therefore, the transfer function for $G(s)$ is again obtained via PRONY method in the form of

$$G(s) = \frac{Y(s)}{I(s)} = \sum_{i=1}^{n} \frac{R_i}{s - \lambda_i} \tag{4-64}$$

where R_i is the residue associated with the identified mode λ_i. R_i indicates how far the corresponding eigenvalue can be moved through feedback

.Based on the eigenvalue sensitivity

$$\frac{\partial \lambda_i}{\partial K} = R_i \frac{\partial (K \cdot H(\lambda_i))}{\partial K} = R_i H(\lambda_i) \tag{4-65}$$

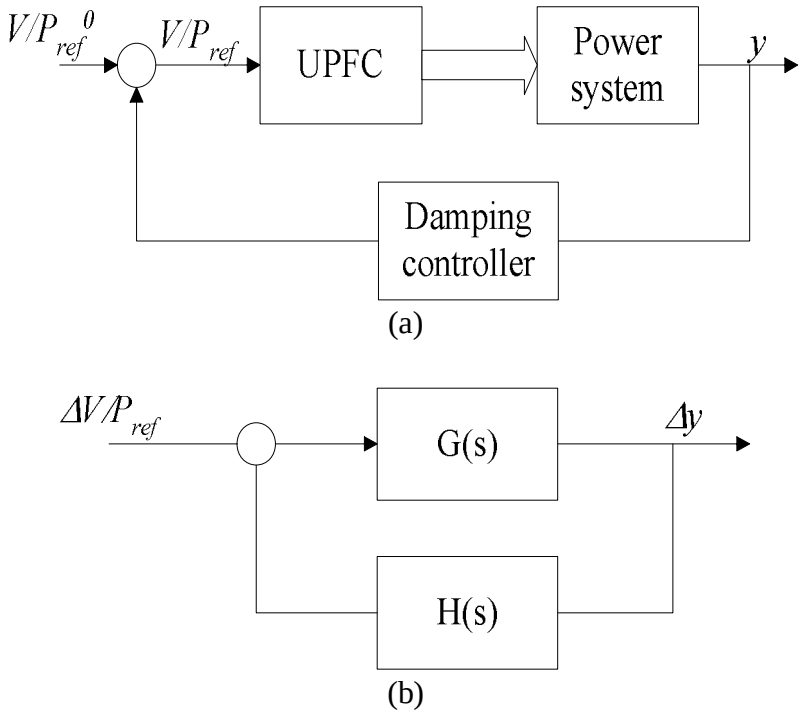

Fig. 4-10 System diagram for UPFC damping controller design

The effect of the controller transfer function in the feedback path is to modify the sensitivity of the eigenvalue of the original system by the value of the controller transfer function evaluated at the original eigenvalue. $H(s)$ is designed to move the loci of the inter-area modes to the left in the complex plane as they depart from the open loop poles. Then the gain of the controller is chosen from the root locus plot for a good damping ratio.

The two area system used in this study is shown in Fig. 4-11. The UPFC is installed on one transmission line. It should control the power flow on line 102-13 and also provide voltage support at bus 101. A pulse signal which lasts for about 0.1 sec is added to the power reference of the UPFC. The responses of the inter-area speed and the power on line 101-13 are shown in Fig. 4-12.

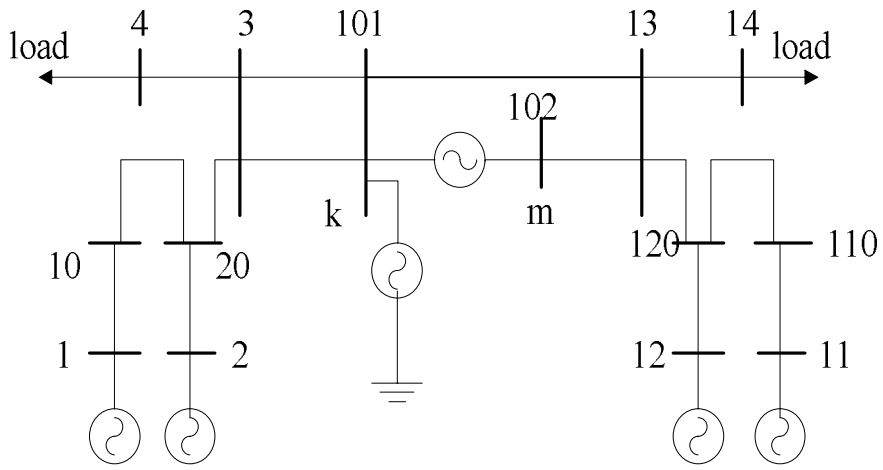

Fig. 4-11. Two Area System

The transfer functions between the two output signals and the power reference are identified and the results are shown in Tables 4-1 and 4-2. Damping controllers are designed based on the phase compensation idea mentioned above. When using inter-area

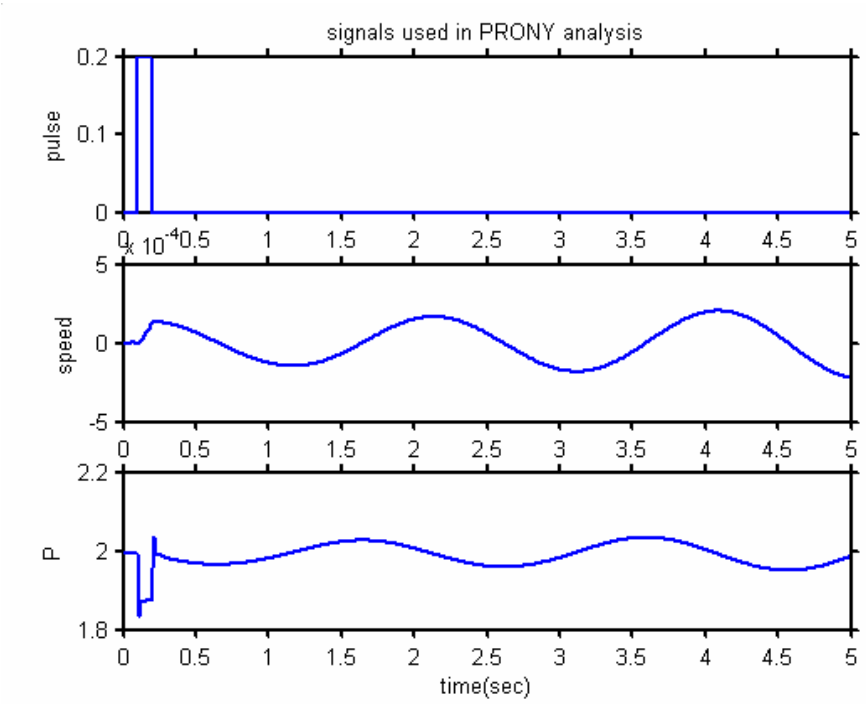

Fig. 4-12 The input and output signals for PRONY analysis

speed as the feedback input, the damping controller designed is a pure gain. When using the parallel line power as the feedback input, the transfer function of the damping controller is

$$H(s) = K\frac{1+0.12s}{1+0.7s}\frac{1+0.12s}{1+0.8s} \tag{4-66}$$

Then root locus plot is then used to determine the gain of the damping controller which leads to a satisfactory damping ratio. The bode plots for the two cases are shown in Figs.4-13 to 4-15. It is observed from Fig. 4-13 that an almost pure damping torque is introduced to the system when the inter-area speed is used as the damping controller input. When using the parallel line power as the controller input, the damping controller does move the unstable inter-area mode to the left half plane as seen in Fig. 4-15. But it also introduces a mode into the system which moves towards the right half plane shown

in Fig. 4-14. So the achievable maximum damping ratio for the inter-area mode is quite limited. Thus, for this two area system, the inter-area mode is chosen as the damping controller input

Table 4-1 Identified Modes and residues of the transfer function between the inter-area speed and the P_{ref}

Mode #	Mode	Residue
1	0.1083 + 3.2162i	3.3149e-003 - 2.5943e-004i
2	-19.074+11.266i	-1.0215e-003 + 3.2597e-003i
3	-7.6072	-2.3600e-004
4	-19.710	4.3090e-003
5	-0.6039 + 6.9219i	7.9764e-005 - 1.4096e-005i

Table 4-2 Identified Modes and residues of the transfer function between the parallel line power and the P_{ref}

Mode #	Mode	Residue
1	-28.333	1.9415
2	0.1083+3.2161i	0.0339 +0.6793i
3	-17.516 +77.552i	0.242+.0302i
4	-18.95+63.815i	0.196+0.13981i
5	-20.57+48.054i	0.025 +0.113i
6	-1.2529	-0.0865
7	-0.7814	0.0544
8	-0.6135 +6.9041i	-.0013+.026i
9	-14.083 +14.594i	0.0122-0.0004i

.

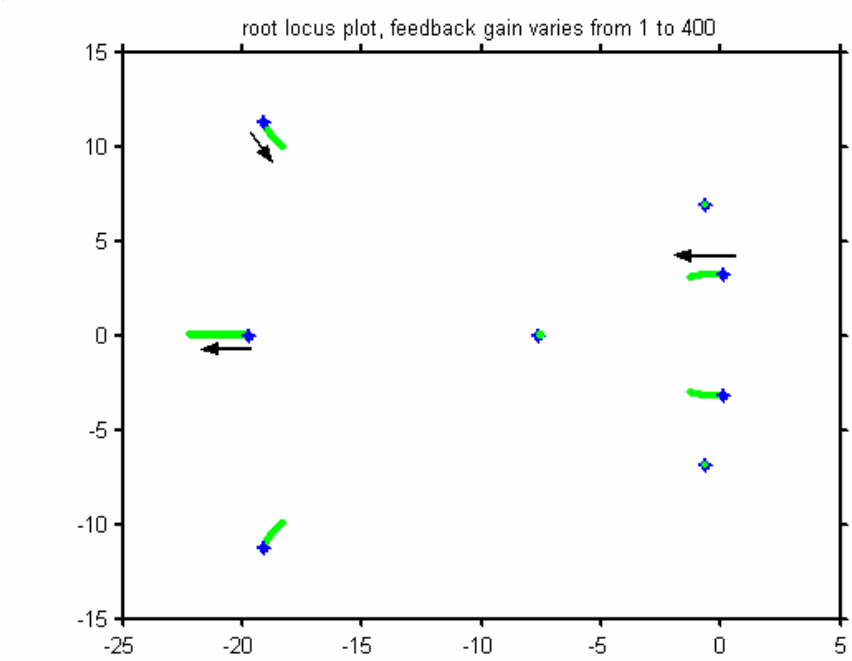

Fig. 4-13 Root Locus plot for damping controller design, using inter-area speed as the controller input

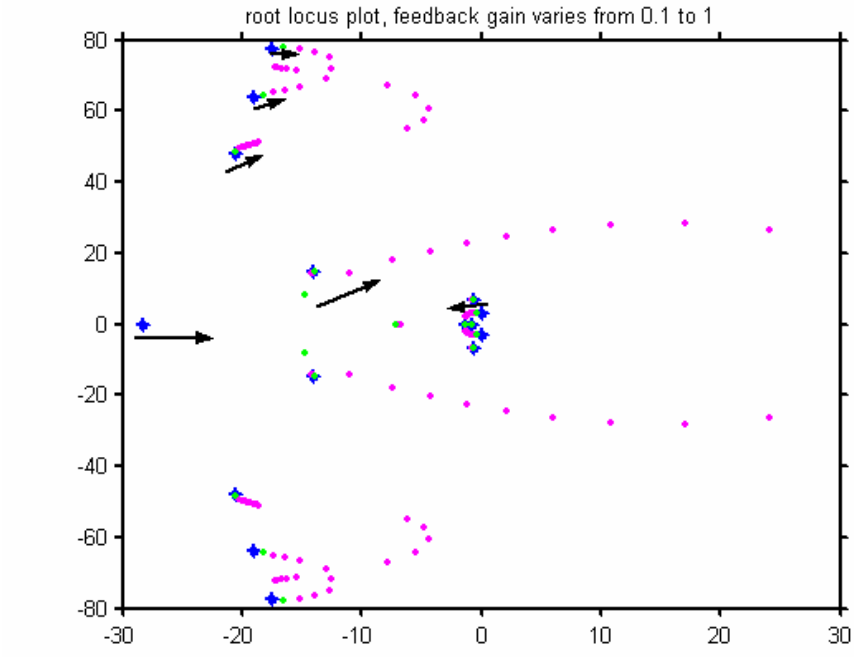

Fig. 4-14 Root Locus plot for damping controller design, using parallel line power as the controller input

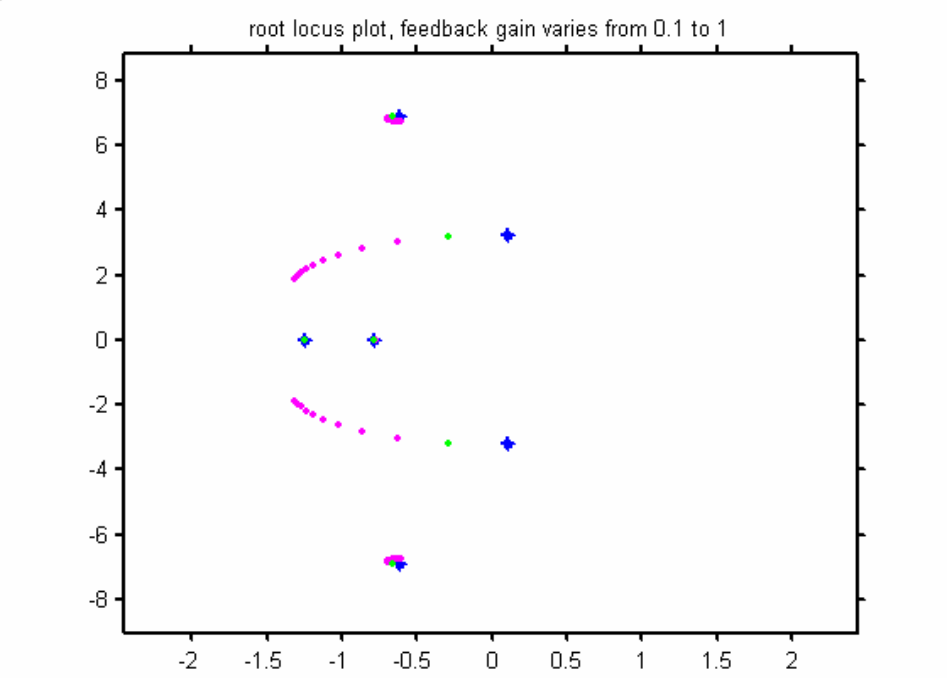

Fig. 4-15 Enlarged parts of the root Locus plot of Fig. 4-12 around the area of inter-area mode

Simulation Results

To test the modeling accuracy and dynamic performance of the UPFC, simulation studies are performed on a two area system shown in Fig. 4-14. This is a modified two area system given in [58]. A UPFC is installed on one transmission line as shown between bus 101 and bus 102. At both buses 4 and 14, there are half of the loads that are constant current loads. The UPFC is supposed to control the power flow on line 102-13 and provide reactive power for voltage support at bus 101. At nominal operating condition, there is about 4 p.u. power transferred on the transmission line from left to right, and line 102-13 carries half of the power transfer.

Rating and parameters of the UPFC

The rating of the UPFC is not the same as that of a traditional electromagnetic device. The UPFC has maximum voltage and current ratings that are almost completely independent of each other [55]. Also, the UPFC does not have the short time thermal reserve capability as most of the electromagnetic devices. Therefore, sufficient design margin should be applied to the UPFC. In practice, a design margin of 100% or more for both the current and voltage are routinely adopted [55].

In the power system shown in Fig. 4-11, the UPFC would be used to double the transfer capability of line 102-13 so that in case of outage of line 101-13, the UPFC can help in transferring the power needed to supply the load. The UPFC is also required to provide reactive power supply to the power system to keep the voltage constant at bus 101. After a careful power flow analysis, it is determined that the UPFC should be able to transfer a maximum 400MW, 200MVAR power flow on the transmission line and provide a maximum 500 MVAR reactive to the system. Considering a maximum 50 MW power transfer between the two converters, the shunt converter should be able to provide a maximum 50 MW and 500MVAR power flow. The rated voltage (voltage base) on the transmission line is 230KV. At nominal voltage, the full load current for the series converter is $I_{series} = \frac{(400 - j200)\cdot 10^6}{\sqrt{3}\cdot 230\cdot 10^3} = 1123A$. The rated voltage of the series converter and its coupling transformer is 0.4 p.u., which is about 53KV per phase. So the MVA rating of the series converter is $3\cdot 1123\cdot 54\cdot 10^3 = 178MVA$. The ratings of the series coupling transformer are the same as those of the series converter. Normally the leakage reactance of a transformer is about 15% on the winding base when the system

voltage is 230KV [55]. The reactance on the system base can be calculated by equation shown in (4-67).

$$Z_{sys} = Z_{winding} \cdot V_{tran}{}^{2} \cdot \frac{MVA_{sys}}{MVA_{tran}} \tag{4-67}$$

where

Z_{sys} is the reactance on the system base

$Z_{winding}$ is the reactance on the winding base

V_{tran} is the rated voltage of the coupling transformer

MVA_{sys} is the system base MVA

MVA_{tran} is the MVA rating of the coupling transformer

Similar calculations are conducted on the shunt converter and its coupling transformer. Table 4-3 shows the ratings of the UPFC and the parameters for the coupling transformer However, the above ratings are determined based on the steady state power flow analysis. During the transient process, both the voltage and current of the converter will vary. Therefore, both the current and voltage ratings of the converters are doubled to ensure a sufficient safety margin.

Power flow control and voltage control

The performance of the UPFC for power flow control and the voltage control is demonstrated by applying step changes to the voltage and power control references of the UPFC, respectively. Three cases were investigated here. Case 1: a 0.2 p.u. step change is made to the power reference of the UPFC at *t = 0.1sec.* The system responses to this change are shown in Figures 4.16-4.19. Case 2: a 0.2 p.u. step change is made to

the reactive power reference of the UPFC at *t = 0.1sec*. The system responses to this change are shown in Figures 4.20-4.23. Case 3: a 0.05 p.u. step change is made to the voltage reference of the UPFC at *t = 0.1sec*. The system responses to this change are shown in Figures 4.24-4.27. The slope factor in the shunt voltage control is set to zero and the UPFC should control the voltages at the reference level. It can be seen from these figures that the UPFC series converter control guarantees the fast tracking of the power flow to the power reference. The sending end bus voltage and the DC capacitor voltages are also controlled to their references. It is also noted that while the power flow on the transmission line is tightly controlled at the reference level, the bus voltages reveal a low frequency oscillation. The oscillation is about 0.5 *Hz* and is unstable. This indicates the need for a damping controller design.

Table 4-3 The ratings of UPFC and the parameters of the coupling transformer

System MVA base	100 MVA
Rated voltage on transmission line	230 KV
Base current	251A
Rated voltage of the series converter and coupling transformer	53KV/phase, 0.4 p.u.
Full load current of the series converter	1123A, 4.5 p.u.
MVA rating of the series converter	178MVA
Series converter coupling transformer impedance	0.0135 p.u.
Rated voltage of the shunt converter and coupling transformer	160KV/phase, 1.2 p.u.
Full load current of the shunt converter	1261A, 5.0 p.u.
MVA rating of the shunt converter	600MVA
Shunt converter coupling transformer impedance	0.036 p.u.

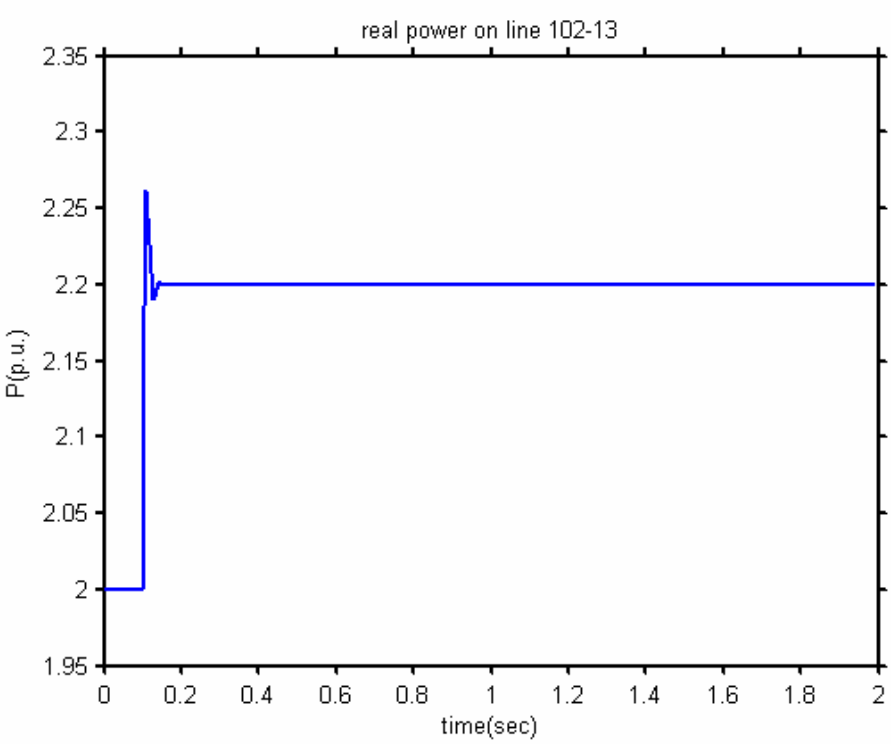

Fig. 4-16 Real power on line 102-13 for case 1

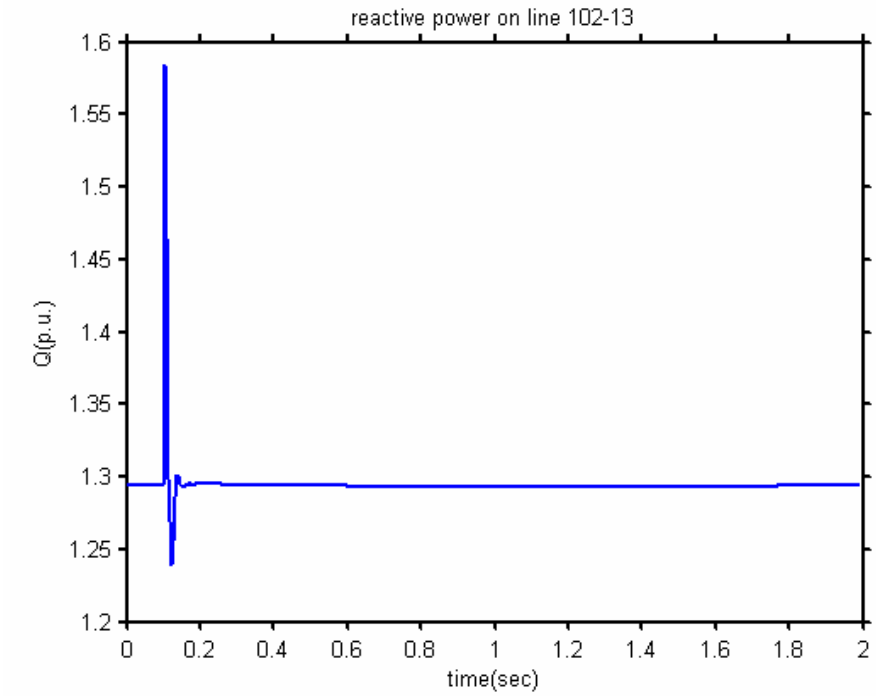

Fig. 4-17 Reactive power on line 102-13 for case 1

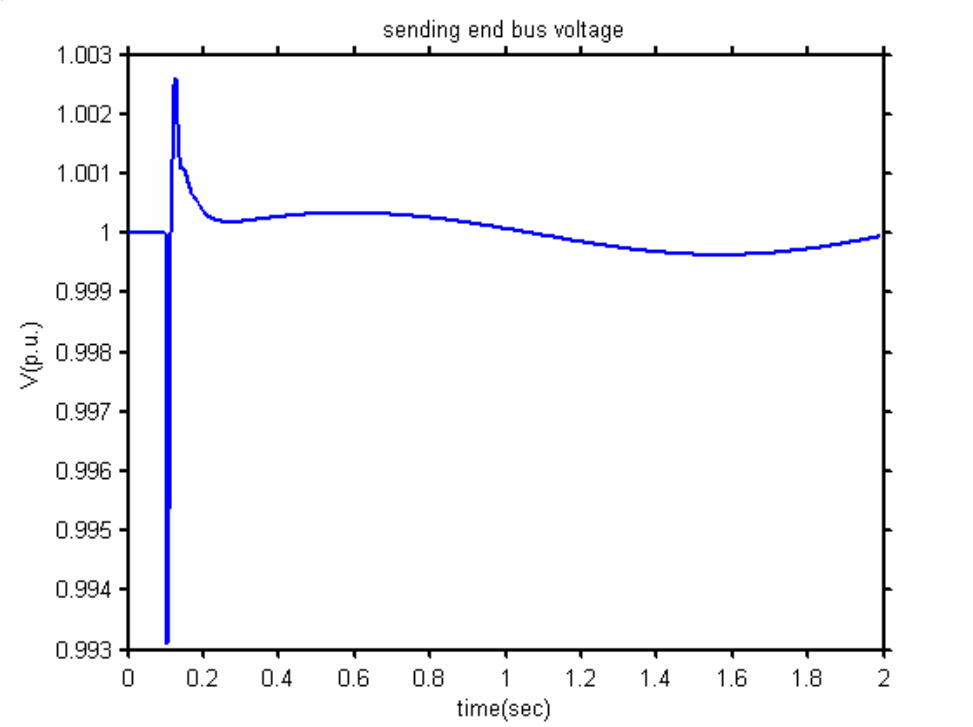

Fig. 4-18 Sending end bus voltage for case 1

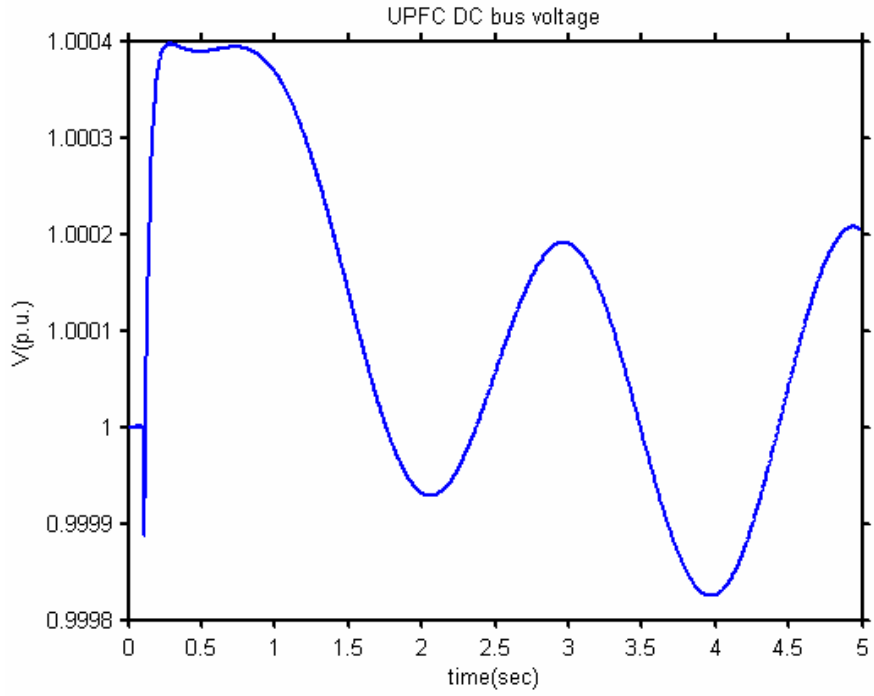

Fig. 4-19 UPFC DC capacitor voltage for case 1

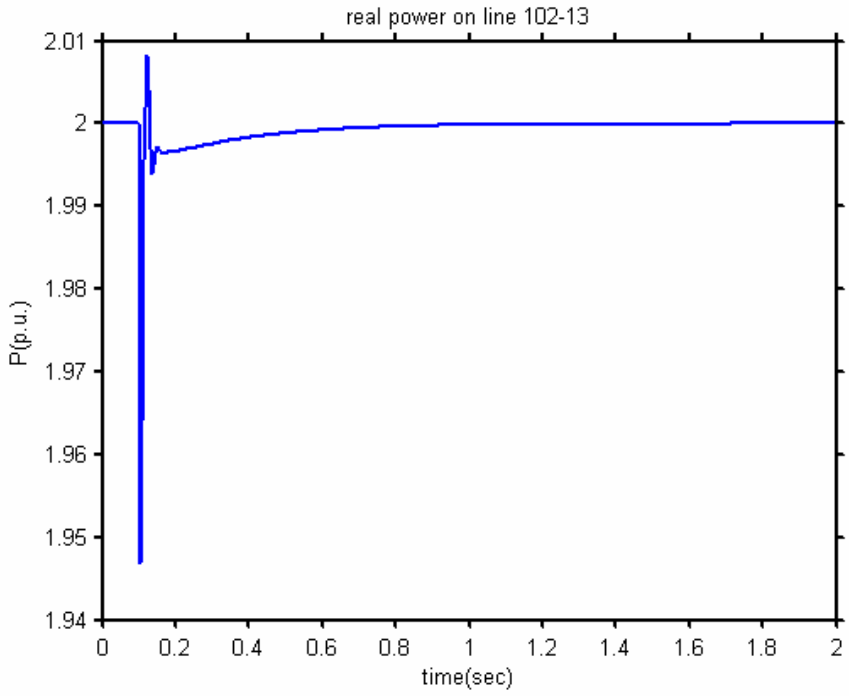

Fig. 4-20 Real power on line 102-13 for case 2

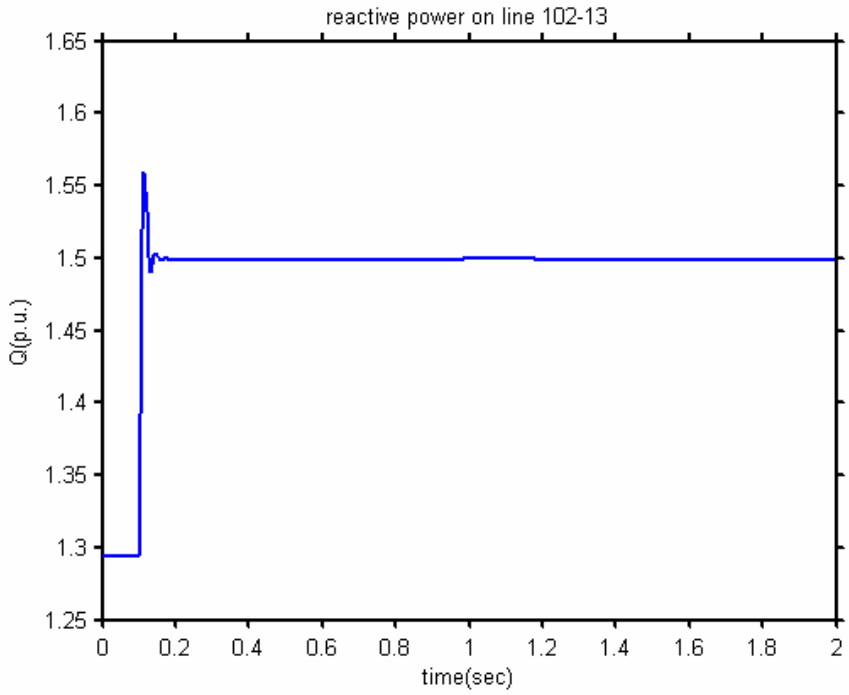

Fig. 4-21 Line reactive power on line 102-13 for case 2

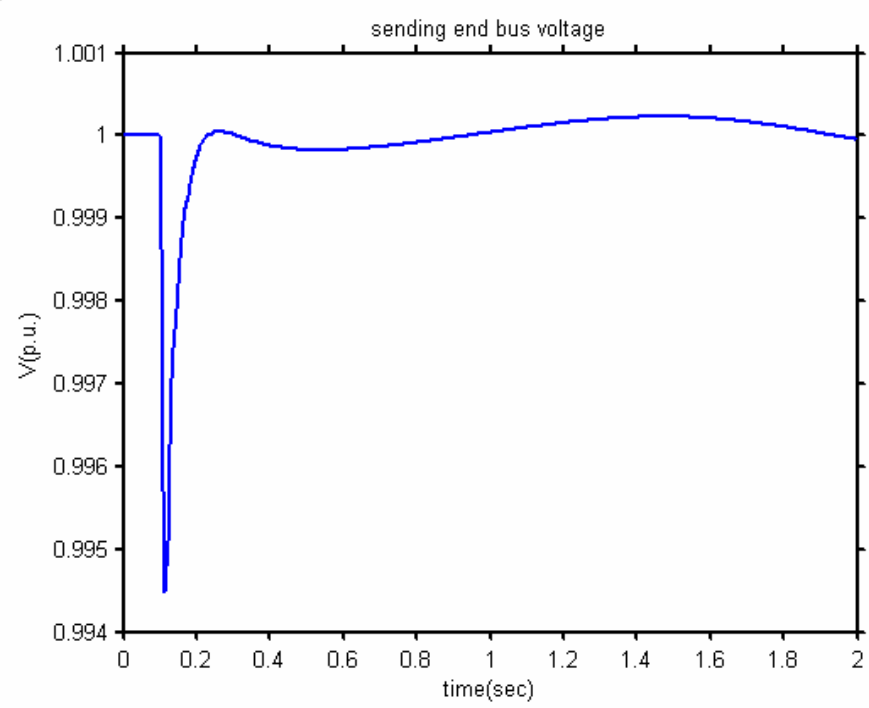

Fig. 4-22 Sending end bus voltage for case 2

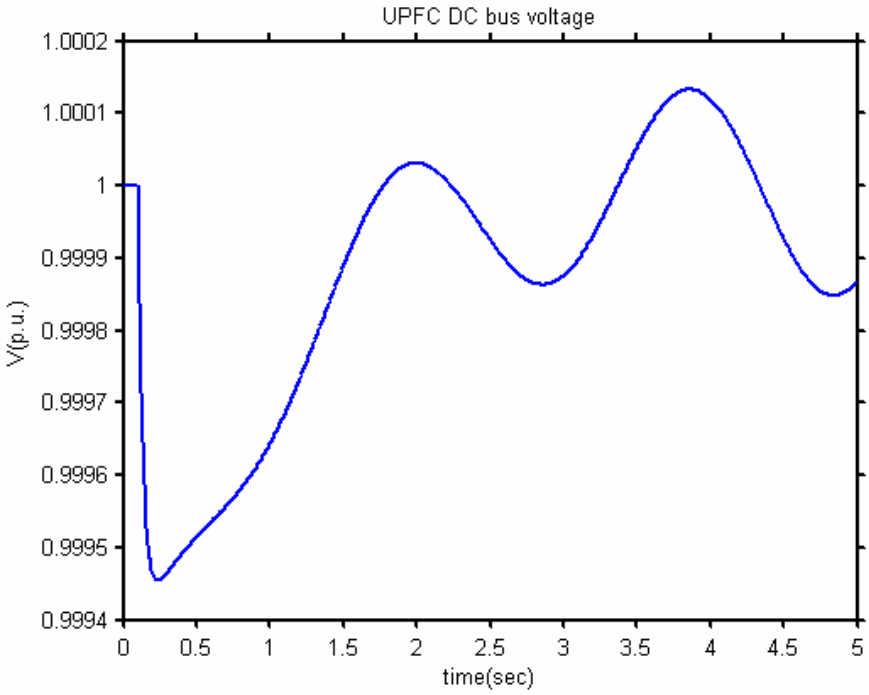

Fig. 4-23 UPFC DC capacitor voltage for case 2

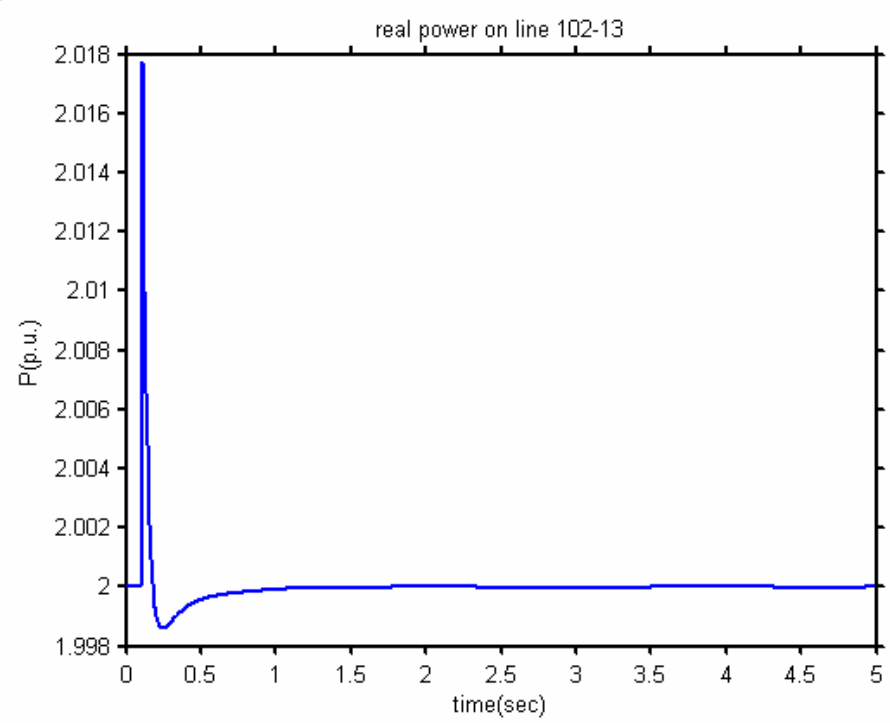

Fig. 4-24 Real power on line 102-13 for case 3

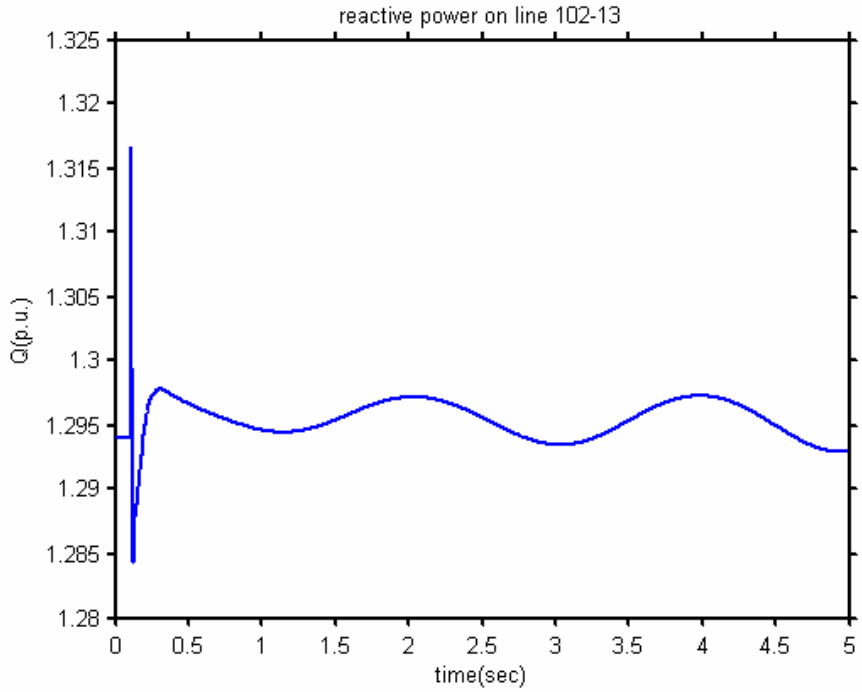

Fig. 4-25 Reactive power on line 102-13 for case 3

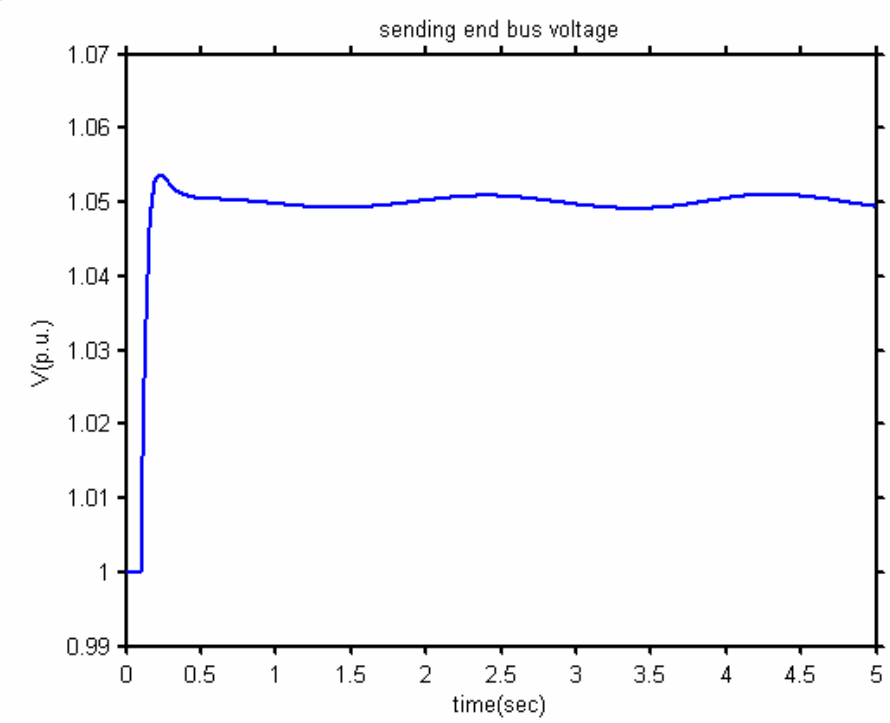

Fig. 4-26 Sending end bus voltage for case 3

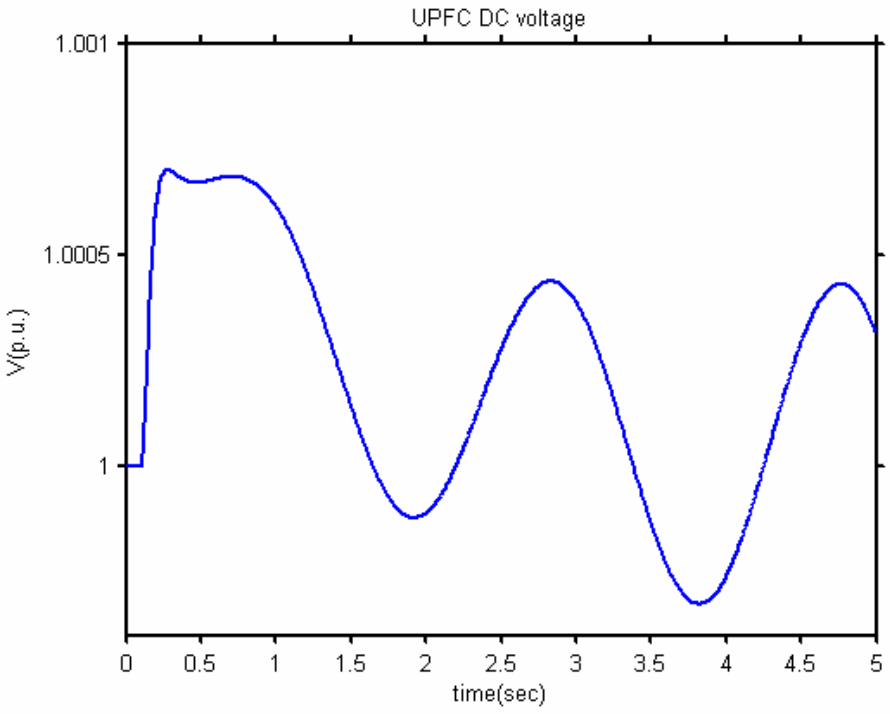

Fig. 4-27 UPFC DC capacitor voltage for case 3: UPFC changing V_{kref}

Load Change

A 14% real load increase is applied at bus 14 and the simulations studies are performed to demonstrate the behavior of the proposed UPFC model. Figures 4.28-4.31 show the power flow on the UPFC line and the UPFC bus voltages. It is clear that the UPFC can keep the power flow and the voltages at the reference level for a small disturbance like a load change. It is also noticeable that an unstable low frequency oscillation is excited because of the disturbance.

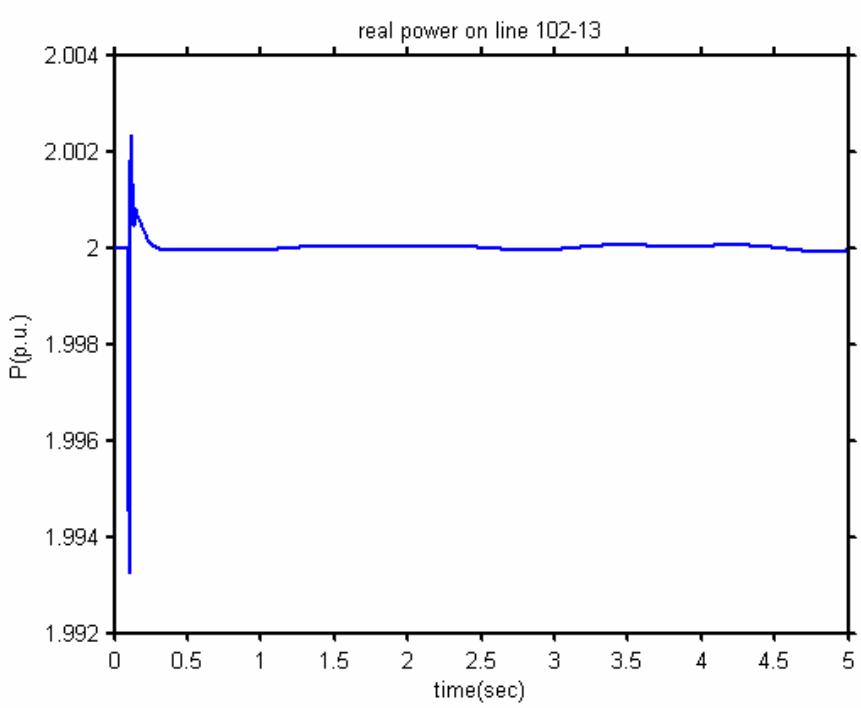

Fig. 4-28 Real power on line 102-13 for load change

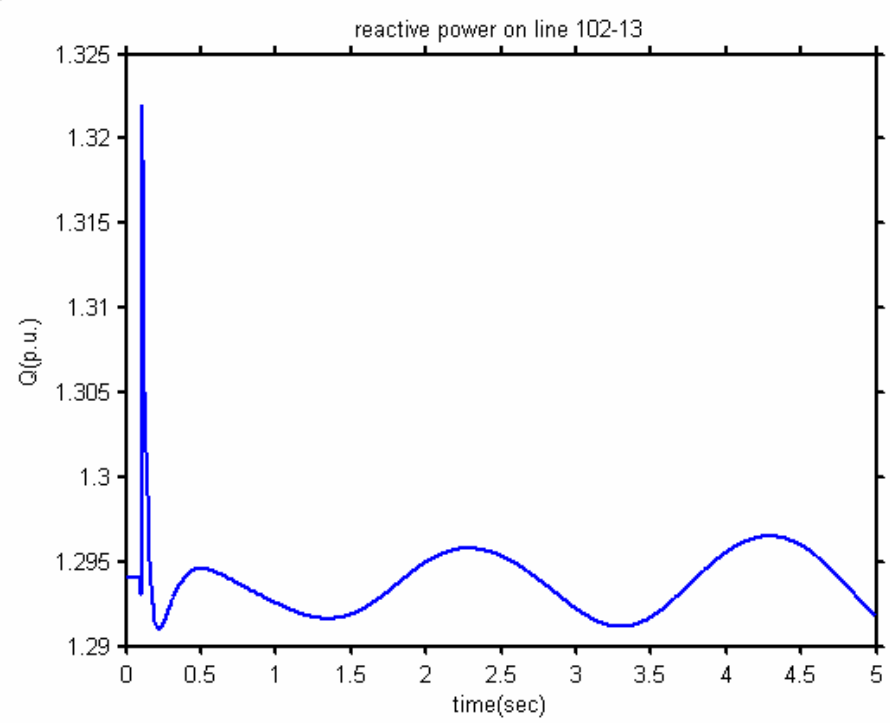

Fig. 4-29 Reactive power on line 102-13 for load change

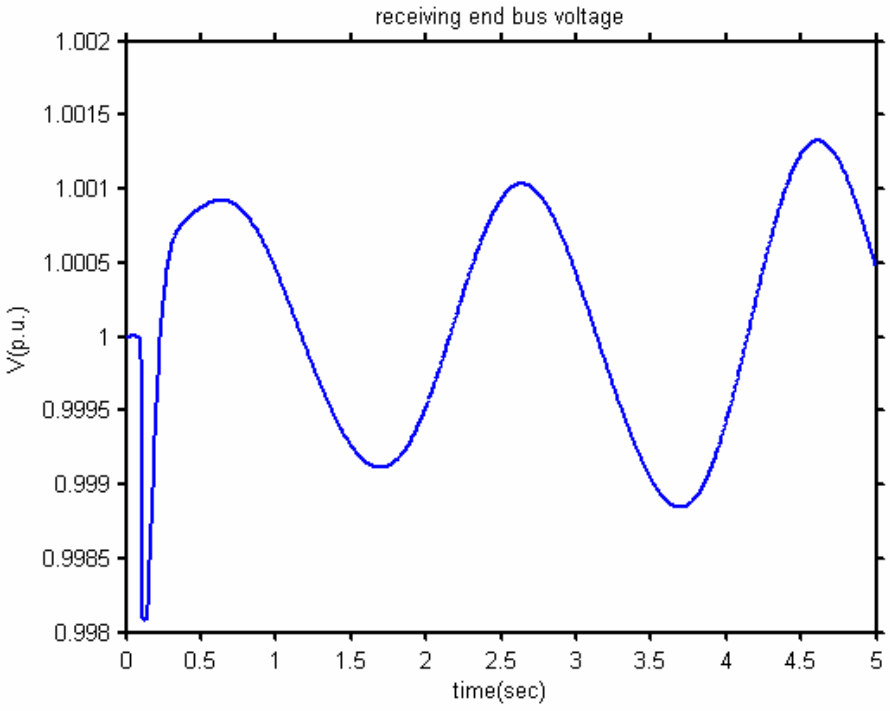

Fig. 4-30 Sending end bus voltage for load change

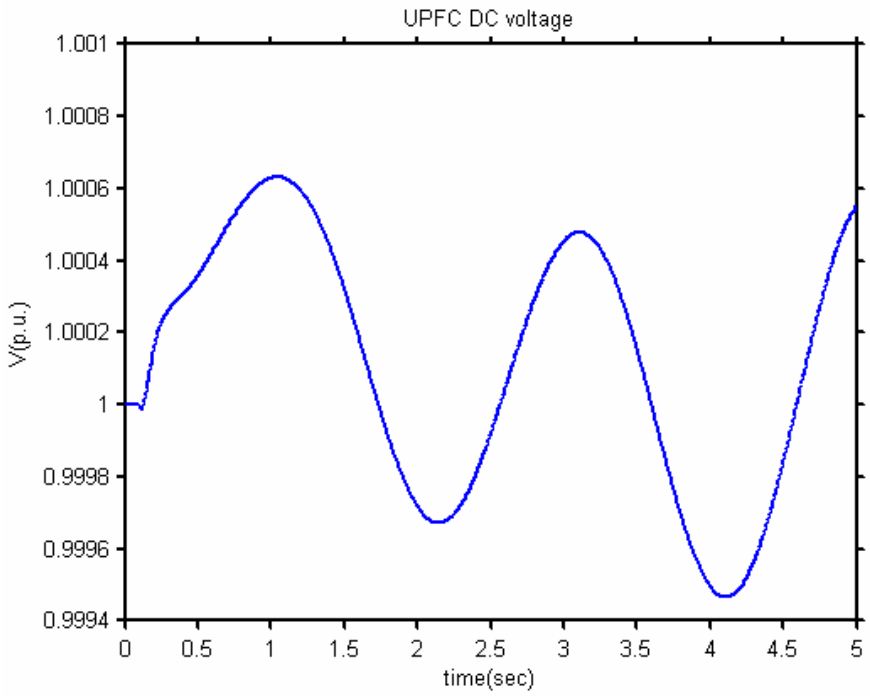

Fig. 4-31 UPFC DC capacitor voltage for load change

Three Phase Fault and Damping Controller Design

Three phase fault is applied at bus 3 on line 3-101 and is cleared after 0.05 *sec*. First no damping controller is installed on the UPFC. The receiving end bus voltage limiter becomes effective after the fault is cleared. And the limits for receiving end bus voltage are 0.9 p.u. and 1.1 p.u. The system responses to this fault are shown in Figs. 4-32 to 4-39. The system responses when only converter voltage limits are considered are also shown in these figures with dotted line. While the power on line 102-13 is tightly controlled by the UPFC, the variation of power interchange between the two areas has to be covered by the power on the parallel transmission line (line 101-13). So power on line 101-13 has large oscillations. The receiving end bus voltage is shown in Fig. 4-33. As can be seen from this figure, the receiving end bus voltage is successfully limited

within the desired range. The converter currents are also shown in Figs. 4-35 and 4-36; these currents are within the current ratings as well. It is seen that the shunt converter current limiter has greatly affected the peak value of the shunt current. But the series converter currents are about the same in these two situations. It reflects that the series converter current is actually well defined within the limit if the proper voltage limit is imposed on the injected series voltage, i.e. the current flow is restricted by the maximum injected voltage capability. It is noticed that a damping controller is needed in order to damp out the low frequency inter-area oscillatory mode.

A damping controller is also designed to damp out the inter-area mode oscillations. The design process has been shown in the previous section. The unstable mode is $0.11 \pm 3.22i$. Inter-area speed $\varpi = \varpi_4 + \varpi_3 - \varpi_2 - \varpi_1$ is used as the damping controller input. The power system responses to this fault are shown in figures 4-37 to 4-. It can be seen that the damping controller successfully damped out the inter-area oscillation. As a compromise, the power on the UPFC line has to experience a large oscillation to counteract the changes in the power exchange between the two areas. The receiving end bus voltage will also undergo some large variation. Therefore, the receiving end voltage limiter is set to be inactive when UPFC is in the damping mode. While the real power experiences large variations in the oscillation damping mode, the reactive power, sending end bus voltage and DC capacitor voltage are kept very close to their references. This again shows that the proposed UPFC model effectively demonstrates the unique characteristics of UPFC to independently control real and reactive power, and the bus voltage.

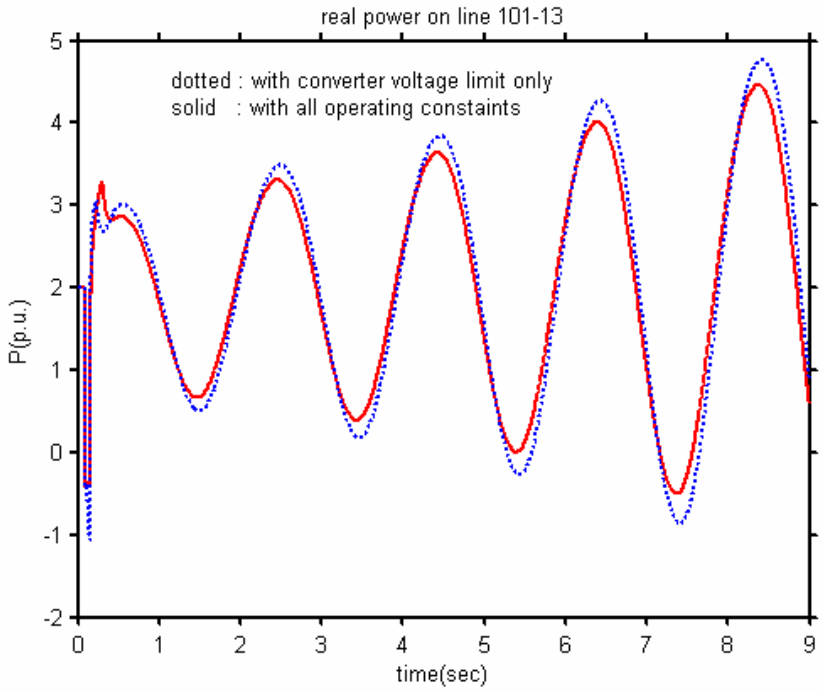

Fig. 4-32 Real power on line 101-13 for case 5: three-phase fault

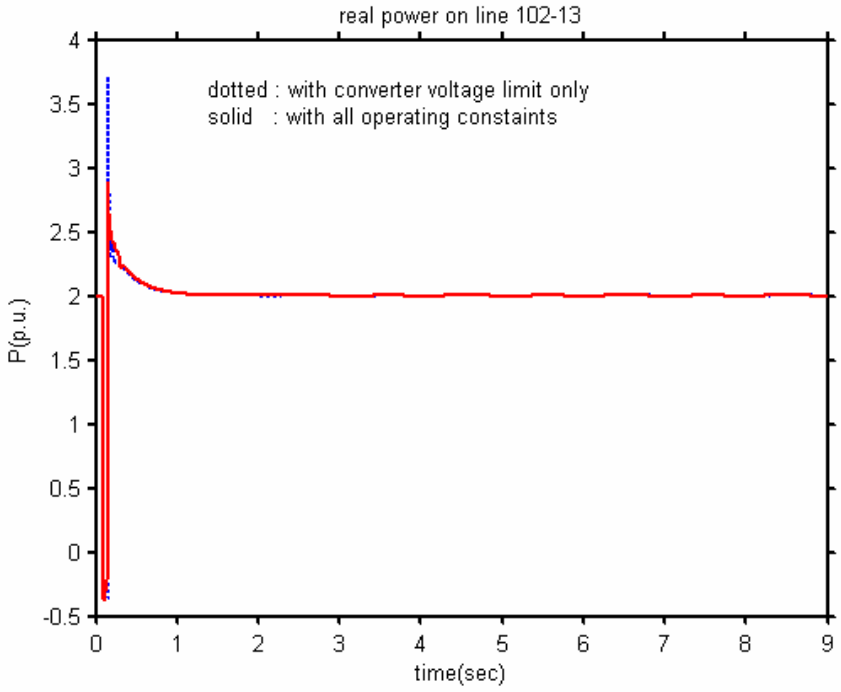

Fig. 4-33 Real power on line 102-13 for three-phase fault

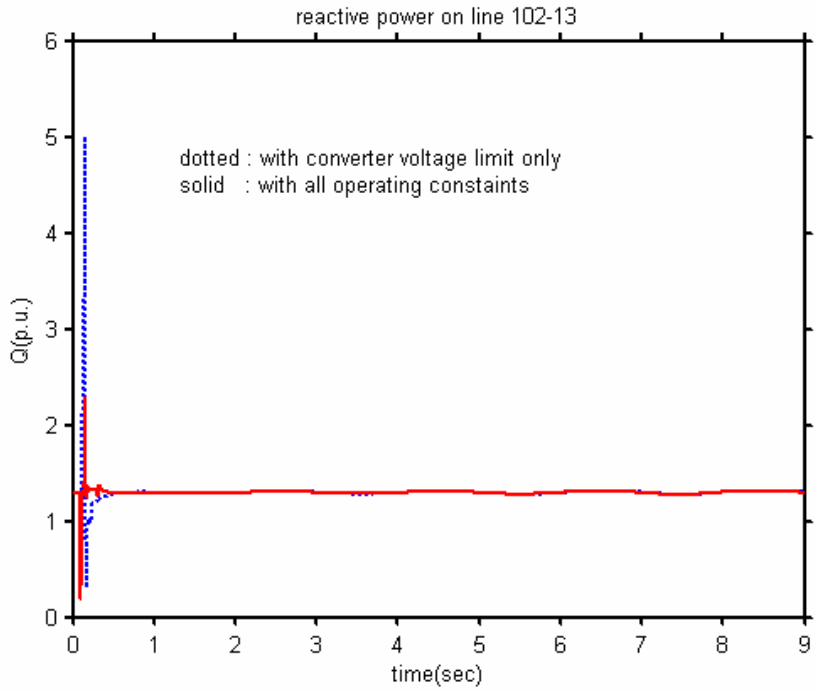

Fig. 4-34 Reactive power on line 102-13 for three-phase fault

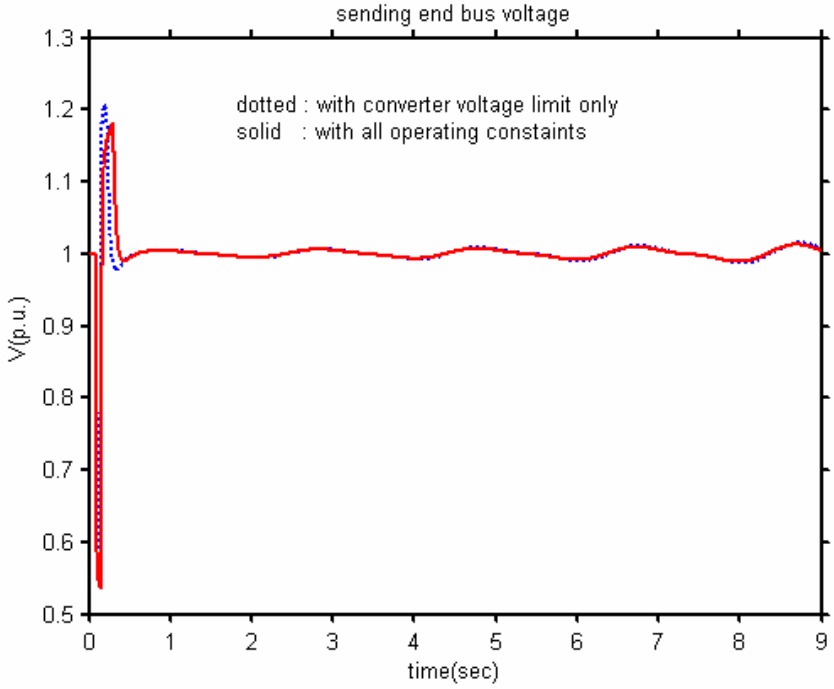

Fig. 4-35 UPFC sending end voltage for three-phase fault

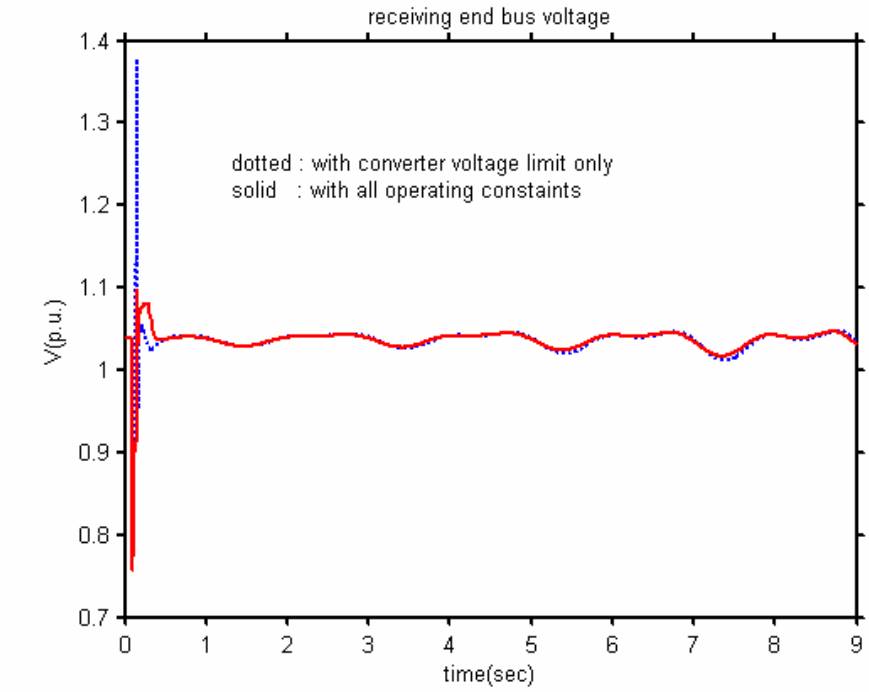

Fig. 4-36 UPFC receiving end voltage for three-phase fault

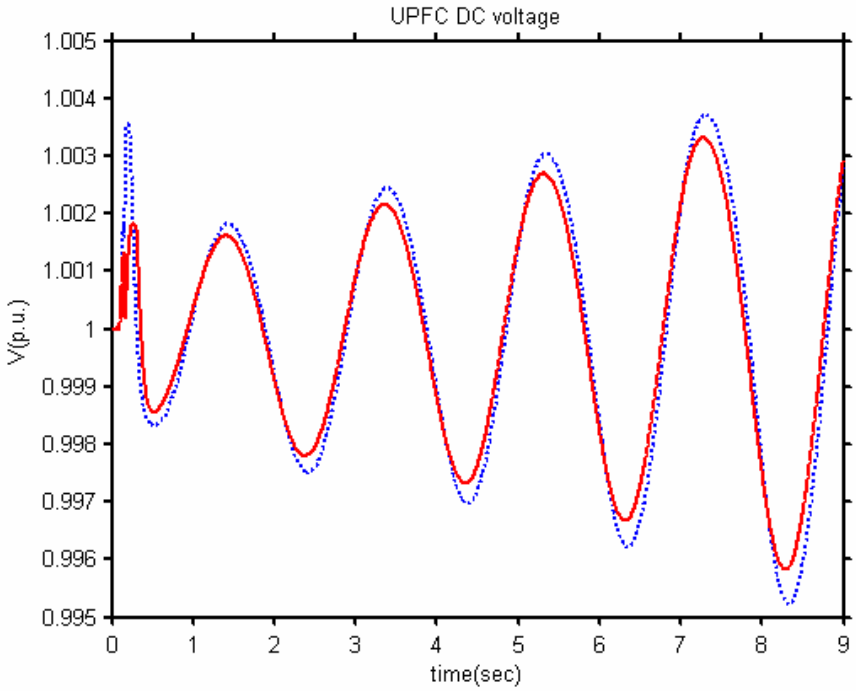

Fig. 4-37 UPFC DC capacitor voltage for three-phase fault

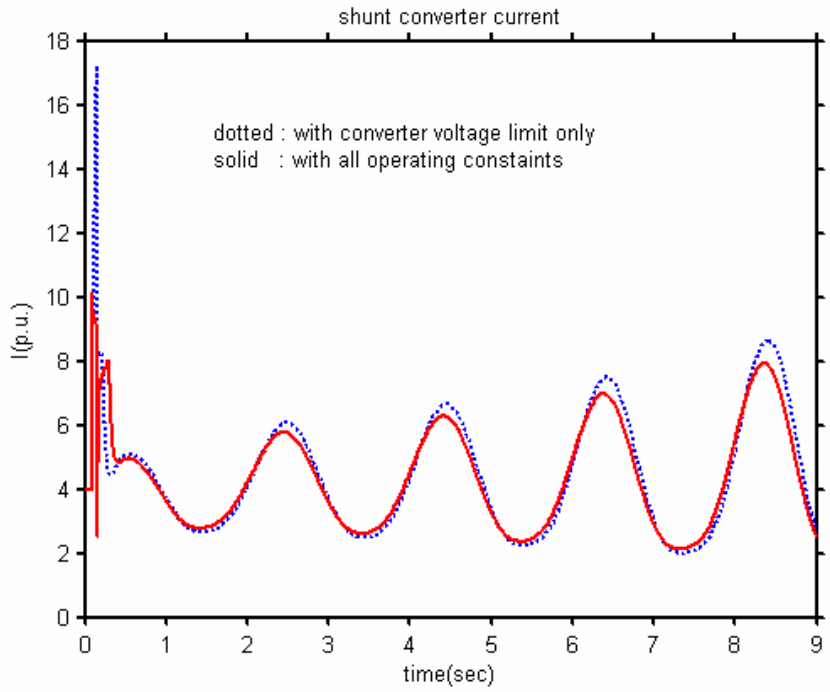

Fig. 4-38 UPFC shunt current for three-phase fault

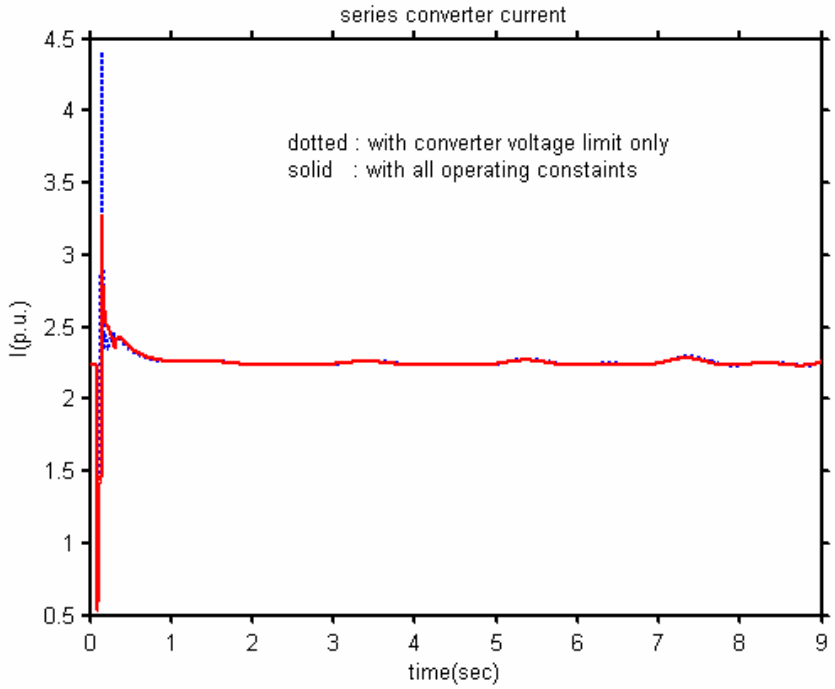

Fig. 4-39 UPFC series current for three-phase fault

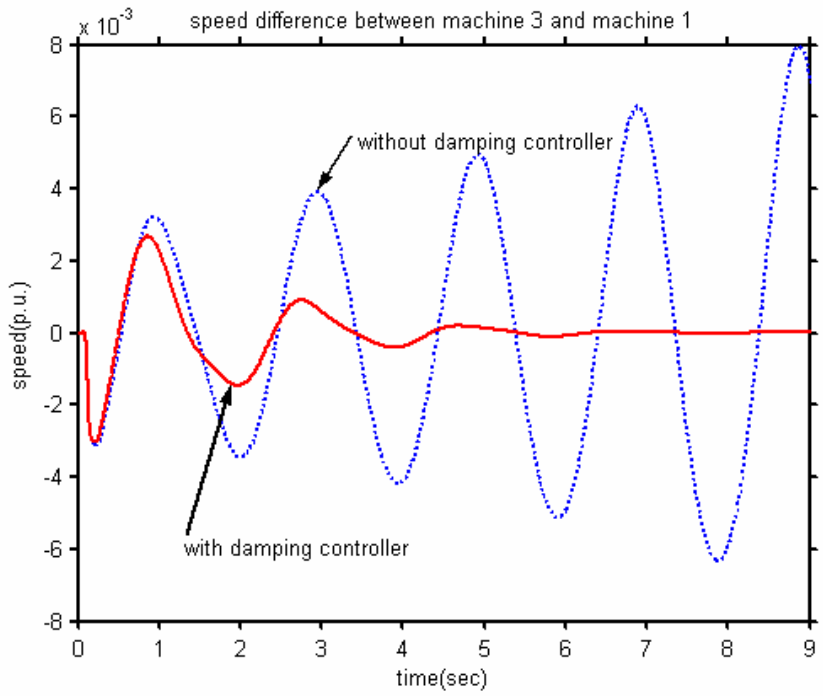

Fig. 4-40 Inter-area speed with damping controller

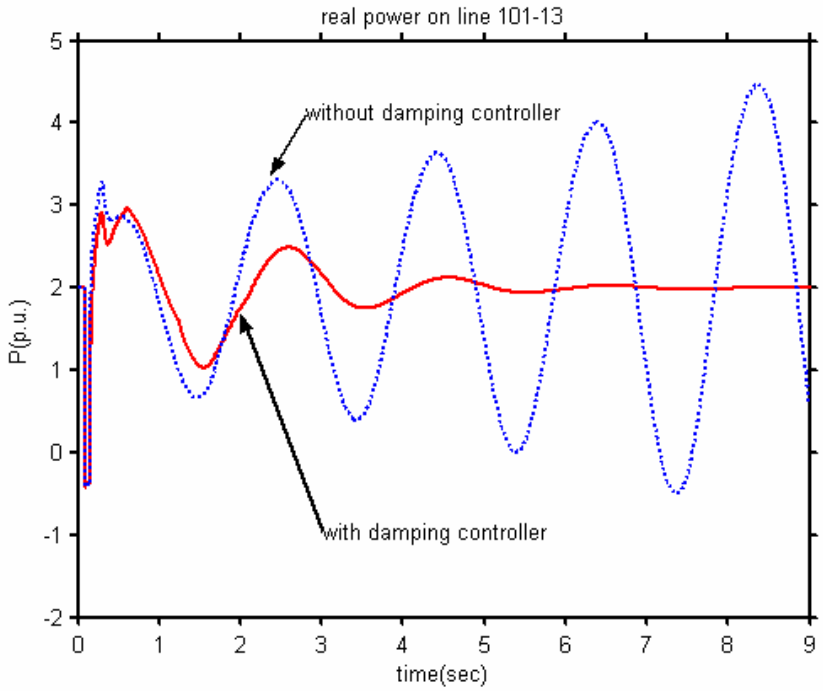

Fig. 4-41 Real power on line 101-13 with damping controller

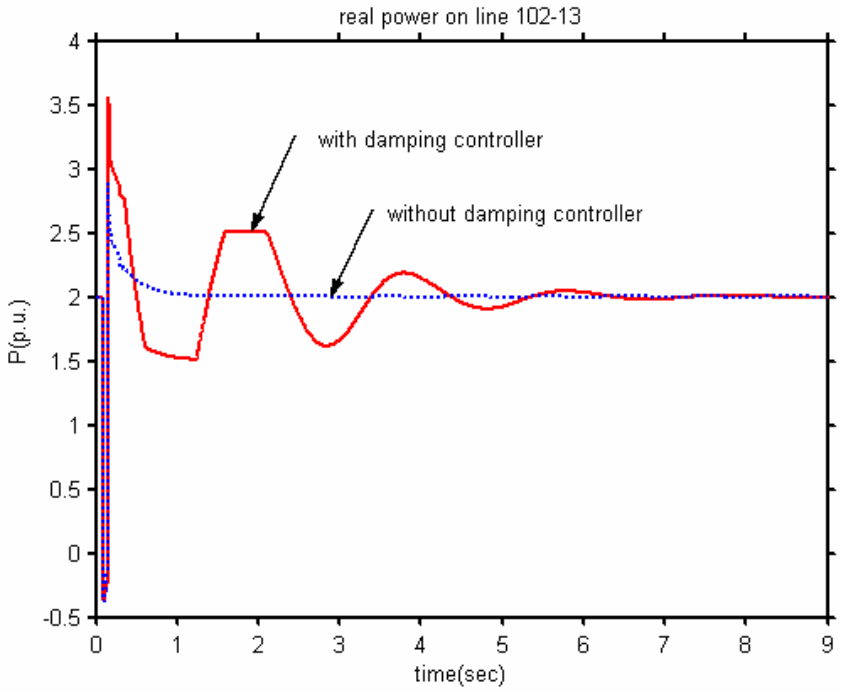

Fig. 4-42 Real power on line 102-13 with damping controller

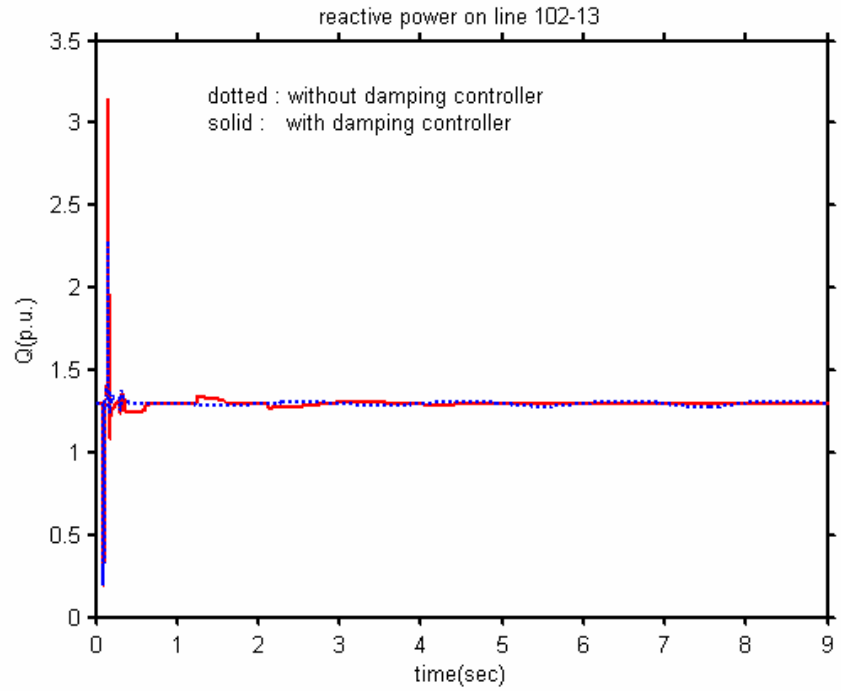

Fig. 4-43 Reactive power on line 102-13 with damping controller

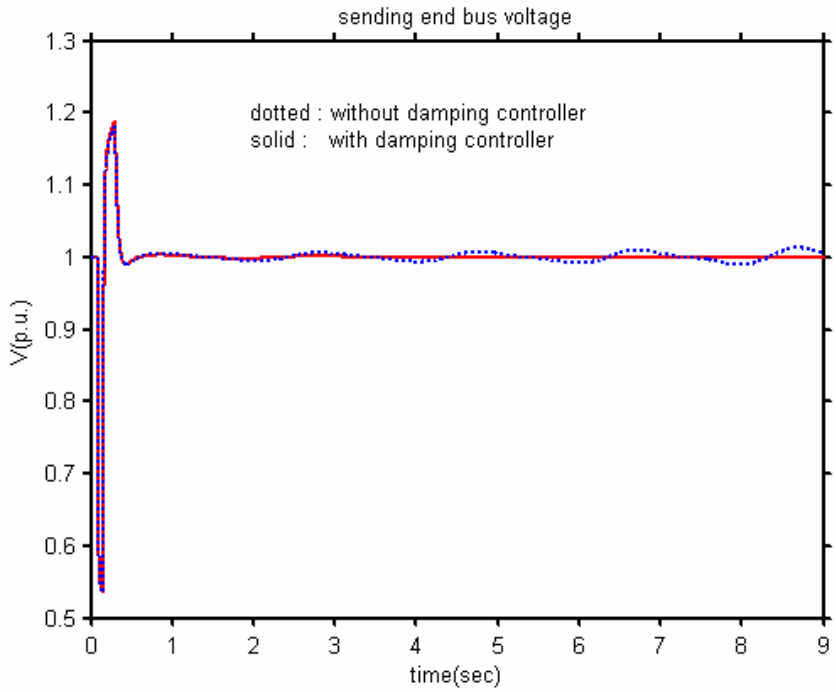

Fig. 4-44 Sending end bus voltage with damping controller

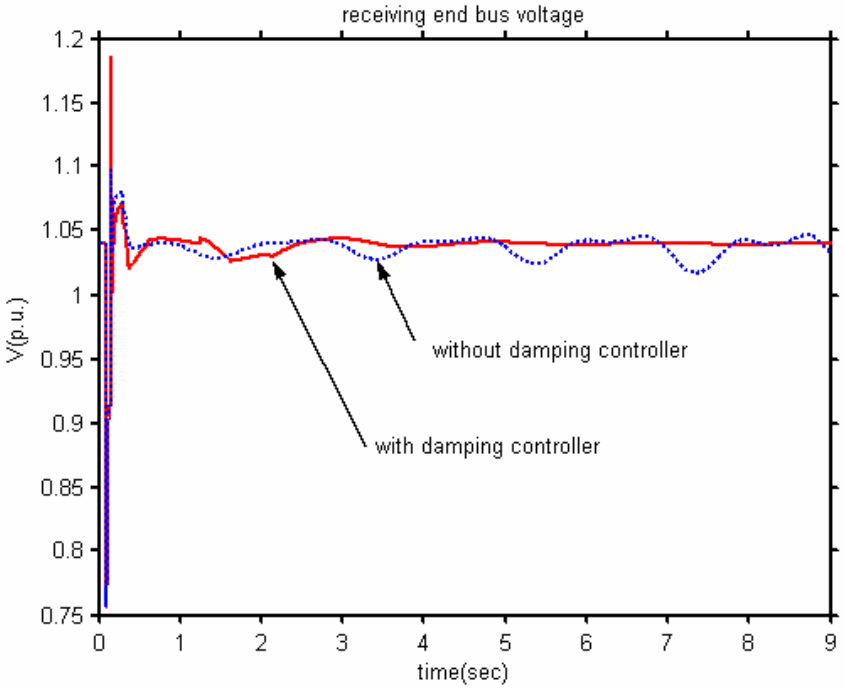

Fig. 4-45 Receiving end bus voltage with damping controller

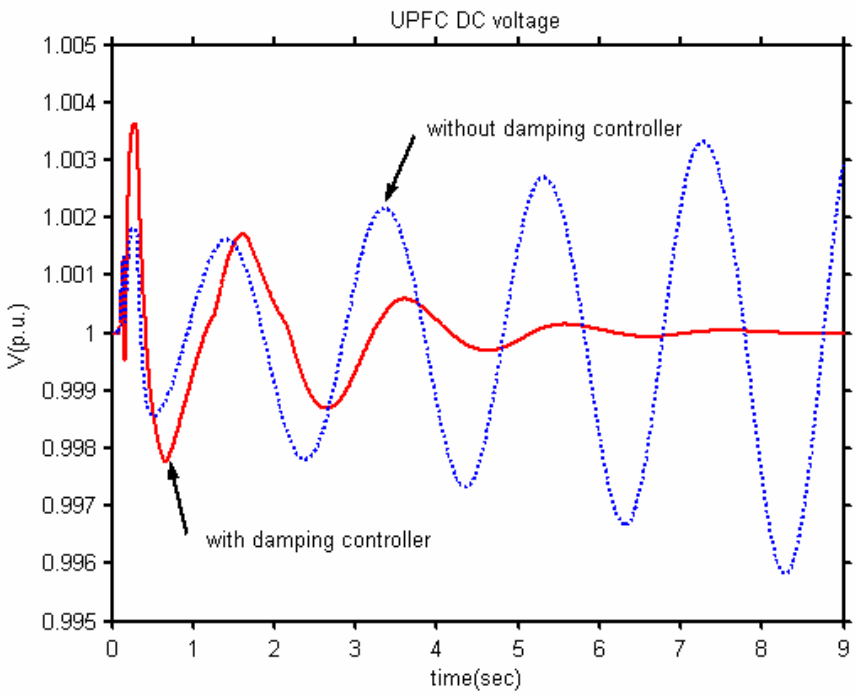

Fig. 4-46 UPFC DC voltage with damping controller

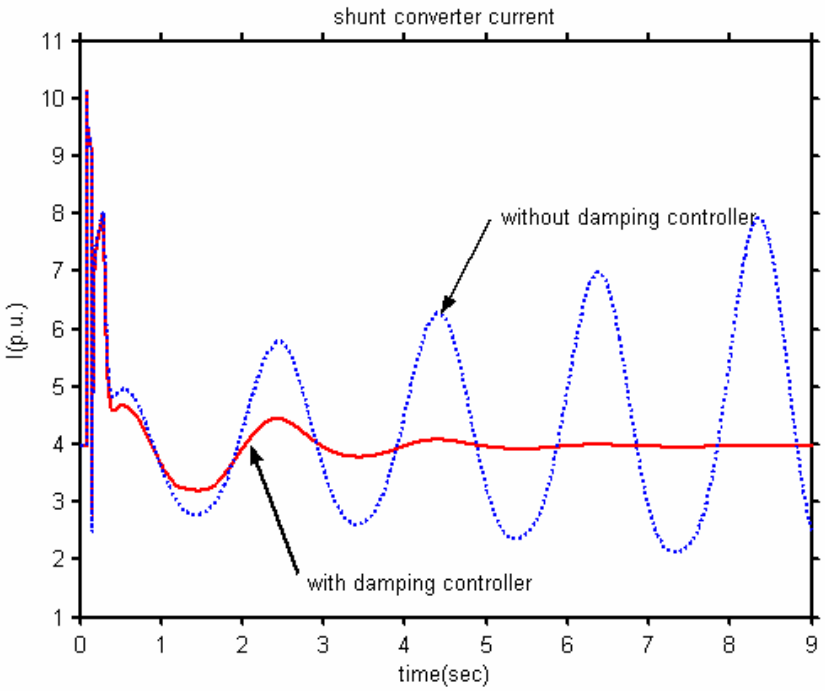

Fig. 4-47 Shunt converter current with damping controller

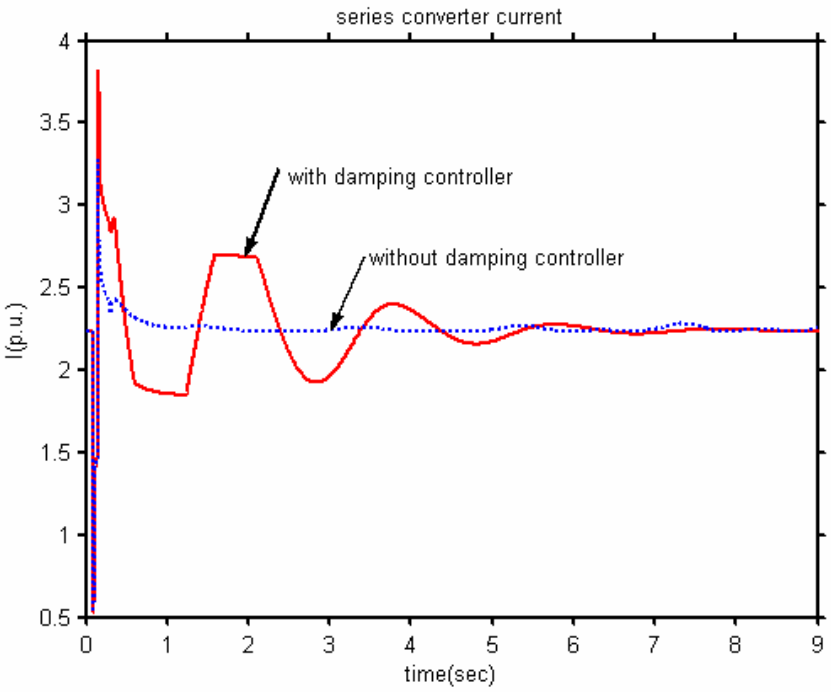

Fig. 4-48 Series converter current with damping controller

CHAPTER 5

CONCLUSIONS

This dissertation presents design methods for power system stabilizers and controllers for various FACTS devices for damping low frequency electro-mechanical oscillations in power systems. A power system stabilizer (PSS) is an excitation system-based damping controller and it is integrated into the excitation system. In general PSS performs better than FACTS controllers in damping local oscillatory modes. The design method for the proposed PSS combines system identification, fuzzy logic control and neural network theories together and the ANFIS PSS yields better damping performance than conventional PSS. While the proposed strategy works very well for PSS design, it did not work as good for control of FACTS devices.

As mentioned above, the PSS is integrated in the excitation system and the signal path from the machine speed to the electrical torque of the generator is rarely affected by external conditions, such as operating conditions or system structure. However, these factors greatly affect the interactions between the FACTS devices and the generators because FACTS devices are normally installed on the high voltage transmission lines that are far away from any generator. They do not affect the power system oscillations in the same way as PSSs. Instead, they do that indirectly by affecting some of the power system network parameters. Therefore, unlike PSS, it is difficult to derive fuzzy rules for damping controllers for FACTS devices.

PSSs use the local generator speed signal as their input and this signal is a good indicator of power system oscillations, especially local oscillatory modes. On the other

hand, single generator speed does not contain as much information about inter-area oscillatory modes as do transmission line local signals like power, current and voltage. Therefore, sometimes it is hard to damp out inter-area mode oscillations using PSSs only. Supplementary controllers can be designed for FACTS devices using the above transmission system variables, or speed difference between two areas, to enhance the damping of inter-area oscillatory modes.

We considered the FACTS damping controller design from a control point of view. We treated this problem as a general feedback control problem. And the problem was divided into three issues: feed-forward plant identification, control input selection, feedback control design and controller gain adjustment. The first issue is solved by the PRONY method, the second is done by analyzing the residues associated with the eigenvalues that are of interest and the third issue is solved by root locus plot and phase compensation. Since the effectiveness of FACTS devices somehow depends on the power system loading conditions, a gain varying strategy was proposed that changes the controller gain according to the transmission line loading condition. Unlike some works that have been done in this area which can only demonstrate their design success in small power systems or simplified power systems, the proposed method can be applied to the damping controller design for any FACTS devices in a power system of any size. This approach was used for damping controller design for SVC, TCSC and UPFC. Simulation results verify the effectiveness of this approach.

Another important work in this dissertation is the modeling of the UPFC, a unique FACTS device. Unlike SVC and TCSC, which are thyristor controlled capacitor and reactor, UPFC is a voltage-sourced converter-based FACTS controller. It operates like

synchronous voltage sources. While SVC and TCSC can be modeled as variable impedances connected in the power system, the modeling of a UPFC, including both steady state modeling and dynamic modeling, is much more complicated. UPFC brings quite a few challenges to power system simulation and study. The first problem is the steady-state power flow calculation. The second problem is the converter control and UPFC dynamics modeling. The third problem is the interface of UPFC and the power systems for transient simulation. The forth problem is the limit setting and practical operating constraint modeling in the simulation. And the fifth problem is the UPFC rating and parameter setting. All these problems are solved and presented in Chapter 4. The proposed model reflected the unique characteristic of the UPFC to control both the load flow and the bus voltage rapidly and independently. A damping controller is also designed for the UPFC. Power flow calculation and dynamic simulation studies demonstrate the potential of the UPFC in increasing the power transfer capability of transmission system and enhancing power system stability.

REFERENCES

[1] Graham Rogers, *Power System Oscillations*, Kluwer Academic Publishers, 2002

[2] F. P. DeMello and C. Concordia, "Concepts of Synchronous Machine Stability as Affected by Excitation Control", *IEEE Transactions on Power Apparatus and Systems*, Vol. 88, 1969, pp. 316-329.

[3] P. Kundur, M. Klein, G. J. Rogers, and M. S. Zywno, "Application of Power System Stabilizers for Enhancement of Overall System Stability", *IEEE Transactions on Power Systems*, Vol. 4, 1989, pp. 614-626.

[4] J. H. Chow, J. J. Sanchez-Gasca, “Pole-placement Designs of Power System Stabilizers”, *IEEE Transactions on Power Systems*, Vol. 4, No. 1, pp271-277

[5] Y. Y. Hsu and C. H. Cheng, "Design of Fuzzy Power System Stabilizers for Multimachine Power Systems", *IEE Proceedings*, Vol. 137, Part C, No.3, 1990, pp. 233-238.

[6] T. Hiyama, "Application of Rule-Based Stabilizing Controller to electrical Power System", *IEE Proceedings*, Vol. 136, Part C, No.3, 1989, pp. 175-181.

[7] T. Hiyama, "Rule-Based Stabilizers for Multi-Machine Power System", *IEEE Transactions on Power Systems*, Vol. 5, 1990, pp. 403-411.

[8] T. Hiyama, "Real Time Control of Micro-Machine System using Micro-Computer based Fuzzy Logic Power System Stabilizer", *IEEE Transactions on Energy Conversion*, Vol. 9, 1994, pp. 724-731.

[9] T. Hiyama, "Robustness of Fuzzy Logic Power System Stabilizers Applied to Multimachine Power System", *IEEE Transactions on Energy Conversion*, Vol. 9, 1994, pp. 451-457.

[10] T. Hiyama, M. Kugimiya, and H. Satoh, "Advanced PID Type Fuzzy Logic Power System Stabilizer", *IEEE Transactions on Energy Conversion*, Vol. 9, 1994, pp. 514-520.

[11] A. Hariri and O. P. Malik, "A Fuzzy Logic Based Power System Stabilizers with Learning Ability", *IEEE Transactions on Energy Conversion*, Vol. 11, 1996, pp. 721-727.

[12] G. P. Chen, O.P. Malik, G.S. Hope, Y.H. Qin and G.Y. Xu, “An Adaptive Power System Stabilizer Based on The Self-optimizing Pole Shifting Control Strategy”, *IEEE transactions on Energy Conversion*, Vol. 8, No. 4, 1993, pp. 639-645.

[13] J. He and O.P. Malik, “An Adaptive Power System Stabilizer Based on Recurrent Neural Networks”, *IEEE transactions on Energy Conversion*, Vol. 12, No. 4, 1997, pp413-418.

[14] P. Shamsollahi and O.P. Malik, “An Adaptive Power System Stabilizer Using On-line Trained Neural Networks”, *IEEE transactions on Energy Conversion*, Vol. 12, No. 4, 1997, pp382-387.

[15] P. Shamsollahi and O.P. Malik, “Application of Neural Adaptive Power System Stabilizer in a Multi-Machine Power System”, *IEEE transactions on Energy Conversion*, Vol. 12, 1997

[16] P. Shamsollahi and O.P. Malik, “Real-Time Implementation and Experimental Studies of a Neural Adaptive Power System Stabilizer”, *IEEE transactions on Energy Conversion*, Vol. 12, 1997

[17] Yuan-Yih Hsu, Chao-Rong Chen, “Tuning of Power System Stabilizers Using an Artificial Neural Network”, *IEEE transactions on Energy Conversion*, Vol. 8, 1992, pp. 612-617.

[18] Jinyu Wen, Shijie Cheng and O.P. Malik, “A synchronous Generator Fuzzy Excitation Controller Optimally Designed with a Genetic Algorithm”, *IEEE Transactions on Power Systems*, Vol. 13, 1998, pp 884-889.

[19] M. A. Abido, "Hybridizing Rule-Based Power System Stabilizers with Genetic Algorithms", *IEEE Transactions on Power Systems*, Vol. 14, 1999, pp. 600-607

[20] Y.L. Abdel-Magid, M.A. Abido, S. Al-Baiyat and A.H. Mantawy, “Simultaneous Stabilization of Multimachine Power Systems via Genetic Algorithms”, *IEEE transactions on Power Systems*, Vol. 14, 1999, 1428-1438.

[21] Y.L. Abdel-Magid, M.A. Abido and A.H. Mantawy, “Robust Tuning of Power System Stabilizers in Multimachine Power Systems”, *IEEE transactions on Power Systems*, Vol. 15, 2000, pp 735-740.

[22] J. Lu, M.H. Nehrir and D.A. Pierre, “A Fuzzy Logic-based Adaptive Power System Stabilizer for Multi-machine Systems”, *Electric Power Systems Research*, Vol. 60, 2001, pp115-pp121

[23] J. Lu, M.H. Nehrir and D.A. Pierre, “A Fuzzy Logic-based Adaptive Damping Controller for Static VAR Compensator”, *Electric Power Systems Research*, Vol. 68, 2004, pp113-118

[24] E.V. Larsen, J.J. Sanchez-Gasca and J.H. Chow, "Concepts for Design of Facts Controllers to Damp Power Swings", *IEEE transactions on Power Systems*, Vol. 10, No. 2, 1995, pp948-955

[25] A.B. Leirbukt, J.H. Chow, J.J. Sanchez and E.V. Larsen, "Damping Control Design Based on Time-Domain Identified Models", *IEEE transactions on Power Systems*, Vol. 14, 1999, pp172-178.

[26] M. Noroozian, M. Ghandhari, G. Andersson, J. Gronquist and I. Hiskens, "A Robust Control Strategy for Shunt and Series Reactive Compensators to Damp Electromechanical Oscillations", *IEEE transactions on Power Delivery*, Vol 12, 2001, pp812-817.

[27] M. Chandhari, G Andersson, and I.A. Hiskens, "Control Lyapunov functions for controllable series devices", *IEEE transactions on Power System*, Vol. 16, 2001, pp689-694.

[28] J.M. Ramirez Arredondo, "A Passivity Approach to Controller Design for TCSC", *IEEE Power Engineering Review*, February 2002, pp55-58.

[29] A.D. Del Rosso, C.A. Canizares and V.M. Dona, "A Study of TCSC Controller Design for Power System Stability Improvement", *IEEE Transactions on Power Systems*, Vol.18, 2003, pp 1487-1495.

[30] E.Z. Zhou, "Application of Static Var Compensators to Increase Power System Damping", *IEEE Transactions on Power Systems*, Vol. 18, 1993, pp 655-661.

[31] J. R. Smith, D.A. Pierre, D.A. Rudberg, I. Sadighi and A.P. Johnson, "An Enhanced LQ Adaptive Var Unit Controller for Power System Damping", *IEEE Transactions on Power Systems*, Vol. 4, 1989, pp443-451.

[32] J. R. Smith, D.A. Pierre, I. Sadighi, M.H. Nehrir and J.F. Hauer, "A Supplementary Adaptive Var Unit Controller for Power System Damping", *IEEE Transactions on Power Systems*, 1989, pp1017-1023.

[33] K.M. Son and J.K. Park, "On the Robust LQG Control of TCSC for Damping Power System Oscillations", *IEEE Transactions on Power Systems*, Vol. 15. 2000, pp1306-1322.

[34] C. Gama, "Brazilian North-South Interconnection control-application and operating experience with a TCSC", IEEE Power Engineering Society Summer Meeting, 1999.

[35] T. Luor, Y. Hsu, T.Guo, J. Lin and C. Huang, "Application of Thyristor-connected Series Compensation to Enhance Oscillatory Stability and Transmission Capability of

a Longitudinal Power System", *IEEE Transactions on Power Systems*, Vol. 14, 1999, pp 179-185.

[36] Y. Y. Hsu and T.S. Luor, "Damping of Power System Oscillations Using Adaptive Thyristor-controlled Series Compensators Tuned by Artificial Neural Networks" *IEE Proceedings*, 1998, pp 137-142.

[37] T.K. Mok, Y. Ni and F.F. Wu, "Design of fuzzy damping controller of UPFC through genetic algorithm", Power Engineering Society Summer Meeting, 2000. IEEE, Vol: 3, pp1889 – 1894.

[38] P.K. Dash, S. Mishra and G. Panda, "Damping Multimodal Power System Oscillation Using a Hybrid Fuzzy Controller for Series Connected Facts Devices", *IEEE Transactions on Power Systems*, Vol. 15, 2000, pp 1360-1366.

[39] L.Y. Dong, L. Zhang and M.L. Crow, "A New Control Strategy for the Unified Power Flow Controller", Power Engineering Society Winter Meeting, 2002. IEEE, Vol.: 1 , pp27-31.

[40] Z. Huang, Y. Ni, C.M. Shen, F.F. Wu, S. Chen and B. Zhang, "Application of Unified Power Flow Controller in Interconnected Power Systems – Modeling, Interface, Control Strategy, and Case Study", *IEEE Transactions on Power Systems*, Vol. 15, No. 2, 2000, pp 817-823.

[41] K. Schoder, A. Hasanovic and A. Feliachi, "Fuzzy Damping Controller for the Unified Power Flow Controller", North American Power Symposium, Canada, 2000, pp 5-21 – 5-27.

[42] K. Schoder, A. Hasanovic and A. Feliachi, "Power System Damping Using Fuzzy Controlled Unified Power Flow Controller", Power Engineering Society Winter Meeting, 2001, IEEE, Vol. 2, pp 617 – 622.

[43] L. Gyugyi, C.D. Schauder, S.L. Williams, T.R. Rietman, D.R. Torgerson, A. Edris "The unified power flow controller: a new approach to power transmission control", *IEEE Transactions on Power Delivery*, Vol. 10, No. 2, April 1995

[44] C. R. Fuerte-Esquivel, E. Acha and H. Ambriz-Perez, "A Comprehensive Newton-Raphson UPFC Model for the Quadratic Power Flow Solution of Practical Power Networks", IEEE *Transactions on Power Systems*, Vol. 15, No. 1, February 2000

[45] C. Schauder, H. Mehta, "Vector Analysis and Control of Advanced Static VAR Compensators", *IEE Proceedings, Generation, Transmission and Distribution*, Vol.140, No. 4, July 1993

[46] B. A. Renz, A. Keri, A.S. Mehraban, C. Schauder, E. Stacey, L. Kovalsky, L. Gyugyi, A. Edirs, "AEP Unified Power Flow Controller Performance", *IEEE Transactions on Power Delivery*, Vol. 14, No. 4, October 1999

[47] C. Schauder, M. Gernhardt, E. Stacey, T. Lemak, L. Gyugyi, T.W. Cease, A. Edris, "Operation of 100 MVAR TVA STACON", *IEEE Transactions on Power Delivery*, Vol. 12, No. 4, October 1997

[48] A. Nabavi-Niaki, M.R. Iravani, "Steady-state and Dynamic Models of Unified Power Flow Controller (UPFC) for Power System Studies", *IEEE Transactions on Power System*, Vol. 11, No. 4, Nov. 1996

[49] I. Papic, P. Zunko, D. Povh, M. Weinhold, "Basic Control of Unified Power Flow Controller", *IEEE Transactions on Power Systems*, Vol. 12, No. 4, November 1997

[50] Claudio A. Canizares, Edvina Uzunovic and John Reeve, "Transient Stability and Power Flow Models of the Unified Power Flow Controller for Various Control Strategies", *Technical Report #2004-09*, University of Waterloo, E&CE, March 2004

[51] Kwang M. Son, Robert H. Lasseter, "A Newton-Type Current Injection Model of UPFC for Studying Low-Frequency Oscillations", *IEEE Transactions on Power Delivery*, Vol. 19, No. 2, April 2004

[52] Manzar Rahman, Mohammed Ahmed, Richard Gutman, Robert J. O'Keefe, Robert J. Nelson, Jianhua Bian, "UPFC Application of the AEP System: Planning Consideration", *IEEE transactions on Power Systems*, Vol. 12, No. 4, November 1997.

[53] C. D. Schauder, L. Gyugyi, M.R. Lund, E.M. Hamai, T.R. Rietman, D. R. Torgerson, A. Edris, "Operation of the Unified Power Flow Controller (UPFC) under Practical Constraints", *IEEE Transactions on Power Delivery*, Vol. 13, No. 2, April 1998

[54] S. Arabi, P. Kundur, "Innovative Techniques in Modeling UPFC for Power System Analysis", *IEEE Transactions on Power Systems*, Vol. 15, No. 1, February 2000

[55] S. A. Waples, A. S. Law, R.J. Nelson and M.G. Gernhardt, "Planning and Operating Ratings for Inverter-Based FACTS Power Flow Controllers", *Proceedings of the American Power Conference*, v 58-2, 1996, p 1555-1561

[56] Narain G. Hingorani, Laszlo Gyugyi, *Understanding FACTS*, IEEE, Inc. 2000

[57] D.A. Pierre, D.J. Trudnowski and J.F. Hauer, "Identifying Linear Reduced-Order Models for systems with Arbitrary Initial Conditions Using Prony Signal Analysis", *IEEE Transactions on Automatic Control*, Vol 37, No.6, June 1992

[58] Cherry Tree Scientific Software, *Power System Toolbox for Matlab*

[59] Prabha Kundur, *Power System Stability and Control*, McGraw-Hill, Inc., 1994.

[60] T.R. Fortescue, L.S. Kershenbaum, B.E. Ydstie, "Implementation of Self-tuning Regulators with Variable Forgetting Factors," *Automatica*, Vol. 17, No. 6, 1981.

[61] T. Takagi, M. Sugeno, "Fuzzy Identification of Systems and its Application to Modeling and Control," *IEEE Trans-SMC*, Vol. 15, 1985.

[62] Martin Brown, Chris Harris, *Neurofuzzy Adaptive Modeling and Control*, Prentice Hall, 1994.

[63] Simon Haykin, "Neural Networks, A comprehensive Foundation," *Prentice Hall*, 1999

[64] R.J. Marks II, S. Oh, P. Arabshahi, T.P. Caudell , J.J. Choi, B.G. Song, "Steepest Descent Adaptation of Min-Max Fuzzy If-Then Rules," *Proc. IEEE/INNS International Joint Conference on Neural Networks, Beijing, China*, November 1992.

[65] J. Shing and R Jang, "ANFIS: Adaptive-network based Fuzzy Inference System," *IEEE Transactions on SMC*, Vol. 23, No. 3, May/June 1993.

[66] Juan J. Sanchez-Gasca, Jow H. Chow, "Performance Comparison of three Identification Methods for the Analysis of Electromechanical Oscillations", *IEEE Transactions on Power Systems*, Vol 14, No. 3, August 1999.

[67] J.F. Hauer, "The use of Prony Analysis to Determine Modal Content and Equivalent Models for Measured Power System Response," IEEE Special Publication 90TH0292-3-PWR, *Eigenanalysis and Frequency Domain Methods for System Dynamic Performance*, 1990.

[68] C.Y. Chung, C.T. Tse, K.W. Wang, A.K. David, C.W. Yu, "Synthesis of sensitivity coefficients for controller parameters of static var compensator", *IEE Proceedings, Generation Transmission and Distribution, Vol. 147, No. 4, July 2000, pp197-201.*

[69] Richard C. Dorf, *Modern Control Systems*, Addison-Wesley Publishing Company, 1992.

APPENDICES

APPENDIX A

SYSTEM PARAMETERS

System Parameters for One-machine-infinite-bus System

Generator Parameters:

X_l = 0.15 *pu*, R_a = 0.0 *pu*, X_d = 2.0 *pu*, $X_d^{'}$ = 0.245 *pu*,

$X_d^{''}$ = 0.2 *pu*, $T_{d0}^{'}$ = 5.0 *sec*, $T_{d0}^{''}$ = 0.031 *sec*, X_q = 1.91 *pu*,

$X_q^{'}$ = 0.42 *pu*, $X_q^{''}$ = 0.2 *pu*, $T_{q0}^{'}$ = 0.66 *sec*,

$T_{q0}^{''}$ = 0.061 *sec*, H = 2.8756 *sec*, D = 0.

Generator base: 991 *MVA*

Exciter Parameters (IEEE type ST3 Model):

T_R = 0.0 *sec*, K_A = 7.04, T_A = 0.4 *sec*, T_B = 6.67 *sec*,

T_C = 1.0 *sec*, V_{Rmax} = 7.57 *pu*, V_{Rmin} = 0 *pu*, V_{Imax} = 0.2 *pu*,

V_{Imin} = -0.2 *pu*, K_J = 200, K_p = 4.365, θ_p = 20 *degree*,

K_I = 4.83, X_L = 0.091 *pu*, K_C = 1.096, E_{fdmax} = 6.53 *pu*,

K_G = 1, V_{Gmax} = 6.53 *pu*

Governor Parameters:

Speed set point: 1 *pu*, Steady-state gain (*1/R*): 25.0

T_s: 0.1 *sec*, T_c: 0.4 *sec*, T_3: 0.0, T_4: 1.25 *sec*, $T_{5:}$ 5.0 *sec*

Other Parameters:

System base: 100 *MVA*

Transformer reactance: 0.1 *pu.*

Transmission line reactance: 0.4 *pu*

The AVR is set to maintain the terminal voltage at 1.05 *pu.*

Voltage of infinite bus: 1.08 *pu*.

System Parameters for the Two-area, Four-machine System

Generator Parameters:

X_l = 0.2 *pu*, R_a = 0.0025 *pu*, X_d = 1.8 *pu*, $X_d^{'}$ = 0.30 *pu*,

$X_d^{''}$ = 0.25 *pu*, $T_{d0}^{'}$ = 8.0 *sec*, $T_{d0}^{''}$ = 0.03 *sec*, X_q = 1.7 *pu*,

$X_q^{'}$ = 0.55 *pu*, $X_q^{''}$ = 0.25 *pu* , $T_{q0}^{'}$ = 0.4 *sec* ,

$T_{q0}^{''}$ = 0.05 *sec*, H = 6.5 *sec*, D = 0.

Generator base: 900 *MVA*

Exciter Parameters:

Exciter 1 (IEEE type DC1 Model):

T_R = 0.01 *sec*, K_A = 46.0, T_A = 0.06 *sec*, $T_B = T_C = 0$,

V_{Rmax} = 1.0 *pu*, V_{Rmin} = -0.9 *pu*, V_{Imax} = 0.0 *pu*,

V_{Imin} = 0.46 *pu*, K_J = 3.1, K_p = 0.33, θ_p = 2.3 *degree*,

K_I = 0.1, X_L = 0.1 *pu*, K_C = 1.0.

Exciter 2 (IEEE type ST3 Model):

T_R = 0.01 *sec*, K_A = 7.04, T_A = 1.0 *sec*, T_B = 6.67 *sec*,

T_C = 1.0 *sec*, V_{Rmax} = 10.0 *pu*, V_{Rmin} = -10.0 *pu*, V_{Imax} = 0.2 *pu*,

V_{Imin} = -0.2 *pu*, K_J = 200, K_p = 4.37, θ_p = 20 *degree*,

K_I = 4.83, X_L = 0.09 *pu*, K_C = 1.1, E_{fdmax} = 8.63 *pu*,

K_G = 1.0, V_{Gmax} = 6.53 *pu*.

Exciter 3 (Simplified Model):

T_R = 0.01 *sec*, K_A = 200, V_{Rmax} = 5.0 *pu*, V_{Rmin} = -5.0 *pu*.

Exciter 4: (IEEE type DC2 Model):

T_R = 0.01 *sec*, K_A = 300.0, T_A = 0.01 *sec*, $T_B = T_C$ = 0,

V_{Rmax} = 4.95 *pu*, V_{Rmin} = -4.9 *pu*, V_{Imax} = 1.0 *pu*,

V_{Imin} = 1.33 *pu*, K_J = 3.05, K_p = 0.279, θ_p = 2.29 *degree*,

K_I = 0.117, X_L = 0.1 *pu*, K_C = 0.675.

Governor Parameters:

Speed set point: 1 *pu*, Steady-state gain (*1/R*): 25.0

T_s: 0.1 *sec*, T_c: 0.4 *sec*, T_3: 0.0, T_4: 1.25 *sec*, $T_{5:}$ 5.0 *sec*

System Parameters (System is symmetric):

line 9-13: R = 0.011 *pu*, X_l = 0.11 *pu*, X_c = 0.1925 *pu*;

Line 6-9: R = 0.001 *pu*, X_l = 0.01 *pu*, X_c= 0.0175 *pu*;

Line 5-6: R = 0.0025 *pu*, X_l = 0.025 *pu*, X_c= 0.0437 *pu*;

Generator transformer reactance: 0.0167 *pu;*

Load transformer reactance: 0.005, tap max: 1.2, tap min: 0.8, tap size: 0.05;

APPENDIX B

JACOBIAN MATRIX FOR UPFC POWER FLOW CALCULATION

$$N_{11} = \frac{\partial P_k}{\partial \theta_k}$$
$$= V_m V_k (G_{cr} \sin(\theta_k - \theta_m) - B_{cr} \cos(\theta_k - \theta_m))$$
$$+ V_k V_{cr} (G_{cr} \sin(\theta_k - \theta_{cr}) - B_{cr} \cos(\theta_k - \theta_{cr}))$$
$$+ V_k V_{vr} (G_{vr} \sin(\theta_k - \theta_{cr}) - B_{vr} \cos(\theta_k - \theta_{vr}))$$
$$+ V_k V_1 (G_1 \sin(\theta_k - \theta_1) - B_1 \cos(\theta_k - \theta_1))$$

$$N_{12} = \frac{\partial P_k}{\partial V_m} V_m = -V_m V_k (G_{cr} \cos(\theta_k - \theta_m) + B_{cr} \sin(\theta_k - \theta_m))$$

$$N_{13} = \frac{\partial P_k}{\partial \theta_m} = -V_k V_m (G_{cr} \sin(\theta_k - \theta_m) - B_{cr} \cos(\theta_k - \theta_m))$$

$$N_{14} = \frac{\partial P_k}{\partial V_{vr}} V_{vr} = -V_k V_{vr} (G_{vr} \cos(\theta_k - \theta_{vr}) + B_{vr} \sin(\theta_k - \theta_{vr}))$$

$$N_{15} = \frac{\partial P_k}{\partial \theta_{vr}} = -V_k V_{vr} (G_{vr} \sin(\theta_k - \theta_{vr}) - B_{vr} \cos(\theta_k - \theta_{vr}))$$

$$N_{16} = \frac{\partial P_k}{\partial V_{cr}} V_{cr} = -V_k V_{cr} (G_{cr} \cos(\theta_k - \theta_{cr}) + B_{cr} \sin(\theta_k - \theta_{cr}))$$

$$N_{17} = \frac{\partial P_k}{\partial \theta_{cr}} = -V_k V_{cr} (G_{cr} \sin(\theta_k - \theta_{cr}) - B_{cr} \cos(\theta_k - \theta_{cr}))$$

$$N_{21} = \frac{\partial P_m}{\partial \theta_k} = -V_m V_k (G_{cr} \sin(\theta_m - \theta_k) - B_{cr} \cos(\theta_m - \theta_k))$$

$$N_{22} = \frac{\partial P_m}{\partial V_m} V_m$$
$$= 2{V_m}^2 (G_{cr} + G_2) + V_m V_2 (-G_2 \cos(\theta_m - \theta_2) + B_2 \sin(\theta_m - \theta_2))$$
$$+ V_m V_k (-G_{cr} \cos(\theta_m - \theta_k) - B_{cr} \sin(\theta_m - \theta_k))$$
$$+ V_m V_{cr} (G_{cr} \cos(\theta_m - \theta_{cr}) + B_{cr} \sin(\theta_m - \theta_{cr}))$$

$$N_{23} = \frac{\partial P_m}{\partial \theta_m}$$
$$= V_m V_2 (G_2 \sin(\theta_m - \theta_2) - B_2 \cos(\theta_m - \theta_2))$$
$$+ V_m V_k (G_{cr} \sin(\theta_m - \theta_k) - B_{cr} \cos(\theta_m - \theta_k))$$
$$+ V_m V_{cr} (-G_{cr} \sin(\theta_m - \theta_{cr}) + B_{cr} \cos(\theta_m - \theta_{cr}))$$

$$N_{24} = \frac{\partial P_m}{\partial V_{vr}} V_{vr} = 0$$

$$N_{25} = \frac{\partial P_m}{\partial \theta_{vr}} = 0$$

$$N_{26} = \frac{\partial P_m}{\partial V_{cr}} V_{cr} = V_m V_{cr} (G_{cr} \cos(\theta_m - \theta_{cr}) + B_{cr} \sin(\theta_m - \theta_{cr}))$$

$$N_{27} = \frac{\partial P_m}{\partial \theta_{cr}} = V_m V_{cr} (G_{cr} \sin(\theta_m - \theta_{cr}) - B_{cr} \cos(\theta_m - \theta_{cr}))$$

$$N_{31} = \frac{\partial Q_k}{\partial \theta_k}$$
$$= V_k V_m (-G_{cr} \cos(\theta_k - \theta_m) - B_{cr} \sin(\theta_k - \theta_m))$$
$$+ V_k V_{cr} (-G_{cr} \cos(\theta_k - \theta_{cr}) - B_{cr} \sin(\theta_k - \theta_{cr}))$$
$$+ V_k V_{vr} (-G_{vr} \cos(\theta_k - \theta_{vr}) - B_{vr} \sin(\theta_k - \theta_{vr}))$$
$$+ V_k V_1 (-G_1 \cos(\theta_k - \theta_1) - B_1 \sin(\theta_k - \theta_1))$$

$$N_{32} = \frac{\partial Q_k}{\partial V_m} V_m = V_k V_m (-G_{cr} \sin(\theta_k - \theta_m) + B_{cr} \cos(\theta_k - \theta_m))$$

$$N_{33} = \frac{\partial Q_k}{\partial \theta_m} = V_k V_m (G_{cr} \cos(\theta_k - \theta_m) + B_{cr} \sin(\theta_k - \theta_m))$$

$$N_{34} = \frac{\partial Q_k}{\partial V_{vr}} V_{vr} = V_k V_{vr} (-G_{vr} \sin(\theta_k - \theta_{vr}) + B_{vr} \cos(\theta_k - \theta_{vr}))$$

$$N_{35} = \frac{\partial Q_k}{\partial \theta_{vr}} = V_k V_{vr} (G_{vr} \cos(\theta_k - \theta_{vr}) + B_{vr} \sin(\theta_k - \theta_{vr}))$$

$$N_{36} = \frac{\partial Q_k}{\partial V_{cr}} V_{cr} = V_k V_{cr} (-G_{cr} \sin(\theta_k - \theta_{cr}) + B_{vr} \cos(\theta_k - \theta_{cr}))$$

$$N_{37} = \frac{\partial Q_k}{\partial \theta_{cr}} = V_k V_{cr} (G_{cr} \cos(\theta_k - \theta_{cr}) + B_{vr} \sin(\theta_k - \theta_{cr})$$

$$N_{41} = \frac{\partial Q_m}{\partial \theta_k} = V_m V_k (G_{cr} \cos(\theta_k - \theta_m) + B_{vr} \sin(\theta_m - \theta_k))$$

$$\begin{aligned} N_{42} &= \frac{\partial Q_m}{\partial V_m} V_m \\ &= -2V_m{}^2 (B_{cr} + B_2) + V_m V_2 (-G_2 \sin(\theta_m - \theta_2) + B_2 \cos(\theta_m - \theta_2)) \\ &\quad + V_m V_k (-G_{cr} \sin(\theta_m - \theta_k) + B_{cr} \cos(\theta_m - \theta_k)) \\ &\quad + V_m V_{cr} (G_{cr} \sin(\theta_m - \theta_{cr}) - B_{cr} \cos(\theta_m - \theta_{cr})) \end{aligned}$$

$$\begin{aligned} N_{43} &= \frac{\partial Q_m}{\partial \theta_m} \\ &= V_m V_2 (-G_2 \cos(\theta_m - \theta_2) - B_2 \sin(\theta_m - \theta_2)) \\ &\quad + V_m V_k (-G_{cr} \cos(\theta_m - \theta_k) - B_{cr} \sin(\theta_m - \theta_k)) \\ &\quad + V_m V_{cr} (G_{cr} \cos(\theta_m - \theta_{cr}) + B_{cr} \sin(\theta_m - \theta_{cr})) \end{aligned}$$

$$N_{44} = \frac{\partial Q_m}{\partial V_{vr}} V_{vr} = 0$$

$$N_{45} = \frac{\partial Q_m}{\partial \theta_{vr}} = 0$$

$$N_{46} = \frac{\partial Q_m}{\partial V_{cr}} V_{cr} = V_m V_{cr} (G_{cr} \sin(\theta_m - \theta_{cr}) - B_{cr} \cos(\theta_m - \theta_{cr}))$$

$$N_{47} = \frac{\partial Q_m}{\partial \theta_{cr}} = V_m V_{cr} (-G_{cr} \cos(\theta_m - \theta_{cr}) - B_{cr} \sin(\theta_m - \theta_{cr}))$$

$$\begin{aligned} N_{51} &= \frac{\partial P_{dc}}{\partial \theta_k} \\ &= V_{cr} V_k (G_{cr} \sin(\theta_{cr} - \theta_k) - B_{cr} \cos(\theta_k - \theta_{cr})) \\ &\quad + V_{vr} V_k (G_{vr} \sin(\theta_{vr} - \theta_k) - B_{vr} \cos(\theta_k - \theta_{vr})) \end{aligned}$$

$$N_{52} = \frac{\partial P_{dc}}{\partial V_m} V_m = V_{cr} V_m (-G_{cr} \cos(\theta_m - \theta_{cr}) - B_{cr} \sin(\theta_{cr} - \theta_m))$$

$$N_{53} = \frac{\partial P_{dc}}{\partial \theta_m} = V_{cr} V_m (G_{cr} \sin(\theta_m - \theta_{cr}) + B_{cr} \cos(\theta_m - \theta_{cr}))$$

$$N_{54} = \frac{\partial P_{dc}}{\partial V_{vr}} V_{vr} = -2V_{vr}{}^2 G_{vr} + V_{vr} V_k (G_{vr} \cos(\theta_{vr} - \theta_k) + B_{vr} \sin(\theta_{vr} - \theta_k))$$

$$N_{55} = \frac{\partial P_{dc}}{\partial \theta_{vr}} = V_{vr} V_k (-G_{vr} \sin(\theta_{vr} - \theta_k) + B_{vr} \cos(\theta_{vr} - \theta_k))$$

$$\begin{aligned} N_{56} &= \frac{\partial P_{dc}}{\partial V_{cr}} V_{cr} \\ &= -2V_{cr}{}^2 G_{cr} + V_{cr} V_k (G_{cr} \cos(\theta_{cr} - \theta_k) + B_{cr} \sin(\theta_{cr} - \theta_k)) \\ &\quad - V_{cr} V_m (G_{cr} \cos(\theta_m - \theta_{cr}) + B_{cr} \sin(\theta_{cr} - \theta_m)) \end{aligned}$$

$$\begin{aligned} N_{57} &= \frac{\partial P_{dc}}{\partial \theta_{cr}} \\ &= V_{cr} V_k (-G_{cr} \sin(\theta_{cr} - \theta_k) + B_{cr} \cos(\theta_k - \theta_{cr})) \\ &\quad + V_{cr} V_m (G_{cr} \sin(\theta_{cr} - \theta_m) - B_{cr} \cos(\theta_m - \theta_{cr})) \end{aligned}$$

$$N_{61} = \frac{\partial P}{\partial \theta_k} = V_m V_k (G_{cr} \sin(\theta_m - \theta_k) - B_{cr} \cos(\theta_m - \theta_k))$$

$$\begin{aligned} N_{62} &= \frac{\partial P}{\partial V_m} V_m \\ &= -2V_m^2 G_{cr} + V_m V_k (G_{cr} \cos(\theta_m - \theta_k) + B_{cr} \sin(\theta_m - \theta_k)) \\ &\quad - V_m V_{cr} (G_{cr} \cos(\theta_m - \theta_{cr}) + B_{cr} \sin(\theta_m - \theta_{cr})) \end{aligned}$$

$$\begin{aligned} N_{63} &= \frac{\partial P}{\partial \theta_m} \\ &= V_m V_k (-G_{cr} \sin(\theta_m - \theta_k) + B_{cr} \cos(\theta_m - \theta_k)) \\ &\quad + V_m V_{cr} (G_{cr} \sin(\theta_m - \theta_{cr}) - B_{cr} \cos(\theta_m - \theta_{cr})) \end{aligned}$$

$$N_{64} = \frac{\partial P}{\partial V_{vr}} V_{vr} = 0$$

$$N_{65} = \frac{\partial P}{\partial \theta_{vr}} = 0$$

$$N_{66} = \frac{\partial P}{\partial V_{cr}} V_{cr} = V_m V_{cr} (-G_{cr} \cos(\theta_m - \theta_{cr}) - B_{cr} \sin(\theta_m - \theta_{cr}))$$

$$N_{67} = \frac{\partial P}{\partial \theta_{cr}} = V_m V_{cr} (-G_{cr} \sin(\theta_m - \theta_{cr}) + B_{cr} \cos(\theta_m - \theta_{cr}))$$

$$N_{71} = \frac{\partial Q}{\partial \theta_k} = V_m V_k (-G_{cr} \cos(\theta_m - \theta_k) - B_{cr} \sin(\theta_m - \theta_k))$$

$$\begin{aligned} N_{72} &= \frac{\partial Q}{\partial V_m} V_m \\ &= 2V_m{}^2 B_{cr} + V_m V_k (G_{cr} \sin(\theta_m - \theta_k) - B_{cr} \cos(\theta_m - \theta_k)) \\ &\quad - V_m V_{cr} (G_{cr} \sin(\theta_m - \theta_{cr}) - B_{cr} \cos(\theta_m - \theta_{cr})) \end{aligned}$$

$$\begin{aligned} N_{73} &= \frac{\partial Q}{\partial \theta_m} \\ &= V_m V_k (G_{cr} \cos(\theta_m - \theta_k) + B_{cr} \sin(\theta_m - \theta_k)) \\ &\quad - V_m V_{cr} (G_{cr} \cos(\theta_m - \theta_{cr}) + B_{cr} \sin(\theta_m - \theta_{cr})) \end{aligned}$$

$$N_{74} = \frac{\partial Q}{\partial V_{vr}} V_{vr} = 0$$

$$N_{75} = \frac{\partial Q}{\partial \theta_{vr}} = 0$$

$$N_{76} = \frac{\partial Q}{\partial V_{cr}} V_{cr} = -V_m V_{cr} (G_{cr} \sin(\theta_m - \theta_{cr}) - B_{cr} \cos(\theta_m - \theta_{cr}))$$

$$N_{77} = \frac{\partial Q}{\partial \theta_{cr}} = V_m V_{cr} (G_{cr} \cos(\theta_m - \theta_{cr}) + B_{cr} \sin(\theta_m - \theta_{cr}))$$